

**REDUCTIVE PRECIPITATION OF SELENITE IN WATER
USING SODIUM SULFIDE**

A Thesis

by

AYA SABRY ABDELMONEIM AHMED SAFAN

Submitted to the Office of Graduate and Professional Studies of
Texas A&M University
in partial fulfillment of the requirements for the degree of

MASTER OF SCIENCE

Chair of Committee,	Ahmed Abdel-Wahab
Committee Members,	Mohamed Nounou
	Mahmood Amani
Head of Department,	Nazmul Karim

August 2016

Major Subject: Chemical Engineering

Copyright 2016 Aya Safan

ABSTRACT

Selenium (Se) is an essential trace element to humans and animals due to its function as an antioxidant and catalyst for the production of active thyroid hormone. However, it is toxic at high concentrations, which can cause diseases and death to humans. Selenium is released to the environment from sewage sludge and industrial facilities such as mining, oil and gas processing, power generation, coal combustion, metals and petrochemical industries. Selenium removal from contaminated wastewaters is necessary due to its toxicity and potential harm to human health and the environment. Selenium can be removed from wastewaters using biological or chemical/physical processes. However, each of these processes has its own limitation. For example, biological treatment of selenium requires several hours of hydraulic residence time and chemical/physical processes either produces unstable selenium-bearing residuals or concentrated liquid waste byproduct.

Reductive precipitation of selenium is an attractive process because it can convert the soluble forms of selenite and selenate to insoluble elemental selenium. This study investigates selenite (Se(IV)) removal from water via reductive precipitation using sodium sulfide at neutral pH. Also, this study investigates the effect of UV light irradiation as an activation method to enhance Se(IV) reduction.

Analysis of precipitated solids using XPS, SEM, and XRD indicated that Se(IV) was reduced to elemental Se or solids composing of Se and sulfur (S) (e.g. $\text{Se}_n\text{S}_{8-n}$). High-resolution S 2p spectra suggested the presence of sulfur oxyanions, monosulfide (S^{2-}),

polysulfides (S_n^{2-}), and elemental sulfur. SEM images showed large irregular aggregates that were dominant at acidic pH than neutral pH, and they were more noticeable in the presence of UV light. Additionally, it was observed from XRD patterns that elemental selenium (layered plate shape) was dominant in the absence of UV light. Whereas, cyclic Se-S precipitates (Se_3S_5) with orange color were dominant in the presence of UV light.

Selenite was effectively removed at neutral pH, regardless of the presence of UV light. UV light did not enhance Se(IV) removal at tested conditions, but it affected the solid morphology and its composition. Complete removal of selenite was achieved in less than five minutes at sulfide dose to initial Se(IV) molar ratios above 11.5.

DEDICATION

I dedicate this thesis to my parents and siblings. I hope this achievement will make them proud when they supported me for the best education. Thank you for your support along the way.

ACKNOWLEDGEMENTS

I would like to thank my committee chair, Dr. Ahmed Abdel-Wahab, and my committee members, Dr. Mohamed Nounou, and Dr. Mahmood Amani, for their guidance and support throughout the course of this research. Many thanks and sincere gratitude to Dr. Bahngmi Jung, who helped, guided and encouraged me continuously throughout the research.

Thanks also go to my friends and colleagues and the department faculty and staff for making my time at Texas A&M University a great experience. Finally, thanks to my parents and siblings for their encouragement, care, and support.

This research was made possible by a grant from the Qatar National Research Fund under its National Priorities Research Program award number NPRP 6-729-2-301. The thesis contents are solely the responsibility of the authors and do not necessarily represent the official views of the Qatar National Research Fund.

NOMENCLATURE

DCP	2,4 dichlorophenol
AOP	Advanced oxidation process
ARP	Advanced reduction process
ATR-FTIR	Attenuated Total Reflectance-Fourier Transform Infrared Spectroscopy
BE	Binding Energy
DDW	Deoxygenated Deionized Water
EPA	U.S. Environmental Protection Agency
FGD	Flue gas desulfurization
FWHM	Full Width at Half Maximum
HA	Humic Acids
ICP-OES	Inductively coupled plasma-optical emission spectrometry
IC	Ion Chromatograph
MCL	Maximum Contaminant Level
MDL	Method Detection Limit
NSPS	New Source Performance Standards
PFOA	Perfluorooctanoic acid
ORP	Oxidation-Reduction Potential
USEPA	The US Environmental Protection Agency
RO	Reverse Osmosis

SEM-EDS	Scanning Electron Microscopy – Energy Dispersive Spectroscopy
Se	Selenium
Se(IV)	Selenite
UV	Ultraviolet light
UV-B	Ultraviolet light from broadband lamp
UV-L	Ultraviolet light from low-pressure mercury lamp
UV-M	Ultraviolet light from medium pressure mercury lamp
UV-N	Ultraviolet light from narrowband lamp
VC	Vinyl chloride
XRD	X-Ray Diffraction
XPS	X-Ray Photoelectron Spectroscopy

TABLE OF CONTENTS

	Page
ABSTRACT	ii
DEDICATION	iv
ACKNOWLEDGEMENTS	v
NOMENCLATURE	vi
TABLE OF CONTENTS	viii
LIST OF FIGURES	x
LIST OF TABLES	xiv
1. INTRODUCTION.....	1
2. BACKGROUND.....	4
2.1 Selenium Chemistry	4
2.2 Oxidation-Reduction Reactions of Se	6
2.3 Ultraviolet (UV) Light as Activating Agent in Advanced Reduction Processes	6
2.4 Sulfide (photo)chemistry.....	8
3. RESEARCH OBJECTIVES AND TASKS	13
3.1 Research Objectives	13
3.1.1 Objective I: Develop Experimental and Analytical Procedures.....	13
3.1.2 Objective II: Evaluate Kinetics and Equilibrium Characteristics	13
3.1.3 Objective III: Characterize the Reaction Mechanism and Produced Solids	14
4. METHODOLOGY	15
4.1 Materials.....	15
4.2 Experimental Procedure	15
4.2.1 Reactor Setup	16
4.2.2 UV Lamps	18
4.3 Analytical Procedure.....	19
5. RESULTS AND DISCUSSION	23
5.1 Screening Experiments for Selenite (Se(IV)) in a Non-Buffered Solution	23

5.2 Screening Experiments for Selenite (Se(IV)) in a Buffered Solution	29
5.3 Effects of Experimental Conditions on Selenite Removal by Sulfide.....	33
5.3.1 Effect of pH	33
5.3.2 Effect of Sulfide Dose.....	54
5.3.3 Effect of Se(IV) Initial Concentration	69
5.3.4 Effect of UV Irradiation.....	70
5.3.5 Effect of Humic Acids	74
5.3.6 Effect of Sulfate and Carbonate on Se(IV) Removal with Sulfide.....	77
5.4 Solid Surface Analysis: XRD Results	79
5.5 Reaction Mechanism of Se(IV) Reduction by Sulfide	83
6. CONCLUSION	87
REFERENCES	89
APPENDIX A	101

LIST OF FIGURES

	Page
Figure 1. Eh-pH diagram for selenium species in water.	5
Figure 2. Distribution of sulfide species in water as a function of pH at 20°C	8
Figure 3. Experimental setup for quartz cells closed reactors.....	17
Figure 4. Experimental setup of beaker open reactor system with mixing.	18
Figure 5. High-resolution C 1s XPS spectra.	22
Figure 6. Effect of UV light on Se(IV) concentration.....	26
Figure 7. Results of screening experiments using different combinations of reducing reagents and UV-light sources in 3 hours.....	26
Figure 8. Visual representation of solids retained on the filter papers with dithionite (a), sulfite (b), sulfide (c), and ferrous iron (d).....	28
Figure 9. Solution color with and without dithionite after four hours of UV-L irradiation.	28
Figure 10. Results of screening experiments in pH 7 buffered solutions after 4 hours of irradiation.	31
Figure 11. The color changes of selenite-sulfide solution with UV-L irradiation (a) and without UV-L irradiation (b) in 4 hours.	32
Figure 12. Effect of pH on Se(IV) removal by sulfide and pH change with time (a) sulfide, no UV and (b) sulfide and UV-L).	35
Figure 13. SEM/EDS analysis of a filter membrane, which does not contain solids.....	36
Figure 14. SEM/EDS results on solids formed in Se-S ²⁻ solution at: (a) pH 4 without UV, (b) pH 4 with UV, (c) pH 7 without UV, and (d) pH 7 with UV.	38
Figure 15. Absorption spectra of sulfide solution prepared in 10 mM phosphate buffer at different pH values with no UV light irradiation.....	39
Figure 16. UV spectra of sulfide solution prepared in anoxic conditions at pH 4 with UV-L irradiation over time.	41

Figure 17. UV spectra of sulfide solution prepared in anoxic conditions at pH 7 with UV-L irradiation over time.	43
Figure 18. UV spectra of sulfide solution prepared in anoxic conditions at pH 9 with UV-L irradiation over time.	44
Figure 19. UV spectra of sulfide solution prepared in anoxic conditions at pH 11 with UV-L irradiation over time.	44
Figure 20. High-resolution O 1s, S 2p, and Se 3d XPS de-convolution spectra of the solids formed in Se(IV)-S(-II) solution in the presence of UV- L at pH 4 and pH 7.	48
Figure 21. High resolution O 1s, S 2p and Se 3d XPS de-convolution spectra of solid formed in Se(IV)-S(-II) solution in the absence of UV- L after 10 min reaction time.....	50
Figure 22. Effect of sulfide dose on selenite removal rate (a) in the absence of UV light, (b) in the presence of UV light.	57
Figure 23. Selenite removal efficiency at different sulfide doses.	58
Figure 24. SEM/EDS analysis results of solids formed in Se-S ²⁻ solution at pH 7 without UV irradiation when sulfide dose was 11.5 times (a), 46 times (b), and 115 times (c) to initial Se concentration.	59
Figure 25. SEM/EDS analysis results of solids formed in Se-S ²⁻ solution at pH 7 with UV irradiation when sulfide dose was 3 times (a), 11.5 times (b), 46 times (c), and 115 times (d) to initial Se concentration.....	60
Figure 26. UV absorbance spectra of Se-sulfide solution at different conditions in the absence of UV light (a) and in the presence of UV-L light (b).....	62
Figure 27. Absorbance spectra of Se-sulfide solution showing the effect of UV-L light over time.	63
Figure 28. Absorbance of sulfide solution over time at 254 nm upon UV-L irradiation	63
Figure 29. High-resolution O 1s, S 2p and Se 3d XPS spectra of solid formed in Se(IV)-S(-II) solution in the absence of UV- L after 10 min at pH 7 with S ²⁻ /Se molar ratio of 11.5 and 115.....	66

Figure 30. High-resolution O 1s, S 2p, and Se 3d XPS de-convolution spectra of the solid formed in Se(IV)-S(-II) solution in the absence of UV- L for 10 min at pH 7 with S ²⁻ /Se molar ratio of 11.5, 46, and 115.	67
Figure 31. High-resolution O 1s, S 2p, and Se 3d XPS spectra of the solid formed in Se(IV)-S(-II) solution in the presence of UV-L and the absence of UV-L light.	71
Figure 32. High-resolution O 1s, S 2p, and Se 3d XPS de-convolution spectra of the solid formed in Se(IV)-S(-II) solution in the presence of UV-L and the absence of UV-L light.	73
Figure 33. Humic acid molecular structure.	74
Figure 34. The effect of humic acids concentration on selenite concentrations at different initial HA concentrations in the absence of UV light (a) and in the presence of UV light (b) when the molar ratio of S ²⁻ /Se was 46.	76
Figure 35. Selenite concentrations and pH changes with 100 mg/L inorganic salts in the absence of UV light (a) and in the presence of UV light (b).	78
Figure 36. Solids formed in Se-S ²⁻ solutions in the absence of UV light (a) and in the presence of UV light (b).	80
Figure 37. XRD pattern of the precipitates formed from selenium-sulfide solution in the absence and in the presence of UV, elemental selenium (03-065-1876) (red dots) and (01-070-9556) (red squares), sulfur (00-042-1278) (blue crosses), Se _{3.3} S _{4.7} (1-071-0247) (blue circles) and Se _{3.02} S _{4.98} (00-031-122) (black peaks).	81
Figure 38. Peak assignments of XRD pattern of the precipitates formed from selenium-sulfide solution in the absence of UV.	82
Figure 39. Peak assignments of XRD pattern of the precipitates formed from selenium-sulfide solution in the presence of UV.	83
Figure A1. Selenite concentrations and pH changes in blank control (no reagent, no UV) (a) and light control (no sulfide, UV-L) (b).	101
Figure A2. Solids produced in Se ⁴⁺ -S ²⁻ solution at pH 4 in a blank (a), light control (b), reagent control (c), and rector (d).	102
Figure A3. Solids produced in Se ⁴⁺ -S ²⁻ solution at pH 7 in a blank (a), light control (b), reagent control (c), and rector (d).	103

Figure A4. Solid formation throughout the experiment at pH 11. (a) Se and no UV-L. (b) Se and Sulfide and no UV-L. (c) Se and UV-L. (d) Se and Sulfide and UV-L.....	104
Figure A5. Absorbance spectra of Se-sulfide solution for different concentration in the absence of UV light (a), in the presence of UV-L light for 10 min (b) and the presence of UV-L light for 30 min.....	105

LIST OF TABLES

	Page
Table 1. Disadvantages of currently available technologies for selenium removal.....	3
Table 2. Previous research work on advanced reduction processes.....	7
Table 3. Experimental conditions of screening experiments without pH adjustment.....	25
Table 4. Experimental conditions of screening experiments in a buffered solutions.	30
Table 5. Experimental conditions for investigating the effect of pH.	34
Table 6. Experimental conditions for investigating the effect of sulfide dose on Se(IV) removal.	56
Table 7. Experimental conditions for investigating the effect of Se(IV) initial concentration.....	69
Table 8. Experimental conditions for investigating the effect of humic acids.....	76
Table 9. Experimental conditions for investigating the effect of inorganics.	77
Table A1. Binding energies of O 1s XPS spectra from the literature.....	106
Table A2. Assignment of S 2p _{3/2} from elemental sulfur collected from the literature	106
Table A3. Assignment of S 2p _{3/2} : sulfides (S ²⁻ , S ₂ ²⁻) and polysulfides (S _n ²⁻) from the published data.....	107
Table A4. Binding energies of S 2p components HSO ₃ ⁻ , SO ₃ ⁻ , SO ₄ ²⁻ , S ₂ O ₃ ²⁻ , S ₂ O ₄ ²⁻ , S ₂ O ₅ ²⁻ , S ₂ O ₆ ²⁻ , S ₂ O ₈ ²⁻ , and S ₄ O ₆ ²⁻ from the published data.....	108
Table A5. Se 3d _{5/2} binding energies of selenium compounds from the literatures...	109
Table A6. Experimental conditions of samples for XPS analysis.....	109
Table A7. Binding energies, full width at half maximum (FWHM), and area for peaks in the Se 3d, S 2p, and O 1s XPS spectra of samples 1-9 in this study.....	110

1. INTRODUCTION

Selenium (Se) is a naturally occurring trace element.¹ It is an essential element in small traces for humans and animals.^{2,3} However, it is toxic at high concentrations.⁴ This makes the margin between nutritional deficiency (< 40 µg/day) and potential toxicity (> 400 µg/day) very narrow.⁵⁻⁷ Therefore, selenium intake should be controlled by humans and animals.

Anthropogenic activities such mining, smelting operations, metal industry, power generation, and petroleum refining release selenium into the environment. High levels of selenium are released from coal or sour crude oils containing sulfur levels larger than 0.5 %.⁵ Cassella et al.⁸ found selenium in the range of 0.03 - 1.4 mg/L in industrial effluents and process wastewater due to its presence in crude oil. Selenium concentration in mining water ranged from 3 µg/L to 12 mg/L.⁹ Vance et al.¹⁰ reported selenium concentrations in wastewater generated from Gaseous Sulfur Desulfurization (FGD) ranged between 1 mg/L and 10 mg/L.

Maximum contaminant level (MCL) of selenium is 50 µg/L according to the US Environmental Protection Agency (EPA) standards for drinking water.^{2,11} The San Francisco Regional Water Quality Control Board set a limit of 50 µg/L of total selenium in the effluent wastewater from refineries.⁸ High concentrations of Se above the MCL may cause adverse health effects to people, including hair or fingernail loss, numbness, and kidney and liver damage.^{2,3,11} Recently, the EPA released a Final Rule, which sets effluent limitations and standards for six distinct wastewater streams from steam electric power

plants. The specific limits of this rule include a daily maximum concentration of 5 $\mu\text{g/L}$ for selenium in FGD wastewaters.¹²

Selenium exists in nature primarily as elemental Se, selenite (Se(IV)), or selenate (Se(VI)).^{3,13} The fate of selenium in water and soil is governed by the mobility of the compound species.^{14,15} With the increase of pH, the solubility and mobility of selenium increase.^{16,17} This is due to the effect of hydroxyl ion in modifying selenium ion adsorption capacity.¹⁵ Elemental selenium is relatively insoluble in water, and it is less toxic compared to other forms.¹⁷

Technologies available for removing selenium from water or wastewater include ion exchange, membrane filtration, biological reduction, co-precipitation, chemical reduction using zero valent iron, adsorption onto activated alumina.^{2,11,18,19} However, these technologies have disadvantages that make them unattractive for selenium removal from wastewaters.^{5,13,20,21} These disadvantages are listed in Table 1.^{22,23} The overall goal of this research is to study the effectiveness of selenite (Se(IV)) removal via reductive precipitation using sulfide at neutral pH and investigate the effect of system variables on the kinetics of selenite removal. Additionally, the application of UV light a method of enhancing Se(IV) removal by producing highly reactive reducing radicals was examined.

Table 1. Disadvantages of currently available technologies for selenium removal.^{22,23}

Treatment Type	Disadvantages
Ion exchange	<ul style="list-style-type: none">• Resin needs to be replaced if it cannot be regenerated; this means high disposal cost. Backwashing for the resins is required.• Anions (such as sulfates and nitrates) can compete with selenium removal• Regenerated streams need treatment/ disposal• Not able to remove selenate
Membrane filtration	<ul style="list-style-type: none">• High capital and operating cost• Pretreatment and chemical addition are needed• Membrane fouling• Frequent monitoring and membranes maintenance• Brine treatment and safe disposal is a challenging task
Biological reduction	<ul style="list-style-type: none">• The difficulty of selenium removal in the presence of high nitrate concentrations. It can be solved by a pre-treatment or proper selection of the microbial communities• Long hydraulic residence time is required
Zero-valent iron	<ul style="list-style-type: none">• High chemical consumption• Waste disposal handling• Low removal efficiency• Long residence time
Ferrihydrite adsorption	<ul style="list-style-type: none">• High chemical consumption• Generation of large quantities of sludge which needs to be disposed as a hazardous waste• Not able to remove selenate; it has to be reduced to selenite first• Release of selenium from ferrihydrite residuals

2. BACKGROUND

2.1 Selenium Chemistry

Elemental selenium is a solid that occurs naturally in the earth as a metallic gray to black crystals.^{3,16} It is found primarily in an anoxic environment such as sediments.¹⁶ Selenium has four oxidation states VI, IV, 0, -II;^{16,17,24,25} selenides (Se(-II)), amorphous or polymeric elemental selenium (Se(0)), selenites (Se(IV)) and selenates (Se(VI)). Se(IV) and Se(VI) are mobile forms of selenium and they are usually found as oxyanions selenates (SeO_4^{2-}) and selenites (SeO_3^{2-}), while Se(0) and Se(-II) are relatively immobile because of the low solubility of their solid phases.^{13,23} Se(IV) is more toxic than other forms, and thus, most of the treatability studies focused on Se(IV) removal.^{13,25} Se(IV) is a weak diprotic acid, and it can exist as H_2SeO_3 , HSeO_3^- , or SeO_3^{2-} ($\text{pK}_{a1} = 2.64$ and $\text{pK}_{a2} = 8.4$) depending on the solution pH.⁶

The Eh-pH diagram of selenium in water is shown in Figure 1.²⁶ This figure is for the selenium-water system at 25 °C, and it shows the thermodynamic equilibrium as a function of pH and oxidation-reduction potential (ORP) conditions.^{22,27,28} The change in pH or redox potential can cause a shift in equilibrium between different molecular forms.²⁸ Nevertheless, these shifts are controlled not only by thermodynamic equilibrium but also by the kinetics of their underlying reactions.²⁸

Based on the Eh-pH diagram, in the pH range of 5-7, the species at equilibrium are Se, HSe⁻, HSeO₃⁻ and SeO₄²⁻.^{16,26} According to literature, SeO₃²⁻ and HSeO₃⁻ are the primary species that exist at neutral environmental pH.⁷ Zero-valent selenium, and hydrogen selenide (H₂Se) can be found under reducing conditions. The pK_a values for hydrogen selenide (H₂Se) are 3.89 and 15, therefore in the pH range of most natural waters, HSe⁻ will be the primary Se species with oxidation state of -II.¹³

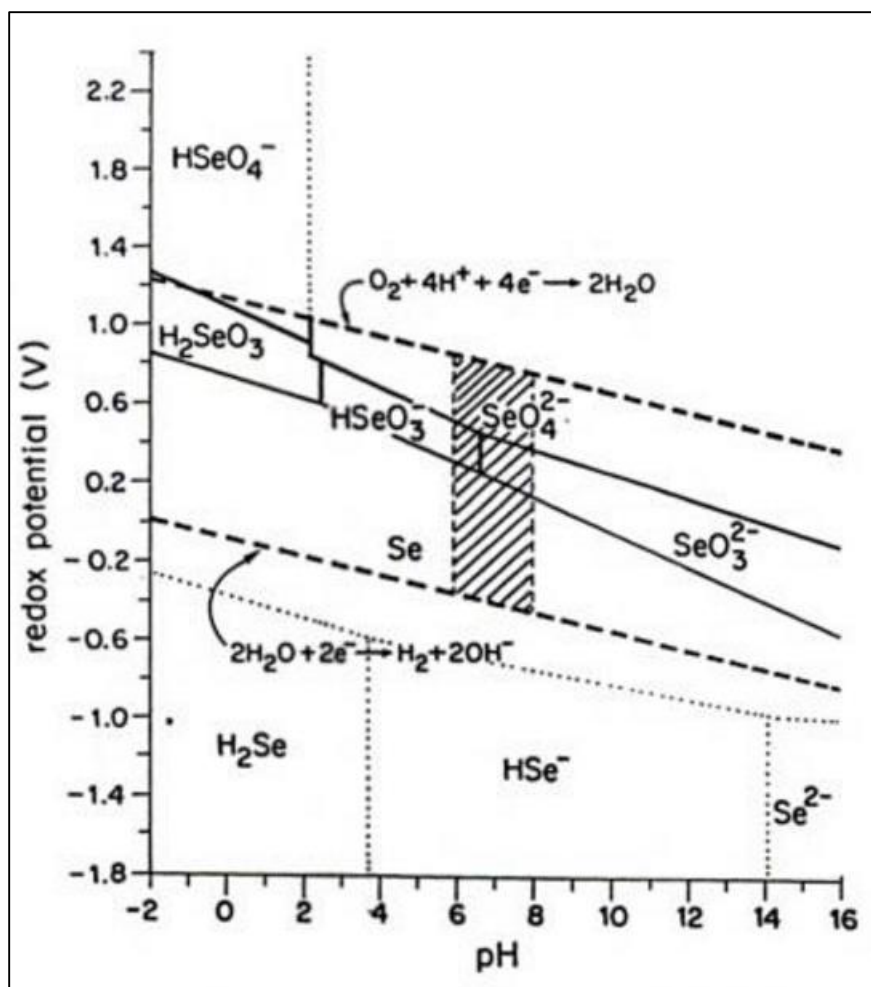


Figure 1. Eh-pH diagram for selenium species in water.²⁶

2.2 Oxidation-Reduction Reactions of Se

The feasibility of contaminate removal via redox reactions is based on the thermodynamic feasibility and kinetics of the reactions.²⁹ Various contaminants are removed from water via redox reactions. Typical contaminants that are removed from water with the aid of redox reactions are heavy metals, cyanides, sulfides and organic pollutants such as phenol, chlorophenols, pesticides, ammonia nitrogen, amines and sulfur containing compounds.³⁰ However, the kinetics of the process can hinder the applicability of redox reaction in water treatment.²⁹ There is a broad range of reducing agents that have been proposed for selenium (IV) removal. These include hydrazinium, zinc powder, metallic copper, and others.^{20,31} Also, some of the studies that investigated selenite reduction utilized stannous chloride, hydroxylammonium compounds, sulfur dioxide, hydrogen peroxide, and nanoscale zero valent iron.³¹⁻³⁶ Additionally, Geoffroy and Demopoulos^{20,21} reported that selenite in zinc refinery acid effluents was reduced by sodium sulfides in less than 10 minutes and with sodium dithionite in less than a minute at very low pH (~ 1.3). They reported that selenium was removed by formation of selenium-sulfur precipitates which were stable at pH values up to pH 7.

2.3 Ultraviolet (UV) Light as Activating Agent in Advanced Reduction Processes

UV light has been widely used in advanced oxidation processes (AOPs)³⁷ and has been recently evaluated in advanced reduction processes (ARPs) as an activating method for reduction of oxidized contaminants in water.³⁸⁻⁴⁵ UV lamps that were used in ARPs include: low-pressure mercury lamp (UV-L) (a monochromatic at 254 nm), broadband UV lamp (UV-B) (wavelength: 280 nm to 320 nm with a major peak at 312 nm) and

medium pressure mercury lamp (UV-M) (wavelength: 320 nm to 380 nm with a major peak at 365 nm).^{40,41} ARPs is a new class of treatment processes that has proven its effectiveness to reduce various oxidized contaminants such as vinyl chloride (VC), 1,2-dichloroethane and perfluorooctanoic acid (PFOA)^{40,44,45}, bromate, nitrate, and perchlorate.^{38,39,43,46}

Reducing agents that have been investigated in ARPs include sulfide, sulfite, dithionite, and ferrous iron. Table 2 summarizes previous research work on advanced reduction processes.

Table 2. Previous research work on advanced reduction processes.^{29,38,40–45}

Target Compound	Reducing Agent	UV lamp type and corresponding wavelength*	Final Product	Ref.
VC	Dithionite, Sulfite, Sulfide and Ferrous iron	UV-L (253.7 nm)	Acetylene and Chloride ion	45
Bromate	Sulfite	UV-M (200 - 600 nm) UV-L (254 nm)	Bromide	46 39
Nitrate	Dithionite	UV-M (200 - 600 nm)	Ammonia	38
perchlorate, PFOA, and DCP [†]	Dithionite, Sulfite, Sulfide and Ferrous iron	UV-L (253.7 nm), UV-B (311 nm), electron beam, ultrasound, and microwave	-	41
1,2-dichloroethane	Hydrosulfite, Sulfite, and Sulfide	UV-M (384 nm) and UV-B (312 nm)	Ethene or ethane	40

*Wavelength of the UV mentioned in the table represent the major/maximum peak for the range of wavelength for UV-M and UV-B.

†DCP: 2,4 dichlorophenol

2.4 Sulfide (photo)chemistry

Sulfide dissociates in water into sulfide ion (S^{2-}), bisulfide ion (HS^-) and hydrogen sulfide (H_2S), where the distribution of species depends on solution pH, as shown in Figure 2.⁴⁷ Sulfide ion is a strong base that reacts with water rapidly to form HS^- and gaseous H_2S based on Eq. (1).⁴⁷ S^{2-} and HS^- are odorless nonvolatile ions, where H_2S is gas with a strong rotten egg smell.⁴⁷

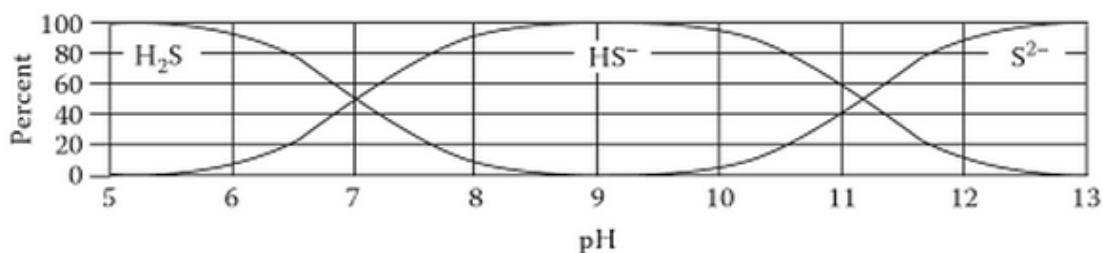
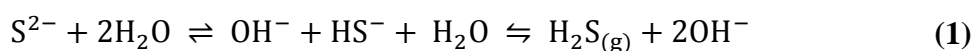
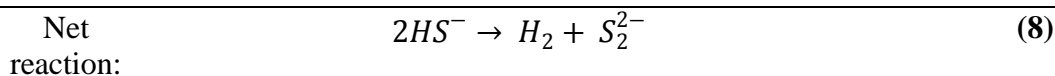


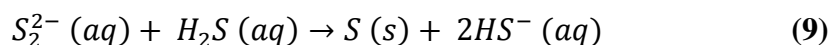
Figure 2. Distribution of sulfide species in water as a function of pH at 20°C.⁴⁷

Sulfide is activated by UV light and produces reductant radicals. According to Liu et al., sulfide solution showed light absorbance peak at a wavelength around 230 nm.⁴² Eq. (2)–Eq. (7)^{48,49} illustrate the photolysis of bisulfide ion (HS^-).



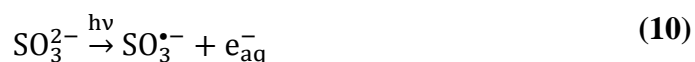


Linkous et al. reported that sulfide ion (mainly bisulfide) produces sulfur when it is oxidized using UV light. The oxidized species is primarily disulfide ion, whereas hydrogen is generated from the reduction of water. The rate of gas generation is a function of pH in the range where HS^- species is dominant.⁴⁸



A literature survey on other reducing reagent chemistry and photochemistry that were utilized in this study are discussed below.

For sulfite, upon irradiating it, sulfite anion radical and hydrated electrons are formed as shown in Eq. (10).^{40,41,50}

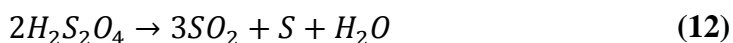


Nevertheless, the dominant species in the solution could be sulfurous acid (H_2SO_3) (with pK_a values of 1.86 and 7.18⁵¹), bisulfite (HSO_3^-) (with pK_a 1.77⁵² and around 7.0⁵³), or sulfite (SO_3^{2-}) (with pK_{a2} of 7.2⁵²) depending on pH.^{40,41} At acidic conditions, bisulfite (HSO_3^-) and metabisulfite ($S_2O_5^{2-}$) (with pK_a value around 1.8⁵³) become more distinct.^{40,41,54} Hence, reducing species at low pH could be HSO_3^- and $S_2O_5^{2-}$ as well. Bisulfite has a thermodynamic equilibrium with metabisulfite⁵⁵ as shown in Eq. (11).

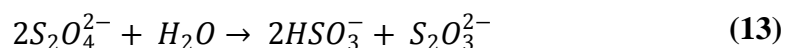


Upon irradiating sulfite solution, bisulfite can absorb minor amount of UV light, and it is unable to produce radicals, nor produce transients during photolysis at room temperature.⁵⁵ On the other hand, metabisulfite can produce sulfite and sulfur dioxide radicals upon irradiation as Hayon et al. reported.⁵⁵ Generally, sulfite aqueous solution shows different absorption peaks at different pH values^{43,56} and initial sulfite concentrations.⁵⁶

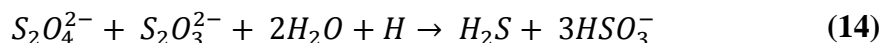
Dithionite is a very strong reducing reagent. According to literature, dithionite ($\text{S}_2\text{O}_4^{2-}$) decomposes to multiple species: sulfite (SO_3^{2-}), sulfate (SO_4^{2-}), bisulfite (HSO_3^-), metabisulfite ($\text{S}_2\text{O}_5^{2-}$), thiosulfate ($\text{S}_2\text{O}_3^{2-}$) and trithionate ($\text{S}_3\text{O}_6^{2-}$). These ions were identified according to Holman et al.⁵⁷ using attenuated total reflectance- fourier transform infrared spectroscopy (ATR- FTIR) spectra at acidic conditions.⁵⁷ The decomposition is highly depended on the acidity of the solution as Cermák et al. reported after extensive studies on dithionate decomposition.⁵⁸ Additionally, Cermák et al. reported that in the absence of oxidizing agents, the major decomposition products of dithionite are thiosulfate, polythionates or hydrogen sulfide.⁵⁸ At extremely acidic conditions, dithionite decomposes to form sulfur dioxide and sulfur as shown below.^{57,59}



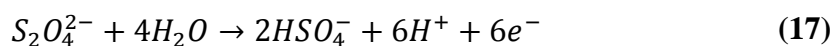
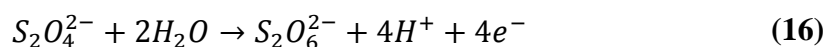
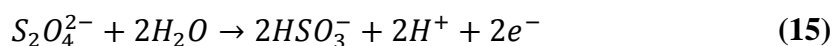
At weakly acidic or weakly alkaline solution, thiosulfate and bisulfite are found to be the products of dithionite decomposition as depicted in Eq. (13).⁵⁸



Geoffroy and Demopoulos reported that dithionite subsequently (Eq. (13)) reacts with thiosulfate, producing hydrogen sulfide as shown in Eq. (14), this makes the decomposition of dithionite is very complex.²⁰



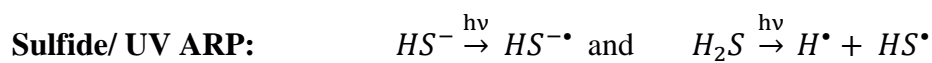
At anaerobic conditions, dithionite readily decomposes to $S_2O_3^{2-}$ and $HSO_3^-/S_2O_5^{2-}$.⁵⁷ This decomposition occurs fast as the pH decreases.⁵⁷ Dithionite is believed to dissociates to sulfur dioxide radical ions (SO_2^{\bullet}) via hemolytic splitting of the weak S-S bond.^{60,61} The most stable decomposition products determined based on literature⁶² are trithionate and thiosulfate ions (stable ions) and no others are likely to be formed. Some of the reduction reactions of dithionite as reported in bleaching reactions in pulp and paper production are as follow (Eq. (15) through Eq. (17)):⁶³



Due to the decomposition of dithionite and the acidic pH of the reaction solution, the actual concentration of dithionite in the solution at the start of the experiment is not necessarily the same as the theoretical concentration.⁵⁷

Furthermore, the absorbance of dithionite was reported to be around 315 nm. However, Amonette et al. observed equilibrium between sulfoxyl radicals and the dithionite. Hence, dithionite might not be necessarily the species giving the absorption at 315 nm.⁶⁴ Lambeth et al.⁶⁵ emphasized the presence of sulfoxyl ion at basic conditions when reducing proteins in the presence of dithionite.

In general, the reactive species in produced upon UV light irradiation are believed to include sulfur dioxide radical ($\text{SO}_2^{\bullet-}$), sulfite radical ($\text{SO}_3^{\bullet-}$), aqueous electron (e_{aq}^-), hydrogen atom (H), and excited bisulfite ion ($\text{HS}^{-\bullet}$), their generation are shown below:⁴⁰



3. RESEARCH OBJECTIVES AND TASKS

3.1 Research Objectives

This research is to investigate the effectiveness of reductive precipitation of selenite (Se(IV)) and the application of UV light as an activating method. The effects of system parameters (pH, reducing reagent dose, initial Se(IV) concentration, reaction time, and the presence of organic matter) on the removal of selenite in the absence and presence of UV light were evaluated. The surface morphology and composition of the precipitates formed were identified using SEM/EDS, XPS, and XRD analysis. The specific objectives of this research are:

3.1.1 Objective I: Develop Experimental and Analytical Procedures

The aim of this task is to develop batch experimental procedures to study the reductive precipitation of selenite and the effectiveness of UV light in reducing the target contaminant. The standard calibration curve for selenite was developed. The maximum detection limit from accuracy and precision tests were determined to define the minimum concentration that can be measured accurately for total soluble selenium. Quartz cells and glass beakers were used as the batch reactor systems in this research.

3.1.2 Objective II: Evaluate Kinetics and Equilibrium Characteristics

This objective aims at identifying the best combination of reducing reagents (sulfite, sulfide, dithionite, or ferrous iron) and UV lamp (UV-L, UV-B, and UV-M) as an activation method through screening tests. Then batch kinetic experiments were conducted, with varying experimental parameters to determine their effects and the optimal conditions for the contaminant removal. The experimental parameters that were

studied are solution pH, reducing agent dose, initial selenite concentration, and light intensity.

3.1.3 Objective III: Characterize the Reaction Mechanism and Produced Solids

This objective is to identify the characteristics of solids formed during the reductive precipitation reactions and to use the results of solution and solids analysis as well as information available in the literature to understand reaction mechanisms of Se(IV) removal.

4. METHODOLOGY

4.1 Materials

Na_2SeO_3 (sodium selenite, Sigma, 99%) was used as the source of Se(IV). Reducing reagents include sulfide (sodium sulfide hydrate, $\geq 60\%$), sulfite (sodium sulfite anhydrous, Na_2SO_3 , Mallinckrodt Chemicals, ACS reagent 98%), dithionite (sodium hydrosulfite, Sigma, $\geq 82\%$), and ferrous sulfate iron ($\text{FeSO}_4 \cdot 7\text{H}_2\text{O}$, ACS reagent, $\geq 99\%$). For the investigation of the effect of natural organic matter and inorganic salts, humic acids sodium salt (Aldrich), sulfate (sodium sulfate anhydrous, EMD, 99.0%) and carbonate (sodium carbonate, VWR, 99.9%) were used. A stock solution of humic acids and inorganic salts was prepared at 1000 mg/L: 0.25 g humic acids sodium salt was dissolved in 250 mL and was mixed for 30 min before use.

All solutions were prepared in 10 mM phosphate solution using 1 M sodium phosphate buffer solution (pH 7.0, BDH) to adjust pH at pH 7. 1.0 N HCl (hydrochloric acid, ACS reagent, 37%) or 1.0 N NaOH (sodium hydroxide, ACS reagent, 97%) was used as needed to adjust pH.

4.2 Experimental Procedure

Batch kinetic experiments for selenite reduction conducted in the presence and the absence of UV light. All solutions were prepared in an anaerobic chamber (Coy Laboratory products Inc. Grass Lake, MI, USA), which contains 99.999% nitrogen and equipped with an oxygen and hydrogen analyzer to monitor their concentrations in the chamber (Coy Laboratory products Inc. Grass Lake, MI, USA).

All reagent solutions were prepared using reagent grade chemicals and deoxygenated deionized water (DDW). DDW (18.2 M Ω) was acquired by a Barnstead Nanopure filter system and purged with N₂ gas (purity > 99.99 %) for approximately two hours. Then, the purged water was stored in the anaerobic chamber until its usage for solutions preparation.

The reducing reagent solution was prepared freshly to avoid any oxidation during storage. A stock solution of Se(IV) was added to a solution including the reducing reagent then the mixture was agitated with a magnetic stirrer. The pH of the solution during the experiment was monitored. Samples were taken at the regular time intervals and filtered using 0.45 μ m or 0.2 μ m membrane filter papers before analysis for Se(IV).²¹

4.2.1 Reactor Setup

In the screening experiments, a closed reactor system of UV-transparent quartz cells of 17 mL volume and 1 cm thickness were used as the batch reactors for experiments outside the anaerobic chamber. The experimental setup is shown in Figure 3. The quartz cells were purchased from Starna company (Starna 32/Q/10, Spectrosil® Quartz) and they have an interior diameter of 47 mm, depth of 10 mm, and the cells are tightly closed with a PTFE stopper.

Another reactor system was used in this research which was an open reactor of a 250 mL beaker that was placed on a stirrer (Thermos Scientific Cimarec stirrer) with a constant speed (around 92 rpm \pm 5.0%⁶⁶) in the anaerobic chamber. The setup for irradiation system in the anaerobic chamber is shown in Figure 4. The breaker was wrapped with aluminum foil to avoid light penetration into the solution during

experiments. The purpose of using this reactor system was to allow solution mixing during the experiments. The distance between the top surface of the solution and the UV lamp installed in the chamber was 4.2 cm.

At a regular time intervals, around 10 mL of the sample was taken out of the reactor using a tight syringe, filtered using 0.45 μm or 0.2 μm membrane filter papers (PALL Life Science, Support $\text{\textcircled{R}}$ -200). The filtrate was analyzed using ICP-OES instrument for total soluble selenium concentration. The filter paper including the solid precipitate was separated from the filter-holder and stored in the anaerobic chamber and dried for solids analysis.

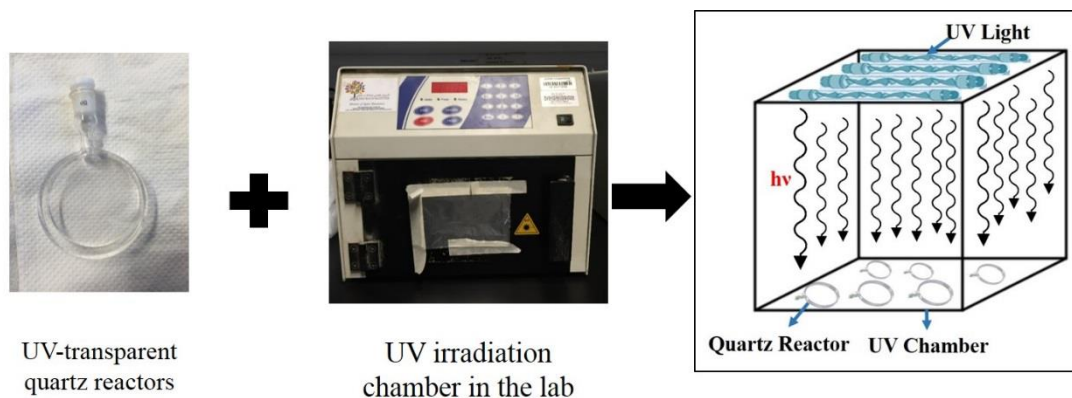


Figure 3. Experimental setup for quartz cells closed reactors.

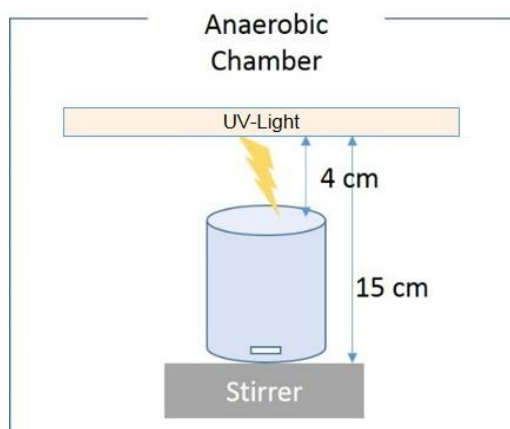


Figure 4. Experimental setup of beaker open reactor system with mixing.

4.2.2 UV Lamps

Four different UV lamps were used in this study: Three UV lamps, T-8C, T-8M, and T-8L were purchased from Vilber Lourmat Company. T-8C lamp is monochromatic at 254 nm (UV-L), and T-8L and T-8M shows a primary wavelength at 365 nm in the range of 320-380 nm (UV-M), and at 312 nm in the range of 280-320 nm (UV-B), respectively. The UV box (14.5 (H) × 33 (D) × 26 (W) cm, BioLink, Vilber Lourmat) is equipped with five individual UV lamps (T-8C, T-8M, and T-8L) of 18 W, as shown in Figure 3. The distance between the lamps and the quartz reactor is 15 cm. Another UV lamp is TUV PL-L Lamp purchased from Philips, which emits short-wave UV radiation at 253.7 nm. The light intensity was measured using ST-512 light meter (UVC, 220-275 nm, calibration point 254 nm) or ST-513 light meter (UVAB, 280-400nm, calibration point 365nm). Before conducting any irradiation experiment and measuring the light intensity, the lamp was warmed up for 10 minutes to reach a constant output. The anaerobic chamber is equipped with a UV-L lamp (TUV PL-L Lamp by Philips that

irradiates short-wave UV with a peak at 253.7 nm), and its light intensity is measured using ST-512 light meter. The light intensity of the TUV PL-L was approximately 6400 $\mu\text{W}/\text{cm}^2$ whereas the light intensity of T-8M UV lamps was around 4600 $\mu\text{W}/\text{cm}^2$; both measured at a vertical distance of 12 cm from the lamp.

4.3 Analytical Procedure

Analytical procedures were developed for Se(IV) concentration measurements. Total selenium concentration in solution was measured using inductively coupled plasma-optical emission spectrometry (Thermo Scientific iCAP 6000 Series ICP-OES) equipped with a recirculating chiller (ThermoFlex 900), and AutoSampler (ASX-260). The conditions of ICP-OES were RF power of 1150 W, pump rate of 50 rpm, nebulizer gas flow of 0.7 L/min and coolant gas flow of 12 L/min. Sulfate analysis was performed by Dionex ion chromatography (ICS-5000). The chromatograph was equipped with AS-AP auto-sampler, a dual gradient pump, anion self-regenerating suppressor (ASRS 300, 2 mm) with a 7.0 mA applied current, and eluent generation module. The mobile phase was 2.4 mM $\text{NaHCO}_3/0.8$ mM Na_2CO_3 at a constant flow rate of 0.25 mL/min and an injection volume of 1200 μL at 30 °C. Perkin Elmer (Lambda 25) UV–Vis spectrophotometer was used for measuring light absorbance via a quartz cell with 1 cm optical path length. The method detection limit (MDL) and method quantification limit (MQL) for selenium were 1.7 $\mu\text{g}/\text{L}$ and 5.6 $\mu\text{g}/\text{L}$ respectively. Selenium species analysis in the stock solutions indicated the presence of small amount of selenate, so it was subtracted from the measured total selenium concentration to give the concentration of selenite in the solution. The pH of the solution was measured by pH-meter (VWR Portable pH-meter (model SympHony

– SP80PC) and Orion, Thermo Scientific, USA with pH meter probe (Orion 8107UWMMD, (ROSS Ultra pH/ ATC Triode, USA))). UV absorbance of reducing reagent solutions was measured using UV-VIS Spectrometer. The solids formed were stored in the anaerobic chamber until being analyzed. Solid samples were analyzed using x-ray photoelectron spectroscopy (XPS), scanning electron microscopy (SEM) - energy dispersive spectroscopy (EDS) and X-ray diffraction (XRD).

The samples were scanned with XRD (Ultima IV, Cu anode) over the range of 0 – 70° at a rate of 1°/min. The sample to be analyzed will be placed into the sample holder (microscope slide glass) ensuring smooth sample Element identification and fitting for the obtained patterns were done using PDXL2 software. The patterns smoothing was made using standard data processing-Rigaku software with Savitzky-Golay's method, and background subtraction was employed using Sonneveld-Visser's method.

For SEM/EDS analysis, the samples were coated with gold Leica EM SCD050 for 120 s at 30 mA and 50 V. The samples will be mounted on a sample holder using carbon tape. Then the non-conducting samples will be coated with a thin layer of gold. SEM-EDS analysis will be performed under vacuum. The particles were captured using Quanta 400 FEI in high vacuum with 10 mm distance between the lenses and the sample, and electron emission at 25.0 kV. The particle images were captured at a magnification in the range 15,000x to 30,000x. The elements were qualified using EDAX-Apollo XP. EDS analysis was conducted using spot analysis for selected particles. Due to small amounts of formed solids, it was not possible to separate enough amount of solids from the filters for

characterization with SEM/EDS. Therefore, the filter papers including solids were analyzed, and the version filter papers without solids were also analyzed for comparison.

For XPS analysis, a Kratos (Manchester, UK) Axis Ultra DLD X-ray Photoelectron Spectrometer (XPS) with a monochromatic Al electrode anode source was used at 75 W. Survey scan for the samples were obtained, along with acquisition of high resolution spectra (narrow scan) to obtain the oxidation states of Se, S, O, and C. The survey scans were recorded with pass energy and sweep of 80 eV and 2 respectively. The narrow scans used 10 eV as pass energy and, at least, sweep of 3. In both scans, the hybrid lens was used, with the emission of 5 mA and voltage of 10 kV. The obtained spectra peaks were corrected according to C 1s binding energy as a reference, as the shift occurs due to charging effect. The narrow scan spectra of Se 3d, S 2p, and O 1s were fitted using XPSPEAK4.1 fitting program with a Gaussian-Lorentzian peak function with a Shirley-type optimization background subtraction corrections. The obtained peaks from XPS analysis are corrected based on the chemical shift in the binding energy of the carbon peak, as shown in Figure 5. In order to calibrate the shifts of spectra, the spectra peak of C 1s at 284.5 ± 0.1 eV was used as a reference.⁷ Then, the adjusted intensity-binding energy spectra of O 1s, S 2p, and Se 3d elements are analyzed, along with survey spectra of the samples. Based on the peak width, it can be resolved into smaller peaks that correspond to the oxidation state of the element. The narrow scan spectra of O1s, S 2p, and Se 3d were fitted using XPSPEAK 4.1 fitting program with Gaussian-Lorentzian function through background subtraction corrections using a Shirley-type optimization. The obtained XPS spectra are quantified in terms of peak position, peak intensity, and the full

width at half maximum (FWHM). Peak position resembles the elemental/ chemical composition; intensity corresponds to the amount of material on the surface, and FWHM indicates the chemical state change and the physical influence.⁶⁷

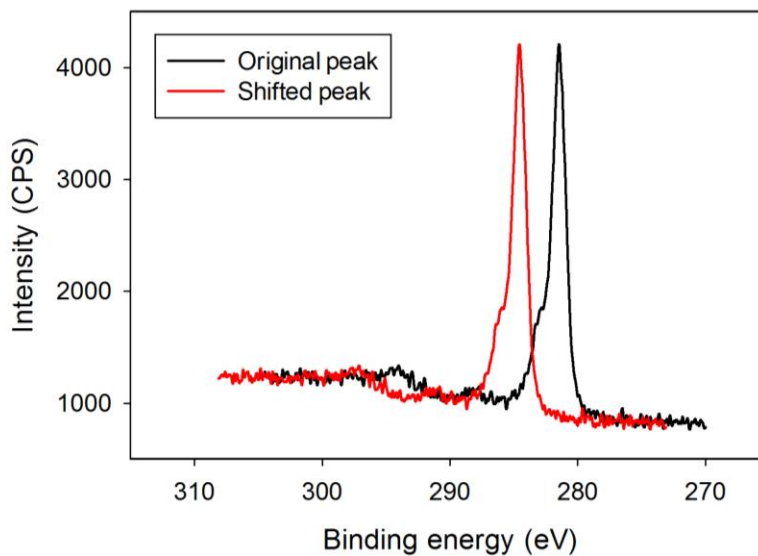


Figure 5. High-resolution C 1s XPS spectra.

Generally, the initial concentration of selenite in experiments is 0.11 mM, unless otherwise specified. The high initial concentration of selenite was considered in order to be able to obtain an adequate amount of solids for the purpose of solid analysis. All experiments were performed at room temperature. For irradiation experiments, samples taken at time zero represent the samples taken right after mixing, but before any irradiation.

5. RESULTS AND DISCUSSION

Batch screening test was performed to identify the best combination of reducing reagents and UV light source that achieves the highest removal efficiency within the shortest reaction time. In the kinetic experiments, three controls were prepared and tested: one includes selenite alone [blank (no reagent, no UV light)], one includes selenite with UV irradiation [reagent control (no reagent, but UV light)] and one includes selenite and the reducing reagent without irradiation [light control (no UV light, but reagent)].

5.1 Screening Experiments for Selenite (Se(IV)) in a Non-Buffered Solution

Combinations of four reducing reagents (dithionite, sulfite, sulfide and ferrous iron) and three different UV-light sources (UV-L, UV-M, and UV-B) each was evaluated for selenite removal. The solution pH was not buffered throughout these experiments. The molar ratio of reducing reagent dose to selenite concentration was fixed at 46 times. The initial pH of the solution with dithionite, sulfite, sulfide or ferrous iron were 5.30, 9.11, 11.97, and 7.50, respectively. The experimental conditions are shown in Table 3. The applied irradiation time was three hours. At regular intervals, around 10 mL of the sample was taken from the reactor, filtered using 0.45 μm membrane filter paper with a disposable syringe filter unit and analyzed for selenite concentration.

Figure 6 shows the results of the control experiments. The experimental results showed that Se concentration was constant with reaction time, regardless of the type of UV light source in the absence of reducing reagent. This indicates that selenite was not reduced by UV light in the absence of reducing reagent.

The results of screening experiments are presented in Figure 7 and show that dithionite-UV-L combination is the most efficient for Se(IV) removal among all combinations. Dithionite/UV-L ARP achieved almost complete Se(IV) removal approaching final concentration of 0.001 mM within 60 minutes reaction time. Selenite removal by ferrous iron was ranged between 70% and 80% regardless of the presence of UV or its light source. Sulfite and sulfide showed less than 5% Se(IV) removal in all cases.

Table 3. Experimental conditions of screening experiments without pH adjustment.

No.	^a Initial Se(IV) conc.	Reducing Reagent		UV irradiation		pH		Removal (%)
	(mM)	Type	Conc. (mM)	Type	Light intensity ($\mu\text{W}/\text{cm}^2$)	Initial	Final	
1	0.109	None	0	None	-	8.79	7.60	0.20
2	0.109	None	0	UV-L	4470	8.79	8.70	0.643
3	0.109	None	0	UV-B	547	8.79	8.70	6.70
4	0.109	None	0	UV-M	1661	8.79	8.70	2.11
5	0.0977	Dithionite	5	None	-	5.30	5.20	0.41
6	0.0977	Dithionite	5	UV-L	4702	5.30	3.40	100
7	0.0977	Dithionite	5	UV-B	640	5.30	3.90	46.0
8	0.0977	Dithionite	5	UV-M	2052	5.30	4.70	10.1
9	0.115	Sulfite	5	None	-	9.11	8.40	1.31
10	0.115	Sulfite	5	UV-L	4374	9.11	9.80	4.10
11	0.115	Sulfite	5	UV-B	210	9.11	8.70	3.49
12	0.115	Sulfite	5	UV-M	1910	9.11	8.70	1.90
13	0.0948	Sulfide	5	None	-	12.0	11.8	0.21
14	0.0948	Sulfide	5	UV-L	4515	12.0	11.8	1.37
15	0.0948	Sulfide	5	UV-B	555	12.0	11.8	3.10
16	0.0948	Sulfide	5	UV-M	1901	12.0	11.7	4.40
17	0.108	Fe ²⁺	5	None	-	7.50	3.30	69.4
18	0.108	Fe ²⁺	5	UV-L	4920	7.50	3.30	73.6
19	0.108	Fe ²⁺	5	UV-B	615	7.50	3.30	80.3
20	0.108	Fe ²⁺	5	UV-M	2074	7.50	3.30	87.2

^a Measured concentrations right after mixing Se(IV) and reducing reagent before starting UV irradiation.

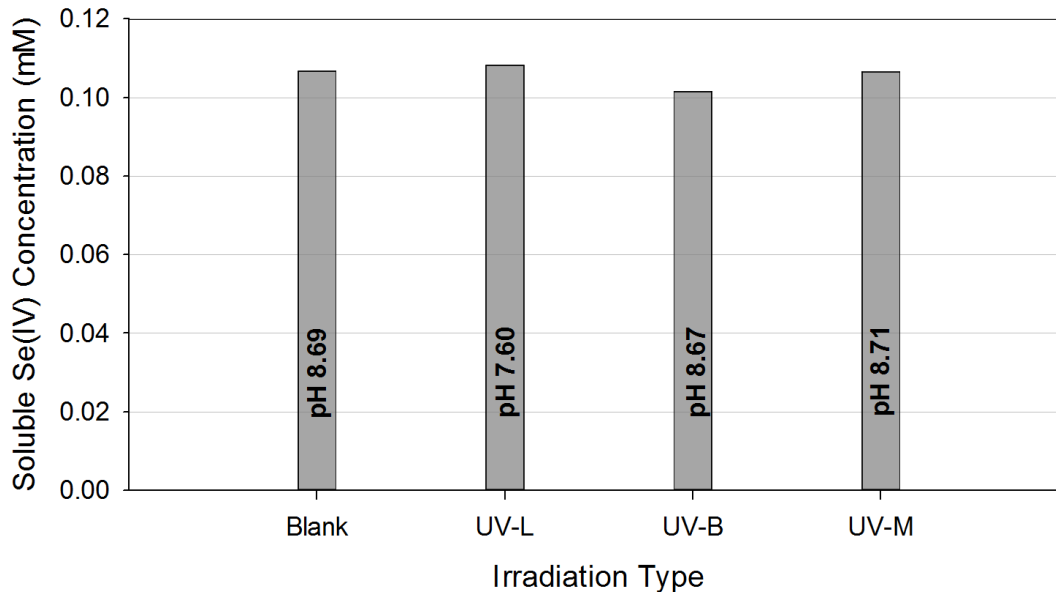


Figure 6. Effect of UV light on Se(IV) concentration. Experimental condition: $[\text{Se(IV)}]_0 = 0.11 \text{ mM}$, reaction time = 3 hrs, the solution pH was not buffered. The pH is the value measured at $t_{\text{irrad}} = 0 \text{ min}$.

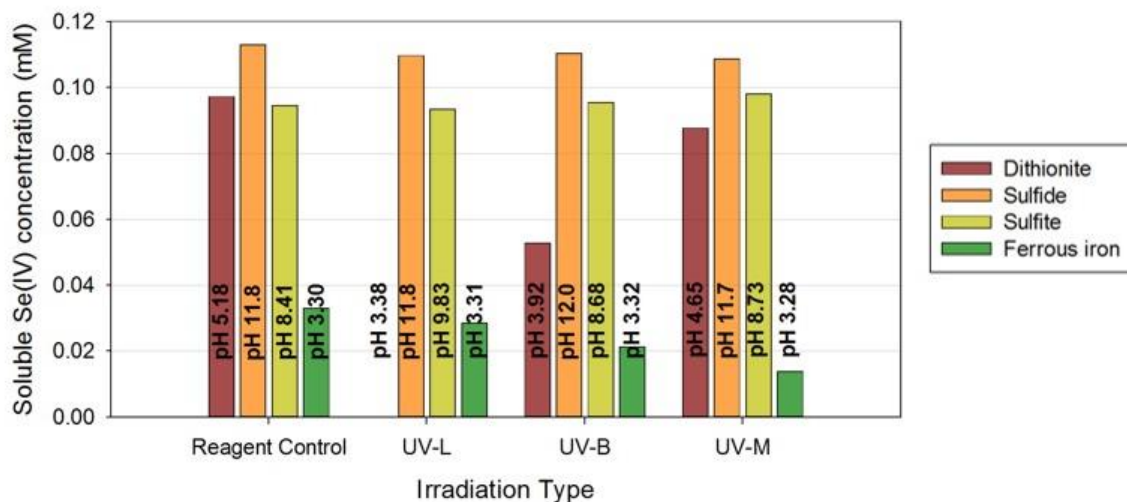
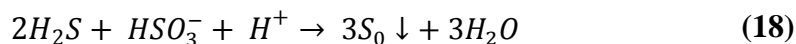


Figure 7. Results of screening experiments using different combinations of reducing reagents and UV-light sources in 3 hours. Experimental conditions: irradiation time = 3 hours, $[\text{Se(IV)}]_0 = 0.11 \text{ mM}$, reducing reagent dose = 5.0 mM, and the solution pH was not buffered.

Figure 8 shows visual images of the filters carrying the precipitated solids at different conditions. The dithionite-UV-L combination showed yellow-colored solids, and the of dithionite-UV-B combination showed orange-colored solids. This indicates that when dithionite decomposition species irradiated with different UV light sources, they can produce different radical species that react with selenite in different ways (Figure 8a).

Demopoulos and Geoffroy²⁰ have found that selenious acid species was effectively reduced in a weak acidic solution using sodium dithionite. They reported that at the pH values of < 1.7 and a dithionite 3 times above initial Se concentration, the precipitation reaction started immediately within less than a minute after the dithionite addition was completed. They obtained a precipitate composed of red amorphous selenium.²⁰ When ferrous iron was used, the color of the solids was orange-yellowish color regardless the presence of irradiation.

The solution color of the Se-dithionite mixture with UV irradiation for 4 hours is shown in Figure 9. The solution color became milky yellow. Geoffroy and Demopoulos²⁰ found a light yellow precipitate in Se-dithionite solution in several minutes after the start of the reaction and turned into a light yellow milky liquid, which was attributed to sulfur precipitates formed during the reaction of dithionite decompositions, Eq. (18). Also, they reported that the precipitates were very fine and stable.



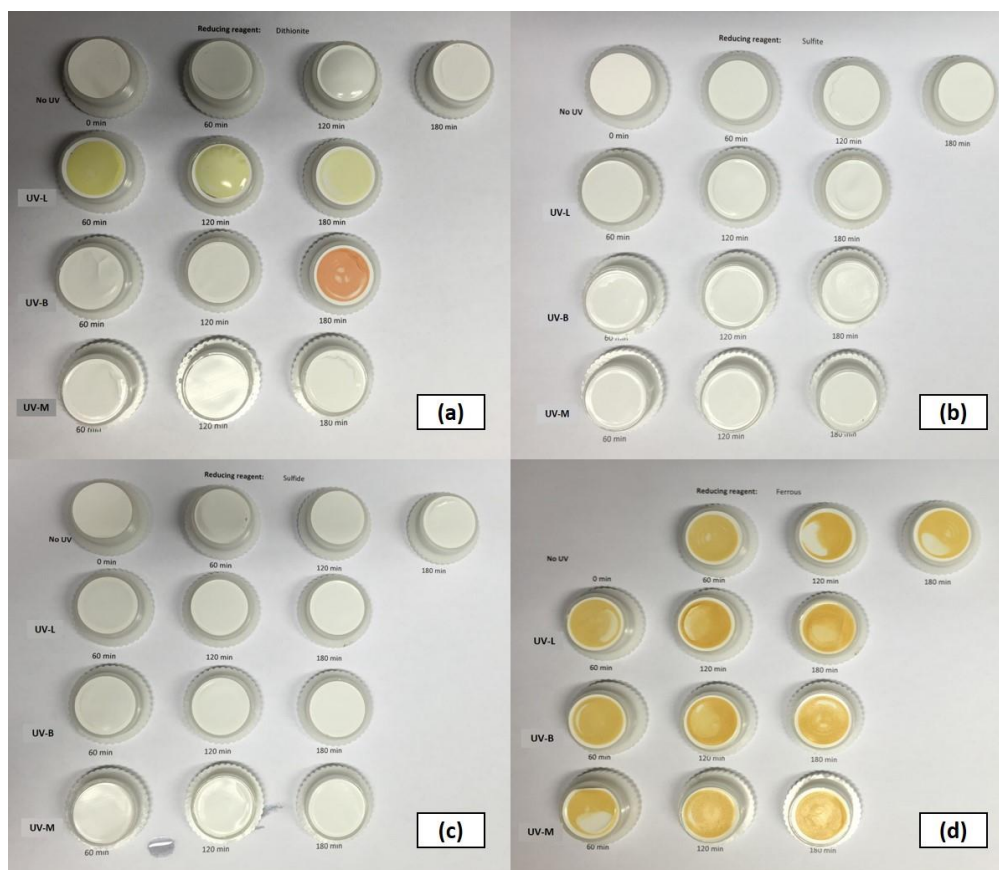


Figure 8. Visual representation of solids retained on the filter papers with dithionite (a), sulfite (b), sulfide (c), and ferrous iron (d).

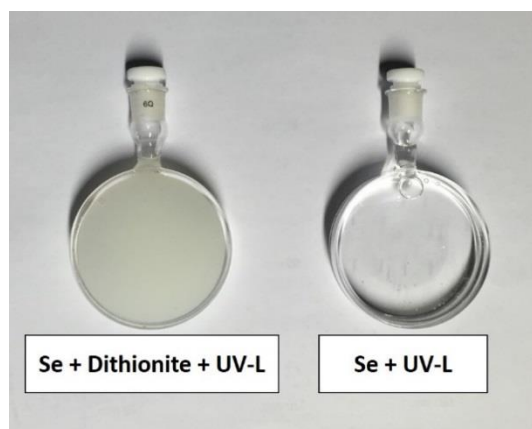


Figure 9. Solution color with and without dithionite after four hours of UV-L irradiation.

5.2 Screening Experiments for Selenite (Se(IV)) in a Buffered Solution

Screening experiments were conducted using reducing reagent solutions prepared in 10 mM phosphate solution to adjust pH at 7. The four reducing reagents and a mixture of dithionite and sulfite were combined with three different UV-light sources to evaluate selenite removal at neutral pH. The molar ratio of reducing reagent dose to initial selenite concentration was 46. The experimental conditions for this set of experiments are shown in Table 4. The applied UV irradiation time was four hours in the UV box.

As shown in Table 4 and Figure 10, there is no significant selenite removal in buffered solutions at pH 7, regardless of UV irradiation, except with sulfide. Selenite was completely removed by sulfide alone and by sulfide-UV-L combination. Selenite removal efficiencies of 97.2% and 99.0% by sulfide/UV-B and sulfide/UV-M, respectively (Figure 10). The solution pH was consistent during the reaction time.

Table 4. Experimental conditions of screening experiments in a buffered solutions.

No.	^a Initial Se(IV) conc.	Reducing Reagent		UV irradiation		pH		Removal (%)
	(mM)	Type	Conc. (mM)	Type	Light intensity ($\mu\text{W}/\text{cm}^2$)	Initial	Final	
1	0.108	Dithionite	5.0	None	-	6.87	6.77	0.00
2	0.0954	Dithionite	5.0	UV-L	4505	6.91	6.79	0.00
3	0.0935	Dithionite	5.0	UV-B	366	7.01	6.51	0.00
4	0.0935	Dithionite	5.0	UV-M	1194	7.01	6.52	3.85
5	0.107	Sulfide	5.0	None	-	7.04	7.52	100
6	0.0957	Sulfide	5.0	UV-L	5030	7.04	7.34	100
7	0.109	Sulfide	5.0	UV-B	342	7.13	7.10	97.2
8	0.109	Sulfide	5.0	UV-M	1204	7.13	7.04	99.0
9	0.0975	Sulfite	5.0	None	-	7.49	7.46	4.10
10	0.109	Sulfite	5.0	UV-L	4688	7.51	7.48	6.24
11	0.118	Sulfite	5.0	UV-B	365	7.12	6.80	5.16
12	0.118	Sulfite	5.0	UV-M	1165	7.12	6.79	2.70
13	0.108	Fe ²⁺	5.0	None	-	7.02	6.89	7.14
14	0.111	Fe ²⁺	5.0	UV-L	4858	6.94	6.50	10.6
15	0.0993	Fe ²⁺	5.0	UV-B	365	6.92	6.65	5.64
16	0.0993	Fe ²⁺	5.0	UV-M	1165	6.92	6.57	8.36
17	0.111	Sulfite/Dithionite	2.5/2.5	None	-	6.99	7.01	2.44
18	0.116	Sulfite/Dithionite	2.5/2.5	UV-L	4932	6.99	6.63	5.44
19	0.113	Sulfite/Dithionite	2.5/2.5	UV-B	406	7.12	6.69	5.24
20	0.113	Sulfite/Dithionite	2.5/2.5	UV-M	1252	7.12	6.68	6.75

^a Measured concentrations right after mixing Se(IV) and reducing reagent before starting UV irradiation.

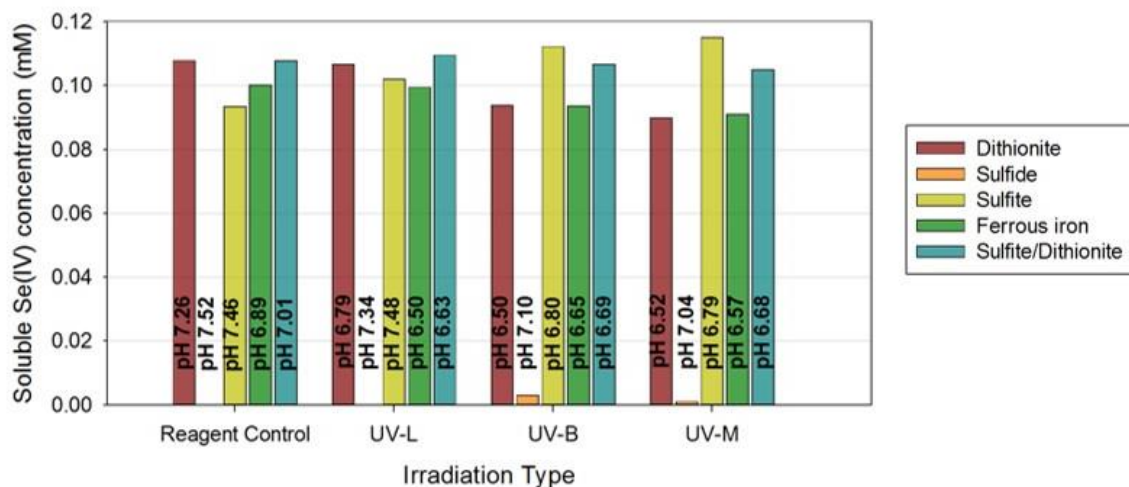


Figure 10. Results of screening experiments in pH 7 buffered solutions after 4 hours of irradiation. Experimental conditions: $[\text{Se(IV)}]_0 = 0.11 \text{ mM}$, reducing reagent dose = 5.0 mM.

In Figure 11, the solution (selenite-sulfide) color was changed from yellow to milky yellow color (Figure 11a) with UV-L irradiation. On the other hand, the solution color did not change over the reaction time of four hours in the absence of UV irradiation (Figure 11b). In the case of UV-B and UV-M irradiation, there was no noticeable change in the solution color.

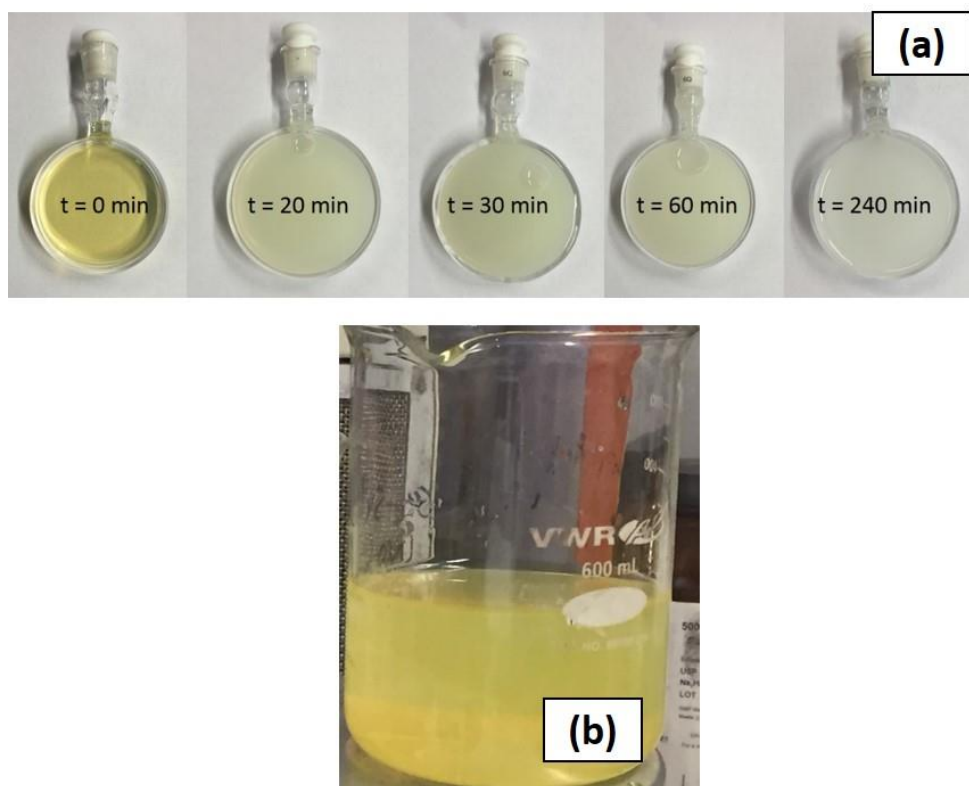


Figure 11. The color changes of selenite-sulfide solution with UV-L irradiation (a) and without UV-L irradiation (b) in 4 hours. Experimental conditions: $[\text{Se(IV)}]_0 = 0.11 \text{ mM}$, light intensity = $4565 \mu\text{W}/\text{cm}^2$, reducing reagent concentration = 5.0 mM , and the solution pH was buffered at pH 7.

Based on the screening tests, it can be concluded that sulfide is the most efficient reducing agent for Se(IV) removal from water at neutral pH. UV light irradiation did not affect Se(IV) removal efficiency, but it affected the color of the solids formed which indicates that the UV light irradiation resulted in the production of solids phases that could be different than those formed with sulfide alone. Therefore, sulfide-UV combination was chosen for further investigation to evaluate effects of experimental conditions, to understand reaction mechanisms, and to characterize the precipitated solids.

5.3 Effects of Experimental Conditions on Selenite Removal by Sulfide

In the presence of sulfide, selenite concentration rapidly decreased in the first few minutes at neutral pH, regardless of the presence or absence of UV light. Geoffroy and Demopoulos²¹ reported that the precipitation reaction between selenious acid and sulfide started immediately upon mixing of the two compounds, and the reaction was completed in less than 10 minutes.

5.3.1 Effect of pH

Batch experiments were conducted to investigate the effect of pH on selenite removal in sulfide solution at three different pH values (pH 4, 7 and 11) in the absence and the presence of UV light. The molar ratio of reducing reagent dose to selenite concentration was 46, and the total reaction time was 30 minutes. The conditions of the experiments that were conducted are shown in Table 5.

Table 5. Experimental conditions for investigating the effect of pH.

No.	^a Initial Se(IV) Conc.	Reducing Reagent Conc.	UV irradiation		pH		Removal
	(mM)	(mM)	Type	Light intensity ($\mu\text{W}/\text{cm}^2$)	Initial	Final	(%)
1	0.0944	0.00	None	-	4.22	4.21	1.27
2	0.0947	0.00	UV-L	6442	4.26	4.37	2.32
3	0.0815	5.00	None	-	3.42	3.66	100
4	0.0966	5.00	UV-L	6282	4.06	4.42	100
5	0.0976	0.00	None	-	7.04	7.06	0.922
6	0.0968	0.00	UV-L	6520	7.07	7.06	1.76
7	0.104	5.00	None	-	7.06	7.12	98.9
8	0.104	5.00	UV-L	5654	6.88	7.12	98.2
9	0.0953	0.00	None	-	11.0	11.0	0.210
10	0.0958	0.00	UV-L	6355	10.98	10.96	1.15
11	0.0955	5.00	None	-	11.0	11.1	4.50
12	0.0980	5.00	UV-L	6535	10.9	11.1	2.55

^a Measured concentrations right after mixing Se(IV) and reducing reagent before starting UV irradiation.

Figure 12 shows no selenite removal at pH 11 and no solids were observed on the filter paper when the solution was filtered. However, selenite concentration was completely and rapidly removed within less than 5 minutes at both pH 4 and pH 7 regardless of the presence of UV irradiation. According to the acid-base equilibrium of sulfide solution, the dominant sulfide species at pH 4 is $\text{H}_2\text{S}_{(\text{aq})}$ and both $\text{H}_2\text{S}_{(\text{aq})}$ and HS^- co-exist at pH 7 while HS^- and S^{2-} species coexist at pH 11 as was shown earlier in Figure 2. The fact that HS^- is present with appreciable concentration at pH 7 and pH 11 and no

selenite removal was obtained at pH 11, this implies that neither HS^- nor S^{2-} reacted with Se(IV) to form Se-containing solids. This also indicates that the sulfide species that reacted with and precipitated Se(IV) is $\text{H}_2\text{S}_{(\text{aq})}$. The reaction mechanisms of Se(IV) removal with sulfide will be discussed later in subsequent sections.

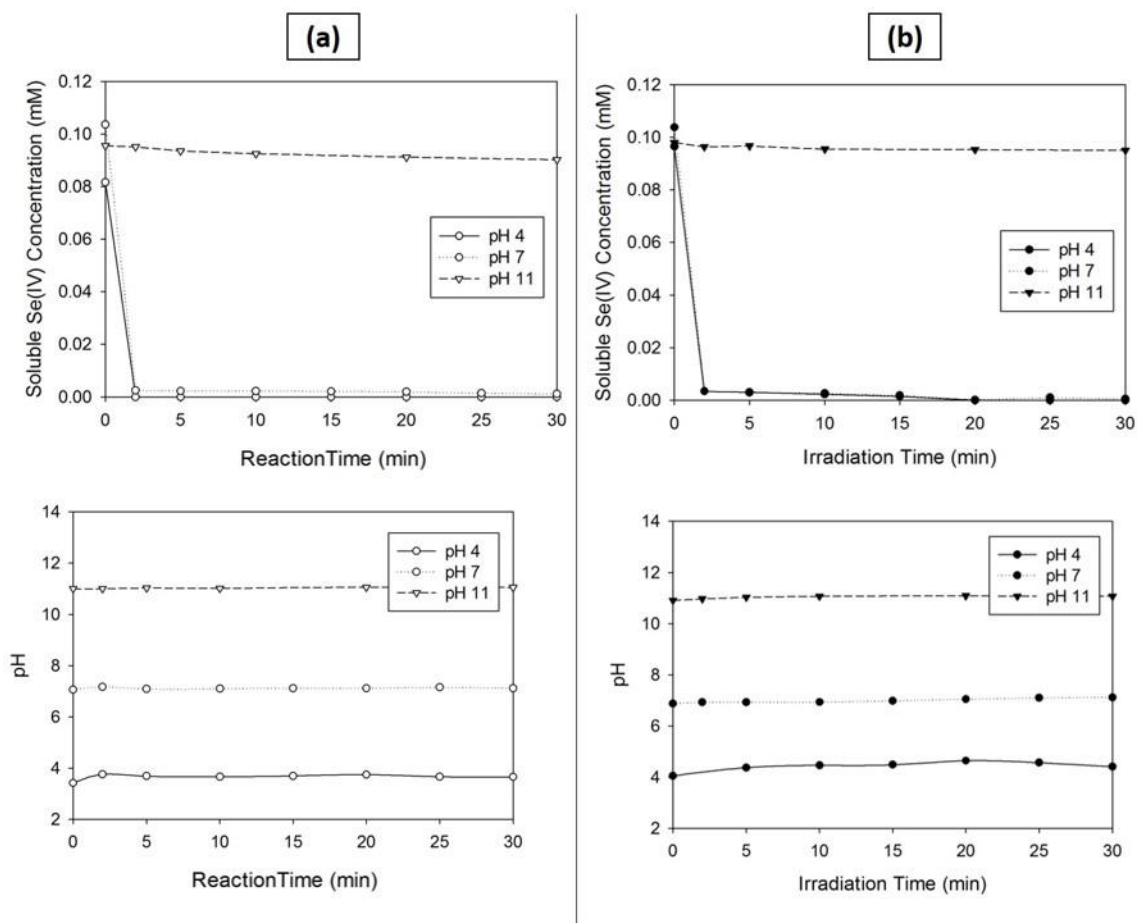


Figure 12. Effect of pH on Se(IV) removal by sulfide and pH change with time (a) sulfide, no UV and (b) sulfide and UV-L). Experimental conditions: $[\text{Se(IV)}]_0 = 0.11 \text{ mM}$, light intensity = $6298 \mu\text{W}/\text{cm}^2$.

The SEM and EDS results of the version filters are shown in Figure 13. The filter papers have 0.2 μm pores, and it is made out of polyethersulfone. EDS results showed the presence of sulfur. As of selenite-sulfur containing samples, selenium absorption peaks were at 1.37 keV (SeL α), 11.22 keV (SeK α) and 12.9 keV (SeK β) approximately, where the last peak was relatively low compared to the other two peaks. As for S absorption peak was at 2.31 keV (S K α).

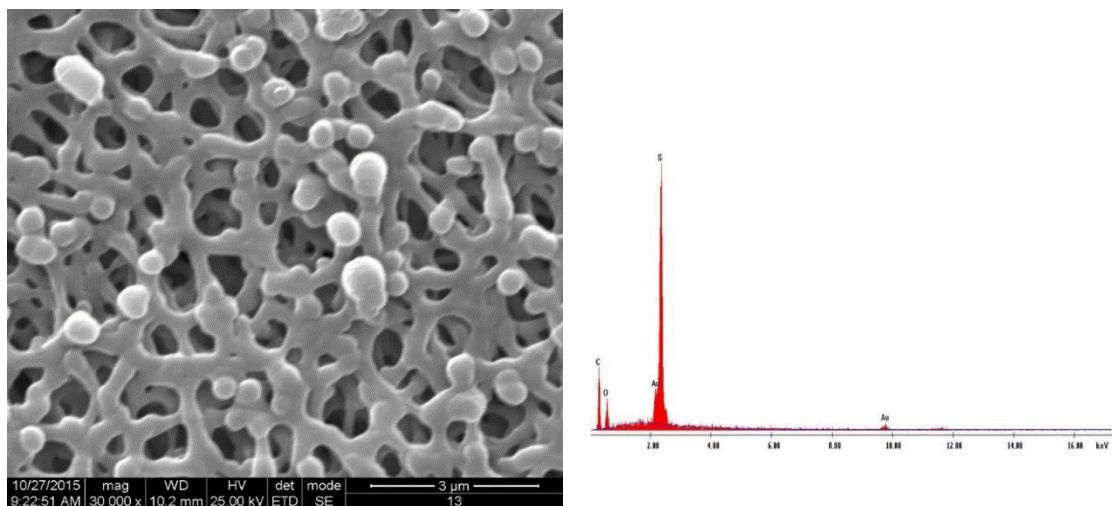


Figure 13. SEM/EDS analysis of a filter membrane, which does not contain solids.

SEM-EDS analysis of precipitated solids was performed, and the ratio between Se and S present in the particles were obtained to understand the nature of solids precipitated. Figure 14 shows that UV irradiation affected the morphology of the solids regardless of the pH of the solution. In the presence of UV light, it is likely that precipitates became more irregular aggregates at both pH 4 and pH 7 (Figure 14), and it was more noticeable

at pH 4 compared to that at pH 7. In the absence of UV irradiation, the precipitates formed larger agglomerates at pH 7 than at pH 4. At pH 4, UV light enhanced the formation of larger irregular aggregates with S/Se wt% ratio of 0.49 in the absence of UV. At pH 7 in the presence of UV, agglomerated irregular solids with S/Se wt% ratio of 0.32 were obtained by EDAX. The low S/Se ratios in these two cases could be attributed to the formation of elemental selenium and/or solids containing both S and Se with high Se stoichiometric ratio in the solids. On the other hand, particles with S/Se wt% ratio around 5 were formed at pH 4 with UV and at pH 7 in the absence of UV. This could be due to the formation of elemental sulfur and/or solids containing both S and Se with high S stoichiometric ratio. Geoffroy and Demopoulos²¹ reported that orthorhombic sulfur was formed from sulfide reaction with Se(IV) reaction, which supports the hypothesis that elemental sulfur is formed with S/Se wt% in EDAX of 5. According to published data,^{21,68} large agglomerates, irregular and amorphous precipitates is likely to be associated with elemental sulfur and Se-S precipitates, whereas, elemental selenium shows more regular and crystallized structure (layered, hexagonal or rectangular and long plate solid). As depicted from the data below, amorphous solids were associated with the high intensity of sulfur, hence, higher S/Se (wt% in EDAX).

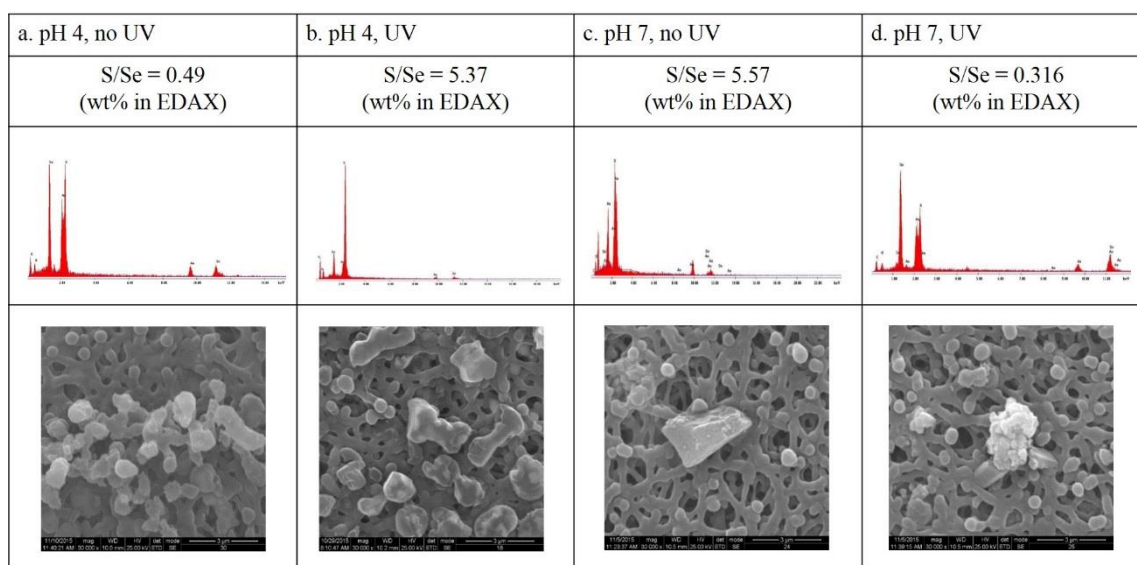
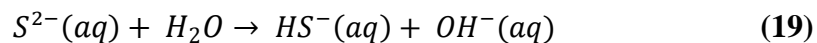


Figure 14. SEM/EDS results on solids formed in Se-S²⁻ solution at: (a) pH 4 without UV, (b) pH 4 with UV, (c) pH 7 without UV, and (d) pH 7 with UV. Experimental conditions: [Se(IV)]₀ = 0.11 mM, [S²⁻]₀ = 5 mM, TUV PL-L lamp, t = 30 min.

To study the characteristics of sulfide species in the solution, the UV absorbance of Na₂S solution was measured at different pH values. Some solutions were irradiated by UV light to investigate photolysis reaction of sulfide, and the results are shown in Figure 15. At pH 3.36, the absorbance spectrum will be due to the presence of H₂S, which was similar to the results obtained by Guenther et al.⁶⁹ and Linkous et al.⁴⁸ Figure 15 shows an absorbance peak at 230 nm, and the intensity increased with increasing the pH value. Therefore, the peak at 230 nm could be attributed to the presence of HS⁻ or S²⁻.

According to Guenther et al.⁶⁹ the absorbance peak at 230 nm corresponds to HS⁻ and hence, it is the species responsible for the UV absorbance in the sulfide solution. Based on Figure 2, the concentration of HS⁻ decreases as pH increases above pH 11. However, the peak at pH 12.5, where dominant species is S²⁻, has a higher intensity than the peaks where HS⁻ is the dominant species. Linkous et al.⁴⁸ reported that Na₂S crystals dissociate,

and the solutions contain bisulfide ion (HS^-), rather than sulfide ion (S^{2-}) due to conjugate base hydrolysis. According to Eq. (19), which could explain the increase in absorbance at 230 nm with pH increase.⁴⁸



Guenther et al.⁶⁹ reported that due to the formation of polysulfides at high pH, the absorption spectrum might be complicated, and the absorption at 230 nm might not only contribute to the presence of HS^- merely.

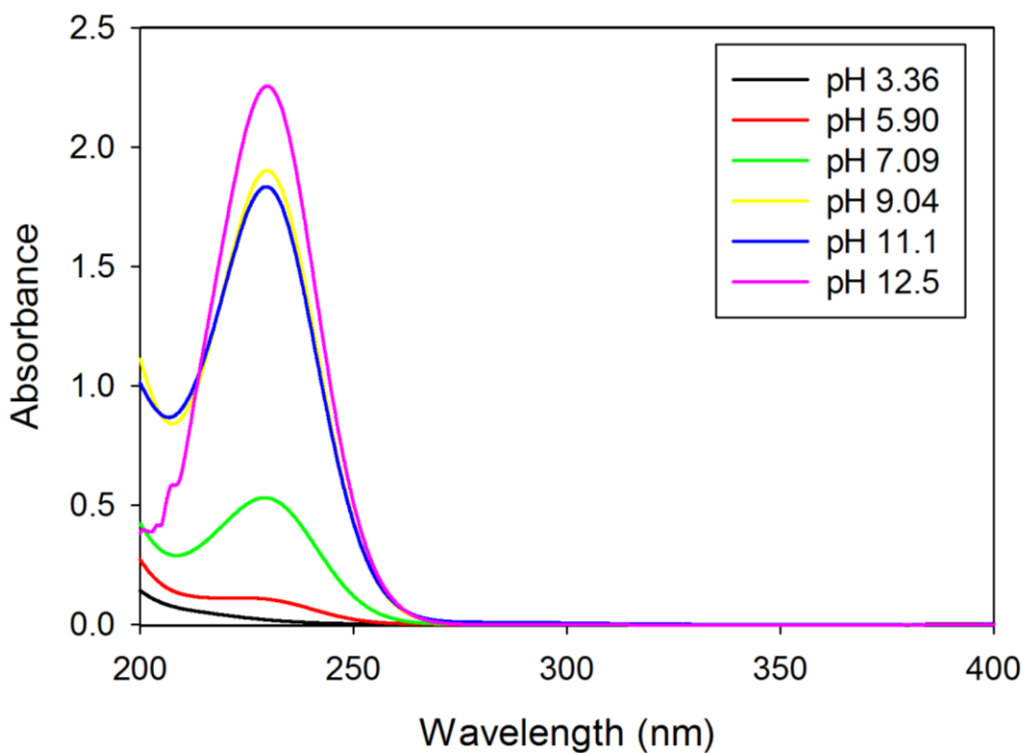


Figure 15. Absorption spectra of sulfide solution prepared in 10 mM phosphate buffer at different pH values with no UV light irradiation. Conditions: $[\text{S}^{2-}]_0 = 0.312$ mM and anoxic condition.

The only observed peak in the range of pH values shown in Figure 15 was at 230 nm. The percentage of HS^- at pH values 3.36, 5.9, 7.09, 9.04, 11.1 and 12.5 calculated by Visual MINTEQ 3.1⁷⁰ at 25 °C are 0.022%, 7.07%, 54.3%, 99.1%, 99.99% and 99.998%, respectively. This proves that at pH values ranging above 9, S^{2-} species dissociates to HS^- which is consistent with the absorbance spectra at 230 nm.

Figure 16 through Figure 19, shows the absorption spectra of sulfide solution irradiated by UV-L lamp. At pH 4, hydrogen sulfide (H_2S) is the dominant species (99.9%⁷⁰). At pH 7, there is almost equal distribution between H_2S and HS^- (45.7% and 54.3% respectively⁷⁰). At pH 9, hydrogen sulfide ion (HS^-) will be dominant species (99.1%⁷⁰). At pH 11, 99.99% of sulfide species exist as HS^- .

The absorption spectra of sulfide solution at pH 4 as shown in Figure 16 did not change with UV-L irradiation over time, and it is similar to the spectrum at pH 3.36 without UV irradiation shown in, Figure 15 with an approximate absorption of 0.214 at 230 nm. This indicates that H_2S species does not undergo photolysis upon irradiation.

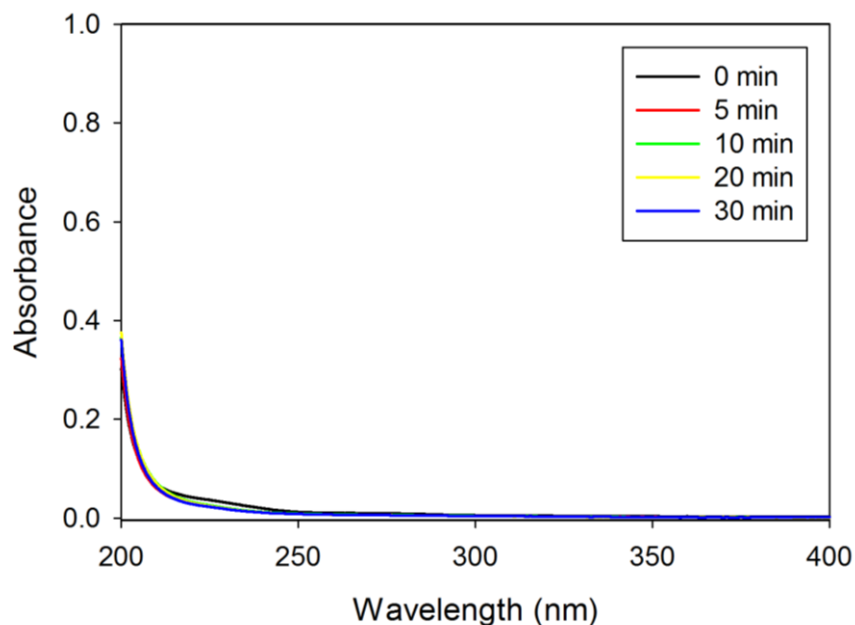
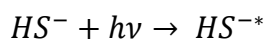
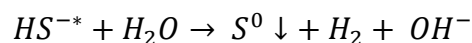
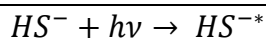
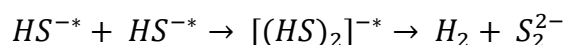


Figure 16. UV spectra of sulfide solution prepared in anoxic conditions at pH 4 with UV-L irradiation over time. Conditions: $[S^{2-}]_0 = 0.312$ mM, light intensity = $4900 \mu\text{W}/\text{cm}^2$, and anoxic condition.

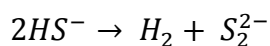
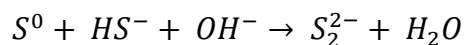
Figure 17 through Figure 19 show decrease in the peak intensity at 230 nm with increasing UV-L irradiation time and a broad peak appears at a higher wavelength which was obvious at pH 7. The broad peak at high wavelengths matches the results reported by Linkous et al.⁴⁸ of a NaHS solution after 273 min photolysis and by Dzhabiev and Tarasov⁴⁹ and Hara et al.⁷¹ for Na_2S solutions undergone photolysis. This broad peak is similar to the peak obtained for S_2^{2-} reported by Linkous et al.⁴⁸ with a slight shift. This indicates that upon irradiation of sulfide solution with UV-L at pH 7, disulfide (and polysulfides) are produced based on the following reaction schemes:⁴⁸



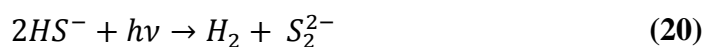
(Scheme 1)



(Scheme 2)



Linkous et al.⁴⁸, Hara et al.⁷¹, and Dzhabiev and Tarasov⁴⁹ reported that upon the irradiation of sulfide solution, hydrogen gas is produced, and its production increases with the increase of light intensity and with the increase of sulfide concentration, which may explain the bubbles observed in the quartz cell when sulfide solution was irradiated. When HS^- is the dominant species in sulfide solution, reaction presented by Eq. (20) takes place and because there is almost equal distribution between H_2S and HS^- at pH 7, the reaction in Eq. (9) also takes place, where the reaction shifts to HS^- again due to the presence of H_2S that serves as an acid equivalent.⁴⁸



In the case of sulfide absorbance at pH 9 and pH 11 (Figure 18 and Figure 19), broad spectra and a small peak at around 305 nm appeared. According to Hara et al.⁷¹, an absorption band appears at 317 nm upon the irradiation of the sulfide solution using a 1000 W Hg high-pressure lamp. Based on the reported data by Hara et al.⁷¹ and Linkous et al.⁴⁸, the broadband peak can correspond to $S_2O_4^{2-}$ or S_2^{2-} .

Absorbance results indicate that sulfide can be irradiated with UV light and converted to other sulfur species with time. The production of these species and their reactions in the S-Se system could cause the change in solid color and morphology that were observed when the solution was irradiated.

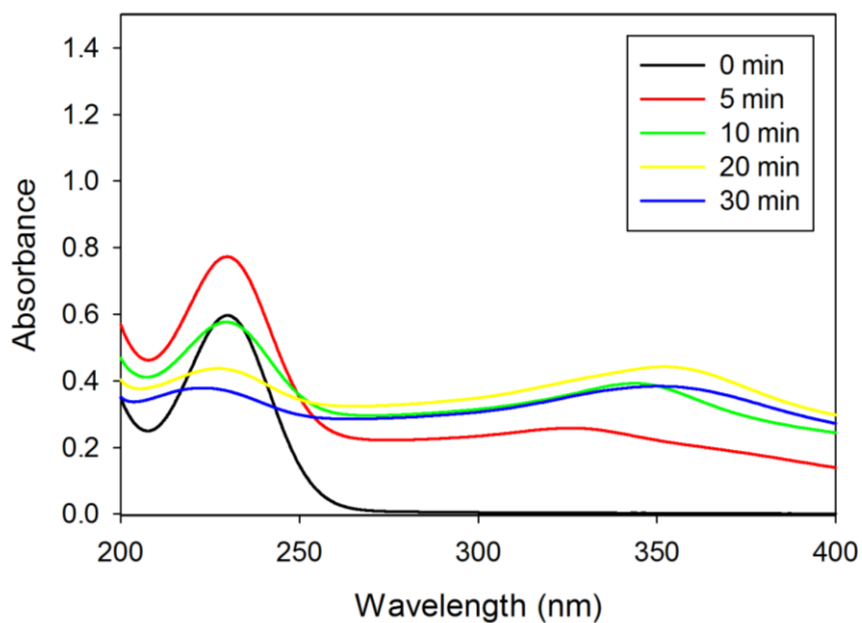


Figure 17. UV spectra of sulfide solution prepared in anoxic conditions at pH 7 with UV-L irradiation over time. Conditions: $[S^{2-}]_0 = 0.312$ mM, light intensity = $4900 \mu\text{W}/\text{cm}^2$.

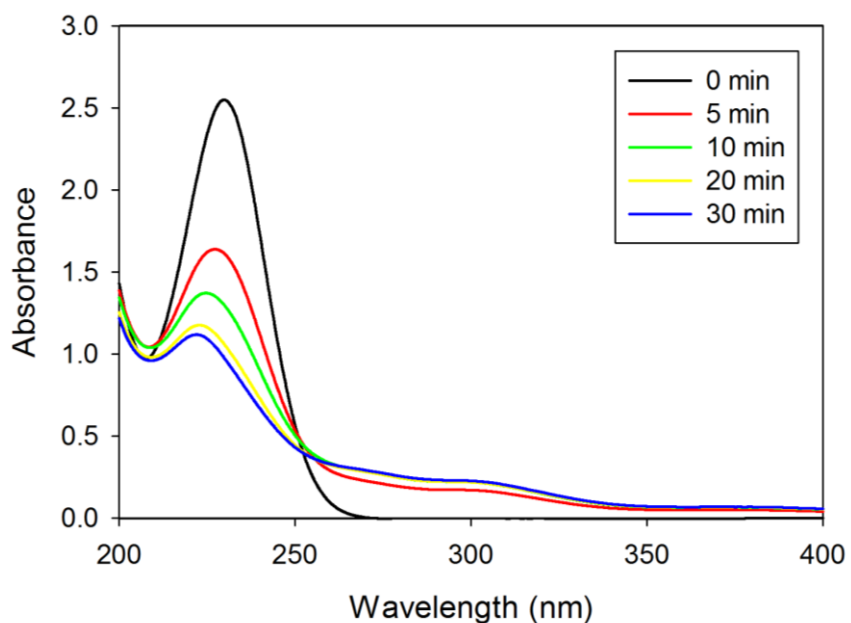


Figure 18. UV spectra of sulfide solution prepared in anoxic conditions at pH 9 with UV-L irradiation over time. Conditions: $[S^{2-}]_0 = 0.312$ mM, and light intensity = $4900 \mu\text{W}/\text{cm}^2$.

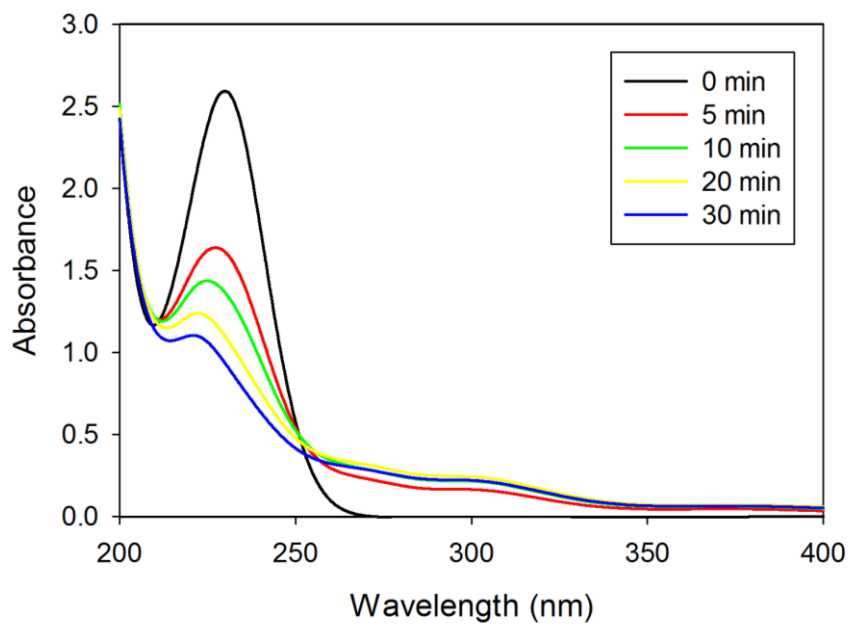


Figure 19. UV spectra of sulfide solution prepared in anoxic conditions at pH 11 with UV-L irradiation over time. Conditions: $[S^{2-}]_0 = 0.312$ mM, light intensity = $4900 \mu\text{W}/\text{cm}^2$.

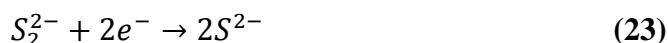
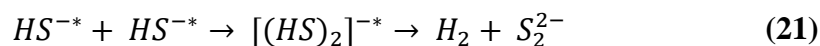
In order to better understand the mechanisms or reactions and precipitated solids composition in Se-S system, XPS analysis was conducted on precipitates formed during Se(IV) reduction experiments. The XPS spectra of solids formed in a solution including Se(IV) and S(-II) were obtained for different pH values, sulfide doses, UV irradiation and reaction time. In order to obtain the oxidation status of the surface of solids, narrow scan spectra for O 1s, S 2p, and Se 3d were acquired. The experimental conditions of the samples investigated by XPS are presented in Table S6. Information about O 1s, S 2p, and Se 3d XPS spectra of solid including binding energy (BE), full width at half maximum (FWHM), and area for peaks of the analyzed samples are provided in Table A7.

Binding energies from the literature are shown in Table A1 through Table A5 for O 1s, S 2p, and Se 3d. Binding energies of S 2p XPS spectra include sulfides (S^{2-} , S_2^{2-}), polysulfides (S_n^{2-}), elemental sulfur, sulfite, bisulfite, sulfate, and sulfur-containing oxyanions.

All the obtained Se 3d XPS peaks lie in the range of binding energies of elemental selenium. Binding energies of elemental Se(0) were found in the range of 54.64 eV - 57.5 eV (refer to Table A5) according to NIST XPS database.⁷² Naveau et al.⁷³ have demonstrated that elemental Se is observed between 54.9 eV and 56.3 eV. Han et al.⁷ reported that reduced species of selenium produce spectra with peaks in the range of 53.7 eV – 56.3 eV. Most of the obtained Se 3d spectra has one peak with a split, and the doublets were in the range of 54.5 – 56.5 eV, where this peak was attributed to elemental selenium.

S 2p XPS obtained peaks lies in the binding energies range of 156 eV - 172 eV. S 2p spectra were fitted with fixed doublets of S 2p_{1/2} and S 2p_{3/2} spin orbitals with binding

energy separation of 1.2 eV, and 2:1 area ratio. Sulfur will be present in various forms due to disproportionation and species such as elemental sulfur (S_0), sulfide (S^{2-}), disulfide (S_2^{2-}), polysulfides (S_n^{2-}), sulfate (SO_4^{2-}), tetrathionate ($S_4O_6^{2-}$), dithionate ($S_2O_6^{2-}$), and thiosulfate ($S_2O_3^{2-}$) could be present. Elemental sulfur is assigned to spectra in the range in the range of 162.9 eV - 164.8 eV. As mentioned previously, Na_2S solution at neutral pH is found in the form of H_2S and HS^- . Additionally, polysulfide ions and sulfide ions can be present during photolysis of HS^- ion according to Eq. (2) and the following equations.



Upon the reduction of selenium, elemental sulfur is formed along with sulfide photochemical decomposition sulfur species such as disulfide ions and polysulfide ions. When selenium reacts with sulfide, it is anticipated that selenium will be reduced, and sulfide will be oxidized. Smart et al.⁷⁴ reported that the binding energy of oxidized sulfur species are as follow: S^{2-} (160.1–161.2 eV), S_2^{2-} (162.1–162.6 eV), S_n^{2-} (161.9–163.2 eV), and S_n^0 (163.0–164.2 eV).

O 1S XPS spectra were found between 530 eV – 534 eV, with two major peaks at 531.4 eV and 533.1 eV. Generally, O 1s peaks are associated with metal oxides, hydroxyl and water have binding energies in the range of 529.5 eV - 533 eV.⁷ O 1s associated with water shows a peak at binding energy in the range of 532.80 eV - 538 eV according to NIST XPS database.⁷²

The effect of pH on the species involved in the solid formation during the experiments was investigated in the presence and the absence of UV-L light. O 1s, S 2p and Se 3d XPS de-convolution spectra of the solid formed are shown in Figure 20 and Figure 21 in the presence and absence of UV, respectively. In the presence of UV-L light (Figure 20) and at pH 4, there are two major peaks centered at 531.6 eV and 533.2 eV which were attributed to HSO_3^- or $\text{S}_2\text{O}_3^{2-}$, and molecular H_2O respectively. However, at pH 7, there are five peaks doublets for a better fitting and simultaneously, the peak at 531.6 eV became asymmetric. The five peaks are located at located at 530.3 eV, 530.9 eV, 531.3 eV, 532.5 eV, and 533 eV. The results of O 1s XPS spectra indicates the production of sulfur-containing anions, which are detected at low binding energies, along with structural hydroxyl anions.

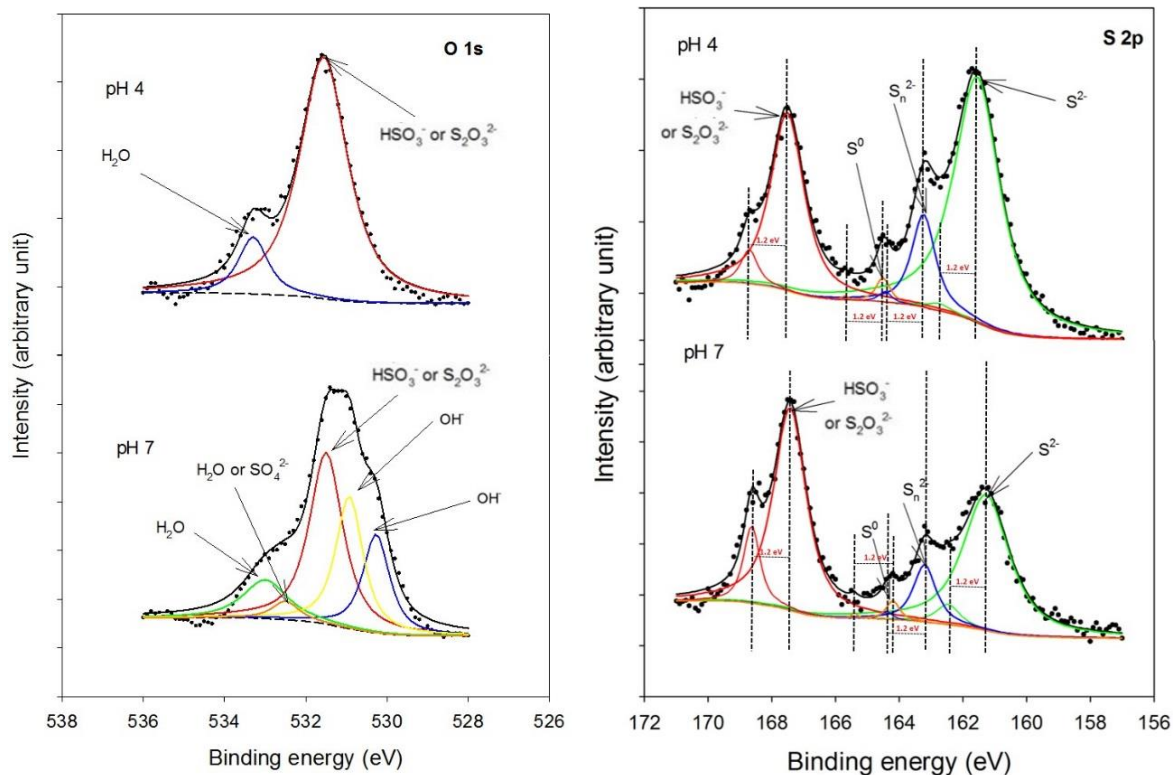


Figure 20. High-resolution O 1s, S 2p, and Se 3d XPS de-convolution spectra of the solids formed in Se(IV)-S(-II) solution in the presence of UV- L at pH 4 and pH 7. Experiment conditions: $[\text{Se(IV)}]_0 = 0.11 \text{ mM}$, $[\text{S}^{2-}]_0 = 5.0 \text{ mM}$, $t = 10 \text{ min}$ at pH 4; $t = 90 \text{ min}$ at pH 7.

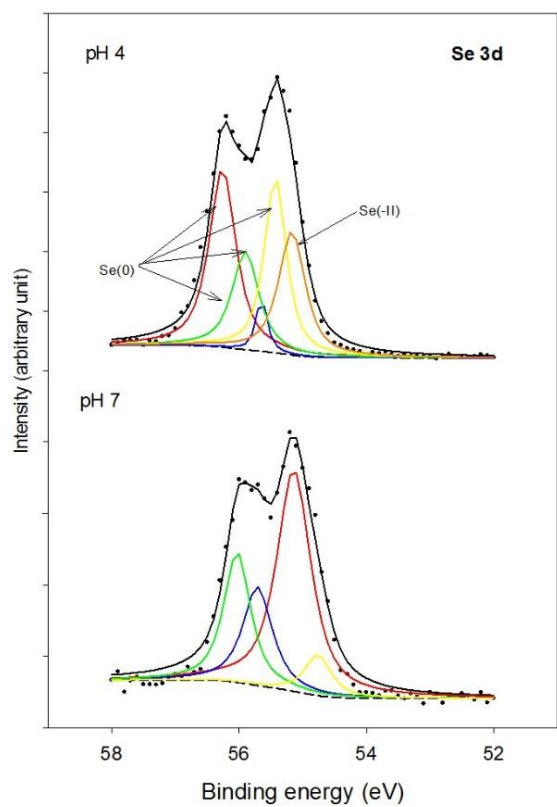


Figure 20. Continued

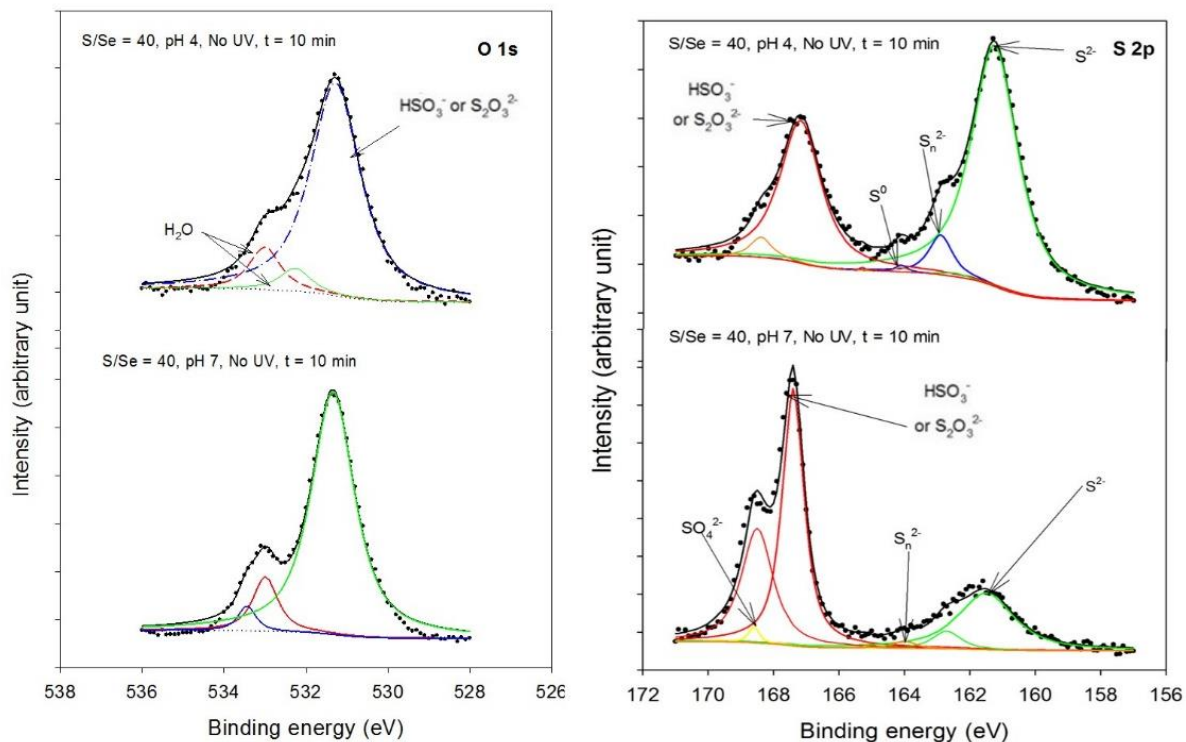


Figure 21. High resolution O 1s, S 2p and Se 3d XPS de-convolution spectra of solid formed in Se(IV)-S(-II) solution in the absence of UV- L after 10 min reaction time. Experiment conditions: $[\text{Se(IV)}]_0 = 0.11 \text{ mM}$, $[\text{S}^{2-}]_0 = 5.0 \text{ mM}$.

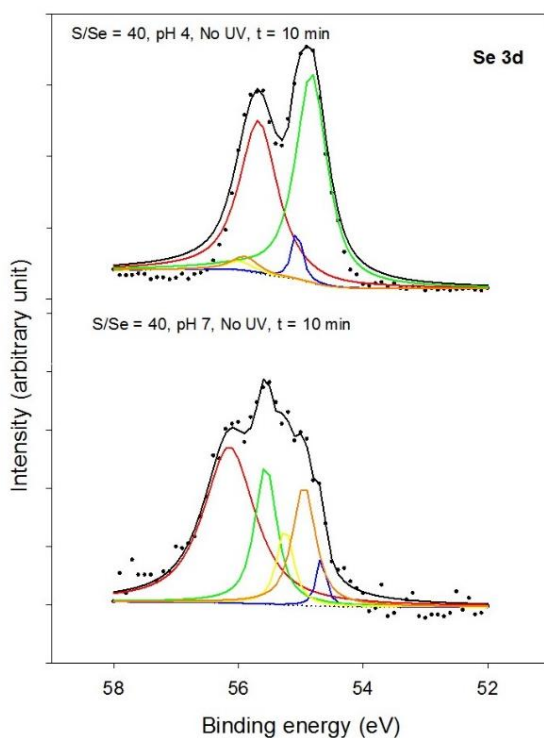


Figure 21. Continued

For S 2p XPS spectra, there are two major areas. At lower binding energies, there are mainly three peaks centered at 161.5 eV, 162.7 eV and 163.3 eV with doublets spin orbitals with 1.2 energy separation as shown in Figure 20, which corresponds to S^{2-} , S_n^{2-} , and S_0 respectively. The peaks at higher binding energies (166 eV – 170 eV) correspond to sulfur-containing oxyanions. The presence of oxyanions is strong evidence for sulfide oxidation in the solutions, which supports the fact that selenite is reduced in the presence and sulfide was oxidized. In this region, there are two constituent peaks, centered at 167.5 eV and 168.7 eV, which may contribute to one species with two different spin orbitals as the energy gap is 1.2 ($S_2O_3^{2-}$ or HSO_3^-). Based on published data, sulfur-containing oxyanions have similar binding energies. Hence, it is difficult to identify the peaks. The

information of binding energies of sulfite, sulfate, bisulfite, and sulfur-containing oxyanions from the published data are tabulated in Table A4. The peak at 1.67.5 eV lies within the range of tetrathionate ($S_4O_6^{2-}$), along with bisulfite (HSO_3^-) and thiosulfate ($S_2O_3^{2-}$). Han et al.⁷ reported that tetrathionate lies in the range of 167.2 eV – 167.6 eV. Also, multiple reports in the literature (Table S4) reported that thiosulfate and bisulfite have binding energy at around 167.7 eV. However, assignment of the peaks of higher binding energy in S 2p spectra was confirmed with the peaks from O 1s spectra. Rickett and Payer⁷⁵ and Lindberg et al.⁷⁶ reported that the peak at around 167.4 eV and 167.2 eV corresponds to bisulfite and thiosulfate, respectively. Hence, tetrathionate was excluded.

When comparing the two energy bands in S 2p spectra, the area percentage of the peaks attributed to S^{2-} were 55.5% and 41.7 % at pH 4 and pH 7, respectively. These results can indicate the presence of sulfur in Se-S precipitates and its formation is favorable at low pH. This observation is supported by SEM/EDS analysis results that show more amorphous agglomerated particles at pH 4. Overall, O 1s and S 2p did not show any shift in binding energies by varying pH. However, Se 3d shifted to higher energy at pH 4 relative to spectra obtained at pH 7. The peaks centered at 55.1 eV and 55.9 eV at pH 7 shifted to 55.4 eV and 56.2 eV at pH 4, respectively. This indicates a change in oxidation state of Se by varying pH from 7 to 4. Reduced Se species (e.g. Se(-I) or Se(-II)) may be oxidized to elemental selenium at low pH.

In the absence of UV-L light, there was no change in the species involving oxygen as it can be revealed from O 1s XPS de-convolution spectra (Figure 21). There are two

constituent peaks centered at 531.6 eV and 533.2 eV which contributes to HSO_3^- or $\text{S}_2\text{O}_3^{2-}$, and molecular H_2O respectively; similar to the case with UV irradiation.

For S 2p XPS spectra, there are two major areas. At pH 4 and at lower binding energies, there are mainly three peaks centered at 161.25 eV, 162.9 eV, and 164 eV which correspond to S^{2-} , S_n^{2-} , and S_0 respectively. The peaks at higher binding energies (166 eV – 170 eV) show two constituent doublets centered at 167.2 eV and 168.6 eV, which may contribute to $\text{S}_2\text{O}_3^{2-}$ or HSO_3^- respectively. Nevertheless, at pH 7, there are only two doublets at low binding energy (161.5 eV and 164 eV), which corresponds to S^{2-} and S_0 , respectively. At higher binding energies, relatively the same peaks as in pH 4 were obtained in addition to a small singlet peak at 168.6 eV, which corresponds to SO_4^{2-} according to binding energies reported in literature. This indicates that the peak at 532 eV in O 1s spectra corresponds to SO_4^{2-} rather than H_2O . When comparing the two energy bands in S 2p spectra, the area percentage of the peaks attributed to S^{2-} was 60.5 % at pH 4, and it was 27.8 % at pH 7. This indicates the presence of Se-S precipitates and its formation is more favorable at low pH even in the absence of UV-L. The percentage of polysulfide detected was more noticeable in the presence of UV at low pH, which supports the dimerization/ photolysis of sulfur-radicals as will be discussed in reaction mechanisms section. In the presence of UV, the area percentages are 11.2% and 9.5% at pH 4 and pH 7, respectively. In the absence of UV, the area percentages are 5.2% and 1.4% at pH 4 and pH 7, respectively. The area percentage of elemental sulfur was less than 2%, except for the sample obtained in the absence of UV at neutral pH, where its area percentage was 69.2%. This significant difference can be due to sulfur sublimation in the XPS under

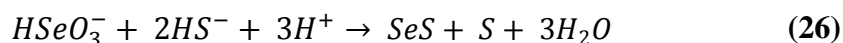
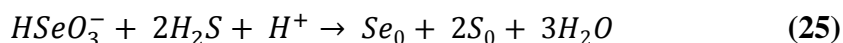
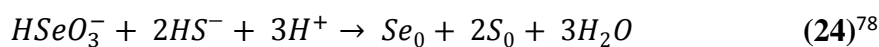
ultrahigh pressure. However, SEM/EDS results confirm the detection of elemental sulfur crystals at neutral pH in the absence of UV (Figure 14c).

From Se 3d XPS de-convolution spectra, it can be revealed that Se 3d shifted to higher binding energy at pH 7. The peaks centered at 55.1 eV and 55.9 eV at pH 7 shifted to 55.4 and 56.2 eV at pH 4, respectively. The peaks centered at 54.8 eV and 56.0 eV at pH 4 shifted to 55.0 eV and 56.2 eV at pH 7, respectively. S 2p and Se 3d high-resolution deconvolution spectra support the reduction of selenite to elemental selenium and selenide with sulfide, in both the presence and absence of UV-L light. Additionally, Se-S precipitates formation may be more favorable at pH 4 than at pH 7. All the peaks shown in the de-convolution spectra of Se 3d corresponds to elemental selenium, except the peak at the lowest binding energy (54.8 eV) that was attributed to a more reduced form of selenium. Naveau et al.⁷³ reported that the peak at a binding energy of 54.8 eV demonstrates Se(-I), or Se(-II) sorbed on pyrite. The formation of Se(-II) is more probable in the form of SeS as S 2p spectra show doublet of S²⁻. The percentage area of Se(-II) is higher at pH 4 regardless of the presence of UV, but 26.2% higher in the absence of UV.

5.3.2 *Effect of Sulfide Dose*

Table 6 shows the experimental conditions used to investigate the effect of initial sulfide dose on Se(IV) removal. Figure 22 shows the effectiveness of Se(IV) removal at different sulfide doses when the initial Se(IV) concentration was 0.11 mM. The initial S²⁻/Se(IV) molar ratio ranged between 0 and 46. The solution of the pH was maintained at pH 7, and it showed less than 0.4 pH unit change during the reaction time. When S²⁻ was above 1.27 mM, Se(IV) was not detected at the first sampling time of 2 min, regardless

the presence of UV light. In the presence of UV irradiation, Se(IV) removal behaved similarly to that observed in the absence of UV. This indicates that the rate of precipitates formation was not affected by UV irradiation at sulfide doses above 11.5 times initial Se(IV) concentration. At neutral pH, the Se(IV) species present are HSeO_3^- (90%) and SeO_3^{2-} (10%).⁷⁷ Based on experimental results and solids analysis described in previous sections, the reactions that were involved in Se(IV) removal with sulfide could be as follows:



Although light absorbance of sulfide solutions showed that HS^- species is converted to other sulfur products under UV irradiation, at high molar ratios of $\text{S}^{2-}/\text{Se(IV)}$ above 11.5, there was still enough HS^- present in the solution to react with Se(IV) and form solids especially, the reaction was very rapid and was complete before HS^- was consumed by photolysis in the presence of UV light. This explains the similar removal rate of Se(IV) in the presence and absence of UV light at high sulfide dose (Figure 23). At low molar $\text{S}^{2-}/\text{Se(IV)}$ ratios, the removal efficiency of Se(IV) removal was slightly less in the presence of UV light than in the absence of UV light. This could be due to the consumption of HS^- by photolysis during UV irradiation.

Table 6. Experimental conditions for investigating the effect of sulfide dose on Se(IV) removal.

No	^a Initial Se(IV) conc.	Sulfide dose.	UV irradiation		pH		Removal
	(mM)	(mM)	Type	Light intensity ($\mu\text{W}/\text{cm}^2$)	Initial	Final	(%)
1	0.0923	0.00	None	-	7.04	7.06	0.975
2	0.0935	0.00	UV-L	6520	7.07	7.06	1.93
3	0.0959	0.065	None	-	7.04	6.98	27.5
4	0.0884	0.065	UV-L	6977	7.09	6.99	13.7
5	0.0874	0.130	None	-	6.90	7.02	50.5
6	0.0856	0.130	UV-L	6977	6.92	7.01	29.1
7	0.0815	0.260	None	-	6.89	7.27	93.1
8	0.0833	0.260	UV-L	6977	6.99	7.25	78.3
9	0.115	1.27	None	-	7.06	7.10	99.9
10	0.101	1.27	UV-L	6950	7.03	7.04	97.4
11	0.102	5.00	None	-	7.06	7.12	100
12	0.102	5.00	UV-L	5654	6.88	7.12	100

^a Measured concentrations right after mixing Se(IV) and reducing reagent before starting UV irradiation.

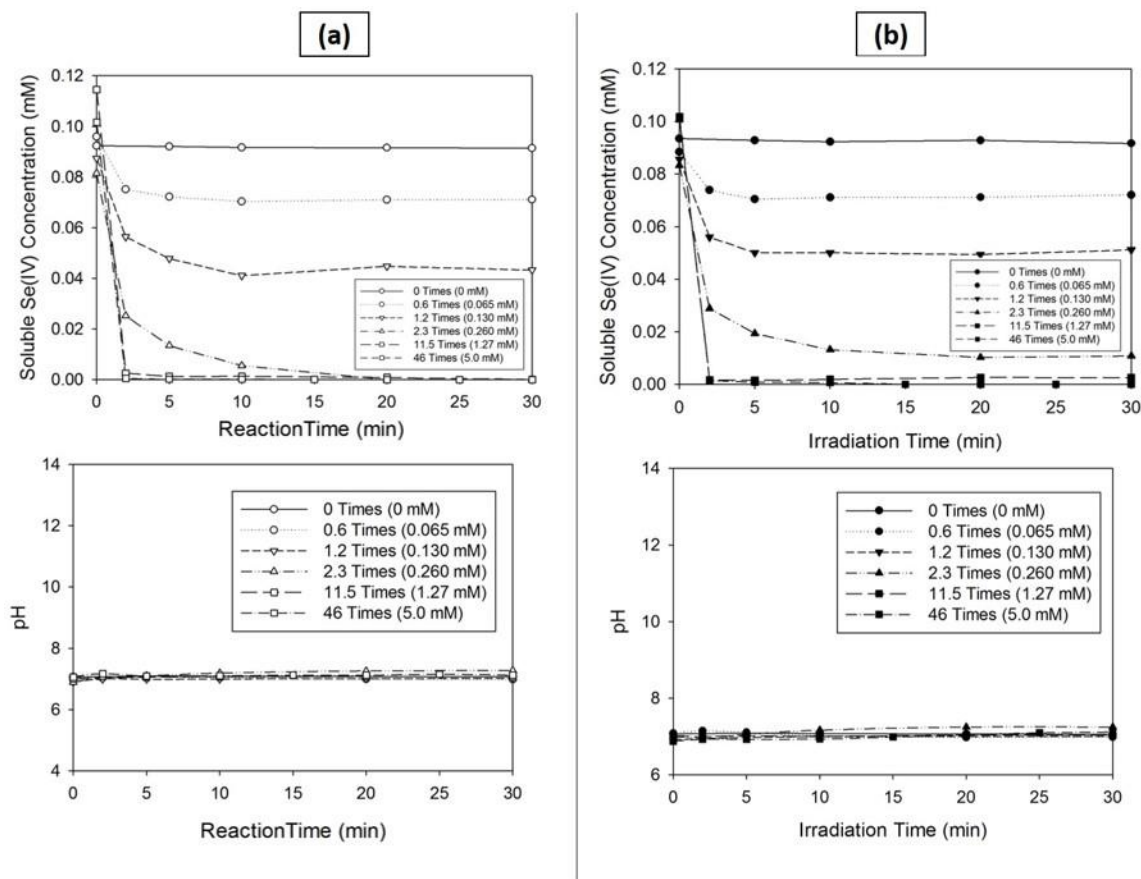


Figure 22. Effect of sulfide dose on selenite removal rate (a) in the absence of UV light, (b) in the presence of UV light. Experimental conditions: $[\text{Se(IV)}]_0 = 0.11 \text{ mM}$, light intensity = $6298 \mu\text{W}/\text{cm}^2$, and pH 7.

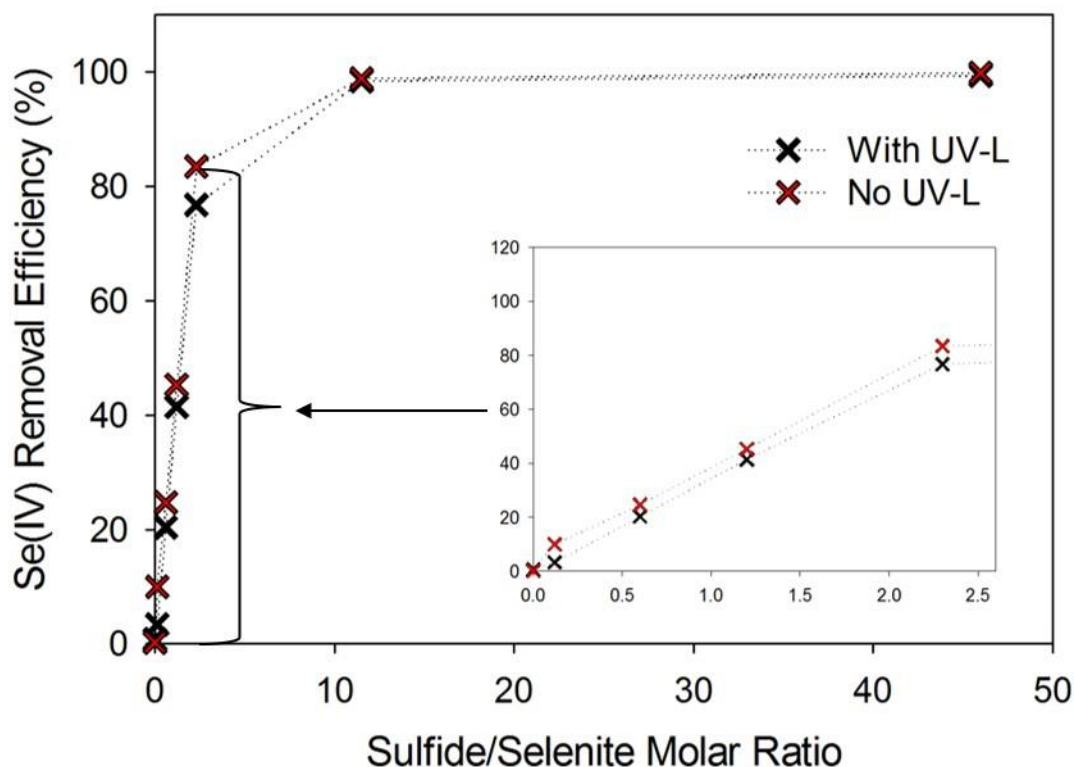


Figure 23. Selenite removal efficiency at different sulfide doses. Experimental conditions: $[\text{Se(IV)}]_0 = 0.11 \text{ mM}$, light intensity = $6298 \mu\text{W}/\text{cm}^2$, $t = 5 \text{ min}$, and pH 7.

Selenite removal efficiency increased linearly with increasing sulfide dose at reached its maximum efficiency at S^{2-}/Se molar ratio of 11.5, regardless of the presence of UV light.

Figure 24 and Figure 25 show the SEM/EDS results in the absence and presence of UV irradiation, respectively. At 115 $\text{S}^{2-}/\text{Se(IV)}$ molar ratio (Figure 24c), more layered precipitates were found compared to that at 11.5 and 46 $\text{S}^{2-}/\text{Se(IV)}$ molar ratios (Figure 24a and Figure 24b, respectively). Figure 25 shows the effect of sulfide dose on results of SEM/EDS analysis of solids formed in a solution containing Se and sulfide at pH 7 after

10 min of irradiation. Commonly, larger agglomerates of precipitates were found at higher sulfide dose in the presence of UV light (Figure 25a vs. Figure 25b). A different structure of precipitates was observed with increasing sulfide concentration. When the molar ratio of S^{2-}/Se is 3.5, smaller precipitates were found. When the molar ratio of S^{2-}/Se increased from 3.5 to 46, the precipitates formed larger agglomerates. When S^{2-}/Se was 115, more regular structures were found that showed higher intensities of Se than S. At 10 minutes, more regular precipitates were found when the ratio of S^{2-}/Se was 115 in the presence of UV irradiation, compared to that in the absence of UV.

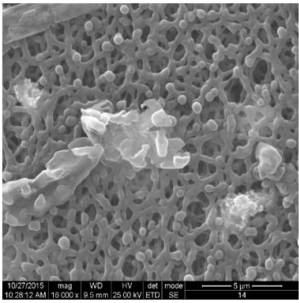
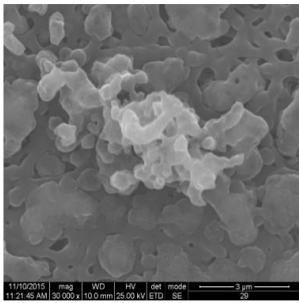
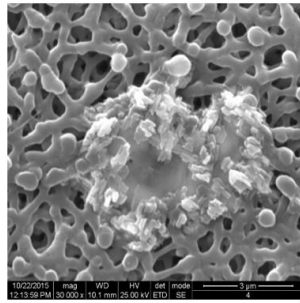
a. 11.5x	b. 46x	c. 115x
S/Se = 0.826 (wt% in EDAX)	S/Se = 1.94 (wt% in EDAX)	S/Se = 0.423 (wt% in EDAX)
		

Figure 24. SEM/EDS analysis results of solids formed in Se- S^{2-} solution at pH 7 without UV irradiation when sulfide dose was 11.5 times (a), 46 times (b), and 115 times (c) to initial Se concentration. Experimental conditions: $[Se(IV)]_0 = 0.11$ mM,

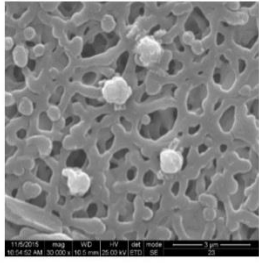
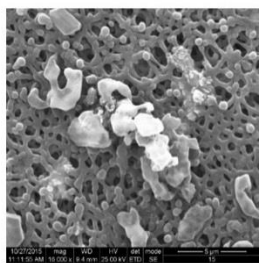
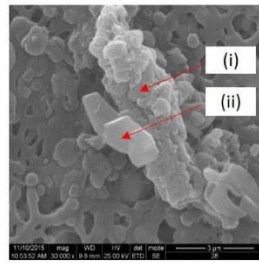
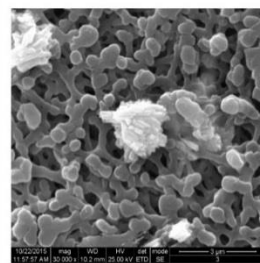
a. 3.4x	b. 11.5x	c. 46x	d. 115x
S/Se = 0.793 (wt% in EDAX)	S/Se = 1.40 (wt% in EDAX)	S/Se = (i)1.10 and (ii) 0.678 (wt% in EDAX)	S/Se = 0.268 (wt% in EDAX)
			

Figure 25. SEM/EDS analysis results of solids formed in Se-S²⁻ solution at pH 7 with UV irradiation when sulfide dose was 3 times (a), 11.5 times (b), 46 times (c), and 115 times (d) to initial Se concentration. Experimental conditions: [Se(IV)]₀ = 0.11 mM, TUV PL-L lamp and t = 10 min.

In order to understand the behavior of selenite-sulfide system in the absence versus the presence of UV light irradiation, light absorbance of the solution at different sampling times was measured as shown in Figure 26. The peak at 230 nm for the molar ratio of reducing reagent dose to selenite concentration 11.5 in the absence of UV-L light did not change significantly with time after 10 min reaction time. In the presence of UV-L light, the peak decreased by 64.4%, 89.9% and 89.9% at 10 min, 30 min, and 60 min respectively. The decrease of the absorption peak at 230 nm with time under UV irradiation indicates the HS⁻ photolysis producing radical species that react with Se(IV) to form elemental selenium, S-Se solids, and/or elemental sulfur. Figure 26b supports the cyclic production of HS⁻ as shown by Eq. (9).

In order to quantify the concentration of HS^- present in the solution, the molar absorptivity of sulfide solution was calculated by varying its dose in the absence of irradiation (Figure A5a). The calculated molar absorptivity was $10165 \text{ L mol}^{-1}\text{cm}^{-1}$ for HS^- present in sulfide solution prepared at pH 7. Figure 27 shown the absorption spectra of sulfide solution under UV irradiation and it supports the photolysis of HS^- over irradiation time and the appearance of a new absorption band at higher wavelengths, which increases over time. The absorbance at 254 nm, which is the wavelength of light produced by UV-L lamp, increased up to 10 min, then starts to decrease slightly as shown in Figure 28. This indicates the effectiveness of UV-L lamp in irradiating sulfide during the first 10 mins. However, upon photolysis of HS^- , the produced species absorb less light at the produced wavelength by UV-L lamp.

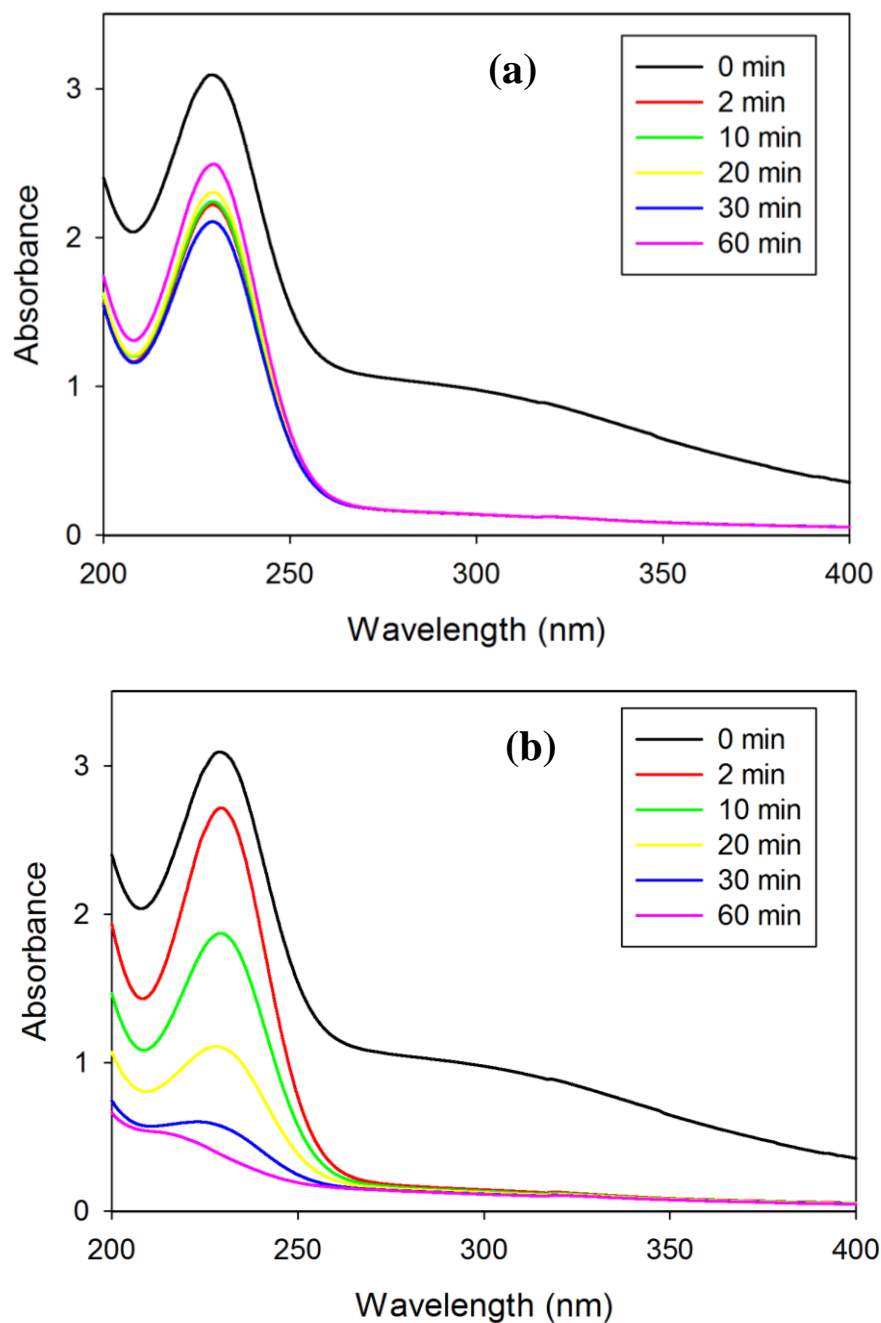


Figure 26. UV absorbance spectra of Se-sulfide solution at different conditions in the absence of UV light (a) and in the presence of UV-L light (b). Experimental conditions: $[\text{Se(IV)}]_0 = 0.11 \text{ mM}$, $[\text{S}^{2-}]_0 = 1.27 \text{ mM}$, light intensity (T-8C lamp) = $4300 \mu\text{W}/\text{cm}^2$, pH 7, and anoxic condition.

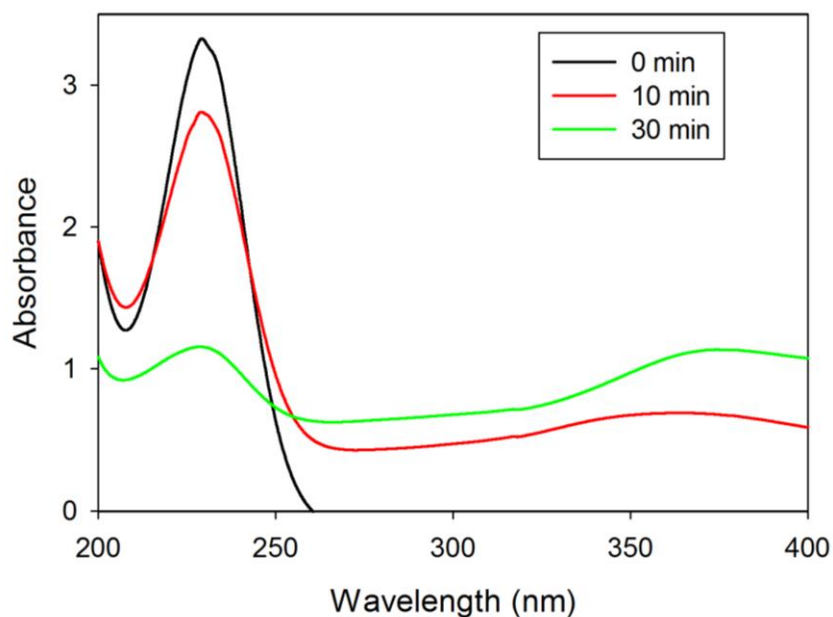


Figure 27. Absorbance spectra of Se-sulfide solution showing the effect of UV-L light over time. Experimental conditions: $[S^{2-}]_0 = 1.25$ mM, light intensity = $4041 \mu\text{W}/\text{cm}^2$, and pH 7.

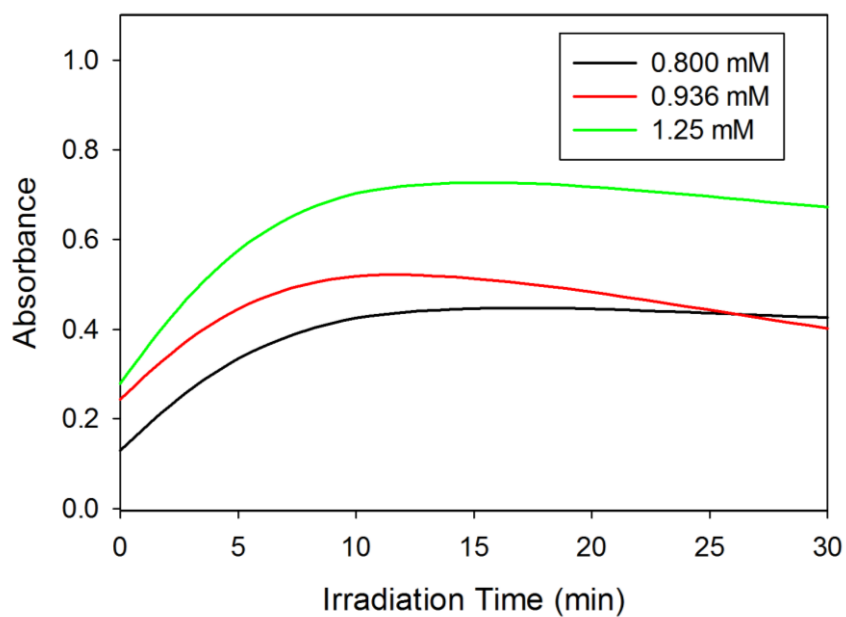
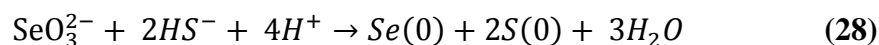


Figure 28. Absorbance of sulfide solution over time at 254 nm upon UV-L irradiation. Experimental conditions: $[S^{2-}]_0 = 1.25$ mM, light intensity = $4041 \mu\text{W}/\text{cm}^2$, and pH 7.

Figure 29 shows O 1s, S 2p, and Se 3d XPS spectra of the solid formed in Se(IV)-S(-II) solution in the absence of UV-L at different sulfide initial doses. Figure 30 shows the deconvolution spectra. O 1s and S 2p XPS spectra at the three different S²⁻/Se molar ratios show a similar trend, except Se 3d XPS spectrum, which was shifted. Additionally, it is observed that at S²⁻/Se molar ratio of 11.5 and 115, peak centered at 531.4 eV in O 1s became asymmetric, showing a shoulder at lower binding energy, which was fitted with two doublets. The shift in the binding energy of Se 3d depends on sulfide dose and shifted to higher binding energy at S²⁻/Se molar ratio of 46. The main peak located at 55 eV (higher binding energy) was shifted towards a lower binding energy at high sulfide doses. This implies that higher sulfide dose in the solution initially can lead to the production of more reduced selenium species such as (Se(-I) and Se(-II)). At S²⁻/Se molar ratio of 115, the peak observed at binding energy 54.8 eV was attributed to Se(-I) or Se(-II), as it was reported by Naveau et al.⁷³ that the peak at a binding energy of 54.8 eV demonstrates Se(-I), or Se(-II) sorbed on pyrite. Figure 30, O 1s XPS de-convolution spectra show three major peaks. For S²⁻/Se molar ratio of 11.5 and 115, the three peaks are at 530.9 eV, 531.5 eV, and 533.1 eV which correspond to OH⁻, HSO₃⁻ or S₂O₃²⁻ and H₂O, respectively. For S²⁻/Se molar ratio of 46, peak at 531.4 eV corresponds to HSO₃⁻ or S₂O₃²⁻, and 533.1 eV and 533.4 eV, which was attributed to H₂O (or 531.1 eV peak corresponds to SO₄²⁻ based on S 2p spectra). It was reported that binding energy at 531.0 eV or 531.1 eV corresponds to hydroxyl ion.⁷⁹ However, except hydroxide ion the peaks ranged between 530 eV and 532 eV may be attributed to O1s from species such as S₂O₃²⁻, S₂O₅²⁻, S₂O₆²⁻, SO₃⁻, and SO₄²⁻. based on the reported data in literature (Table A1). S 2p XPS de-convolution spectra

show two major areas. Low binding energy region (158 eV – 166 eV) shows two constituent doublets with S 2p_{3/2} peaks at 161.2 eV, 162.4 eV, and 164.1 eV which correspond to S²⁻, S_n²⁻ and S₀ respectively. In the high binding energy region (166 eV – 170 eV), there are two constituent doublets. The peaks at 167.4 eV and 168.6 eV may contribute to S₂O₃²⁻ or HSO₃⁻. At S²⁻/Se molar ratio of 46, SO₄²⁻ peak appears at 167.4 eV. Se 3d XPS de-convolution spectra show five major peaks and most peaks found between 54 eV and 56 eV, which is attributed to elemental Se(0) according to binding energy values reported in the literature (Table A5). The lowest energy peaks found between 54.5 and 54.8 eV (Figure 30) may be attributed to surface-bound Se(-II) or Se(-I).⁷³ The high-resolution XPS de-convolution spectra of S 2p and Se 3d again supports the observation that Se(IV) was reduced to Se(0), and elemental sulfur was produced by sulfide oxidation. This supports the following reaction between selenium and sulfide.



The peak at lower binding energy for S 2p de-convolution spectra that are located between 160.40 eV and 160.91 eV is consistent with results reported by Doyle et al.⁸⁰, which was attributed to monosulfide at surface defects.⁸⁰ Hence, the peaks observed at low energy can be S²⁻ or due to surface defects. The percentage of the low binding energy band are 43.4%, 45.7%, and 29.9% for S²⁻/Se molar ratio of 11.5, 46 and 115, respectively. The percentage of Se(0) calculated from the peak area, are 84.8%, 73.4% and 96.9% for S²⁻/Se molar ratio of 11.5, 46 and 115, respectively which is an indication of the formation of a crystal monoclinic elemental selenium.^{81,82}

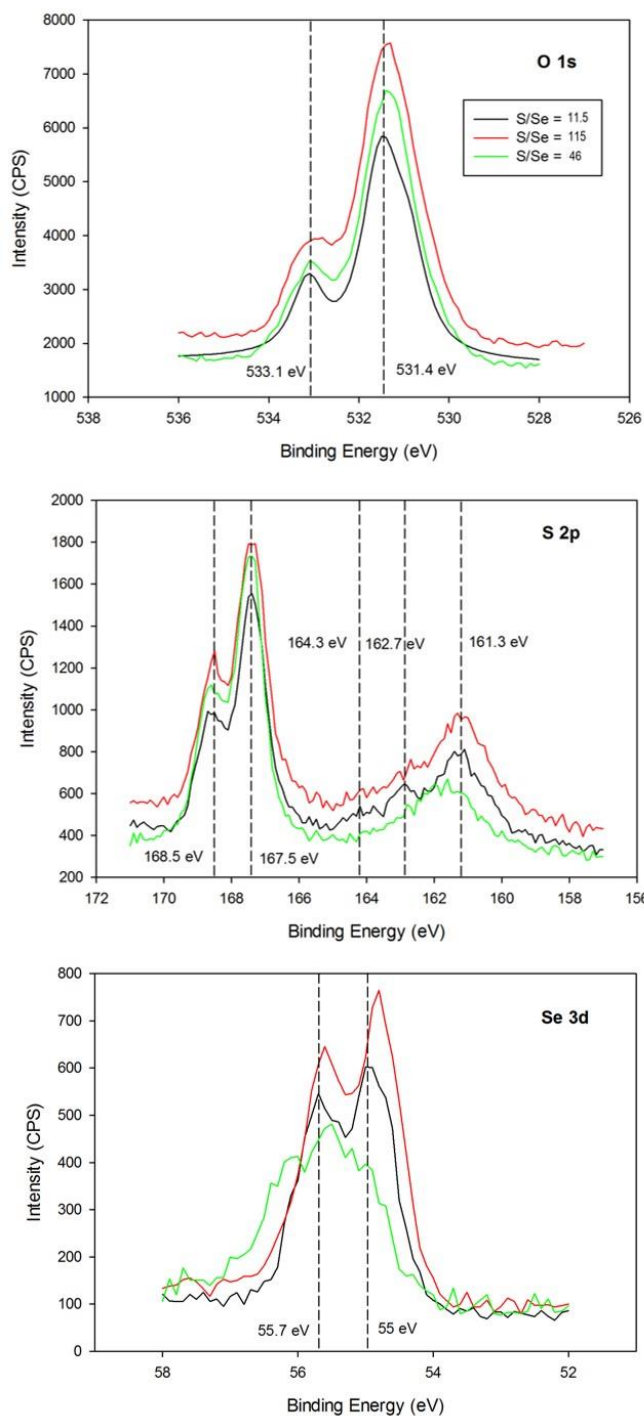


Figure 29. High-resolution O 1s, S 2p and Se 3d XPS spectra of solid formed in Se(IV)-S(-II) solution in the absence of UV- L after 10 min at pH 7 with S^{2-}/Se molar ratio of 11.5 and 115. Experimental conditions: $[Se(IV)]_0 = 0.11$ mM, $[S^{2-}]_0 = 5.0$ mM, and pH 7; $[Se(IV)]_0 = 0.11$ mM, $[S^{2-}]_0 = 1.27$.

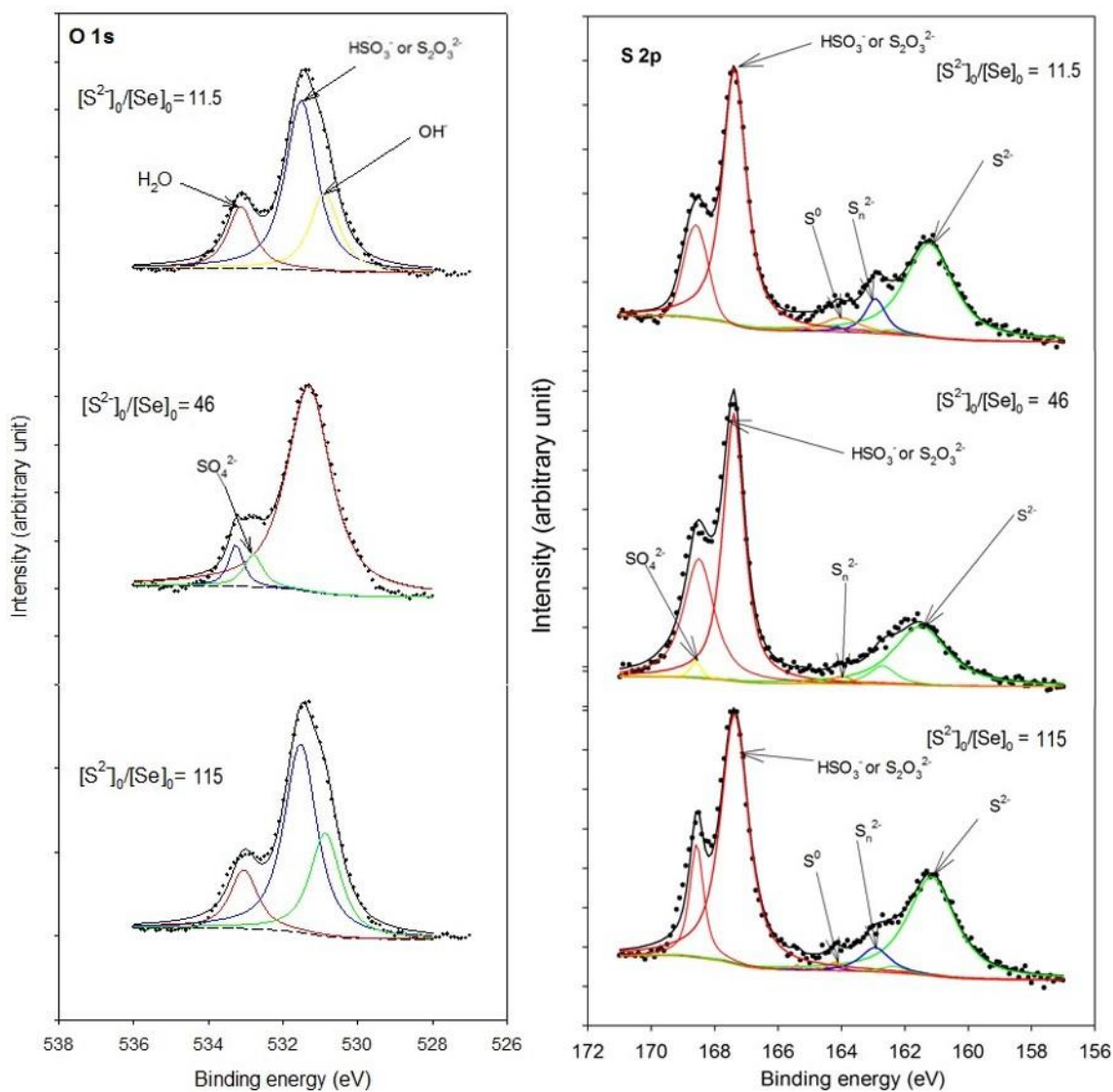


Figure 30. High-resolution O 1s, S 2p, and Se 3d XPS de-convolution spectra of the solid formed in Se(IV)-S(-II) solution in the absence of UV- L for 10 min at pH 7 with S^{2-}/Se molar ratio of 11.5, 46, and 115. Experimental conditions: $[Se(IV)]_0 = 0.11$ mM.

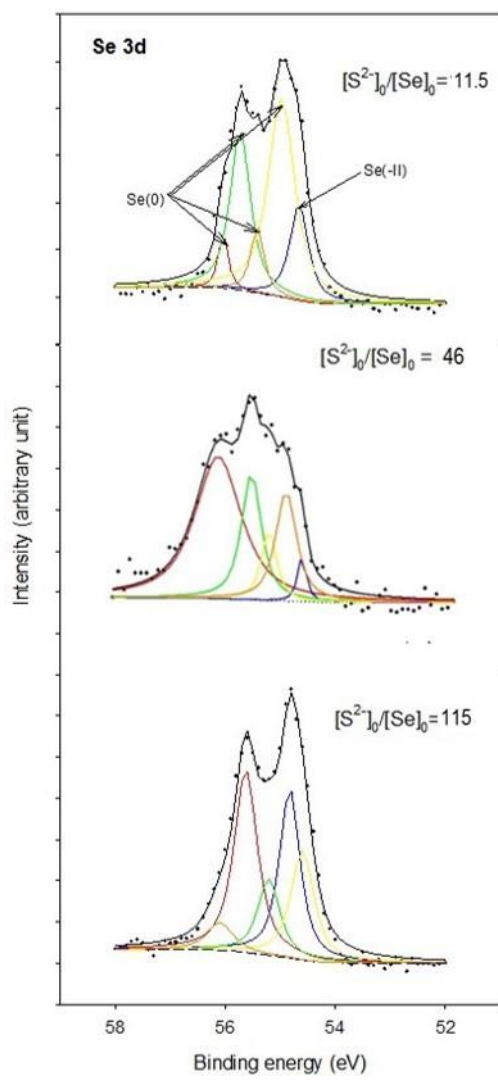


Figure 30. Continued

5.3.3 Effect of Se(IV) Initial Concentration

The effect of the initial Se(IV) concentration on the effectiveness of its removal was investigated and the experimental conditions and Se(IV) removal efficiencies are shown in Table 7. Initial Se concentration was investigated at 0.0011 mM, 0.011 mM, and 0.11 mM. The applied UV irradiation time was 30 minutes in the anaerobic chamber using TUV PL-L lamp. Results shown in Table 7 indicate that low removal efficiencies were obtained at low initial Se(IV) concentrations in the presence of UV light irradiation. This could be because at low Se(IV) concentration, sulfide dose is low too, and it could have been photolyzed by UV light and consumed producing species with low concentrations that are not effective in reducing Se(IV).

Table 7. Experimental conditions for investigating the effect of Se(IV) initial concentration

No.	^a Se(IV) Initial Conc.	Reducing Reagent Conc.	Radiation		pH		Removal
	(mM)	(mM)	Type	Light intensity ($\mu\text{W}/\text{cm}^2$)	Initial	Final	(%)
1	0.102	5.00	None	-	7.06	7.12	100
2	0.102	5.00	UV-L	5654	6.88	7.12	100
3	0.00728	0.510	None	-	7.06	7.04	98.8
4	0.00778	0.510	UV-L	6755	6.98	7.13	80.3
5	9.24×10^{-4}	0.0513	None	-	7.04	7.02	94.5
6	9.93×10^{-4}	0.0513	UV-L	5714	7.01	7.09	53.5

^a Measured concentrations right after mixing Se(IV) and reducing reagent before starting UV irradiation.

5.3.4 *Effect of UV Irradiation*

As mentioned earlier, experimental results showed that UV irradiation did not affect the efficiency of Se removal as compared to results without UV light at the same sulfide doses. Yet, UV irradiation affected the characteristics of solids formed as indicated by the different colors of the precipitated solids when the solutions were not or were irradiated with UV light. The effect of UV-L irradiation on the nature of the solid formed was evaluated by analyzing samples using XPS at neutral pH after 10 min irradiation at S^{2-}/Se molar ratio of 11.5. O 1s, S 2p, and Se 3d XPS spectra of the solid formed in Se(IV)-S(-II) solution in the absence and presence of UV-L for the two cases are shown in Figure 31. At S^{2-}/Se molar ratio of 11.5 (Figure 31), there was no significant shift observed for the narrow scan of O 1s and S 2p. However, in the presence of UV, there was a slight shift to higher binding energy in Se 3d spectra. The major peaks shown in Se 3d de-convolution spectra (Figure 32) are attributed to elemental Se indicate that selenite (Se(IV)) was reduced to Se(0) in a solution, regardless of the presence of UV.

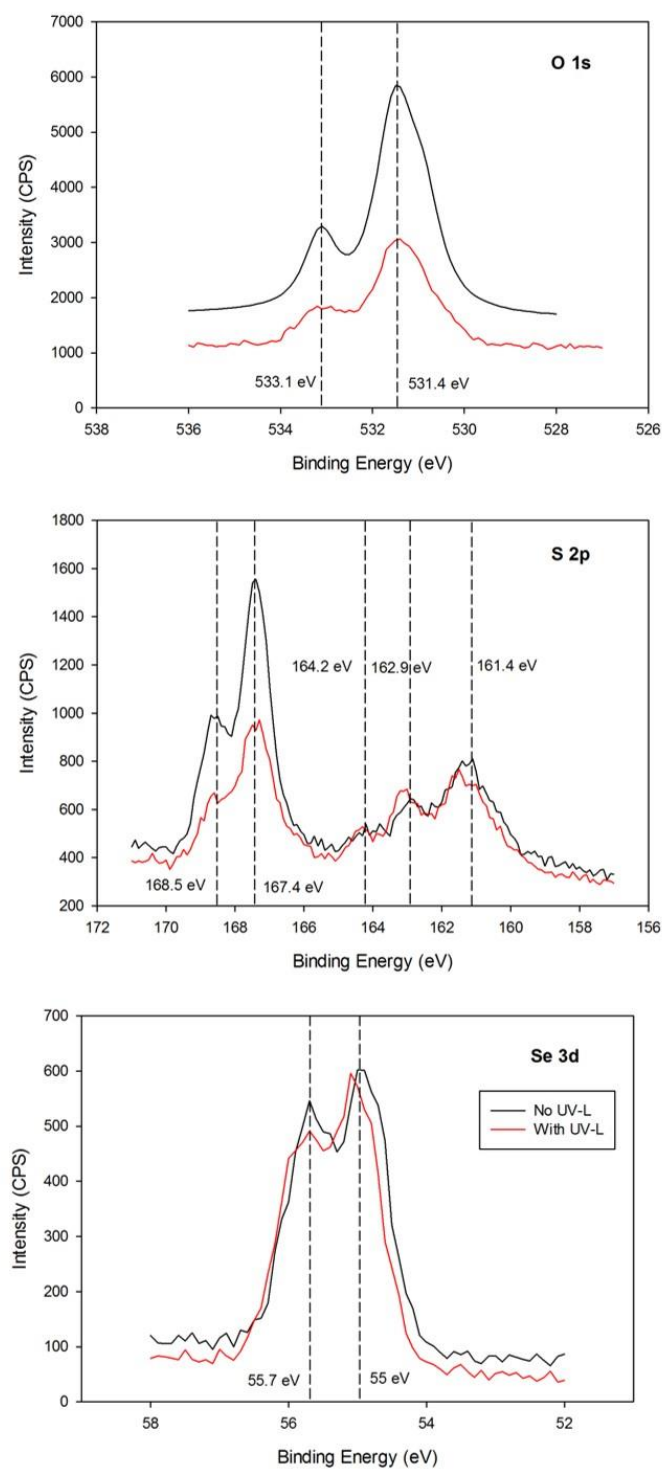


Figure 31. High-resolution O 1s, S 2p, and Se 3d XPS spectra of the solid formed in Se(IV)-S(-II) solution in the presence of UV-L and the absence of UV-L light. Experiment conditions: $[\text{Se(IV)}]_0 = 0.11 \text{ mM}$, $[\text{S}^{2-}]_0 = 1.27 \text{ mM}$, pH 7, $t = 10 \text{ min}$.

High-resolution deconvolution spectra at S^{2-}/Se molar ratio of 11.5 for O 1s, S 2p, and Se 3d are shown in Figure 32. At S^{2-}/Se molar ratio of 11.5, the peak observed at 533.1 eV which is attributed to molecular H_2O decreased with UV irradiation as compared to that in the absence of UV (Figure 32) (with peak areas of 856 and 1599 with UV and no UV, respectively). The other two peaks at 530.9 eV and 531.5 eV contribute to OH^- and HSO_3^- or $S_2O_3^{2-}$, respectively. For S 2p de-convolution spectra, three major doublets were present at low binding energy, including elemental sulfur, with area percentage of 2.82 % and 0.786 % in the presence and absence of UV, respectively. At a higher binding energy of S 2p and in the absence of UV irradiation, the peaks assigned from $S_2O_3^{2-}$ or HSO_3^- increased by 13.9%. This indicates that sulfide was oxidized to high oxidation states. Se 3d XPS de-convolution spectra show five major peaks with most peaks found between 54 eV and 56 eV, which can be attributed to elemental Se(0), except the peak at 54.7 eV attributes to Se(-II). The percentage of Se(0) in the sample calculated from the peak are 74.4% and 84.8% in the presence and absence of UV, respectively.

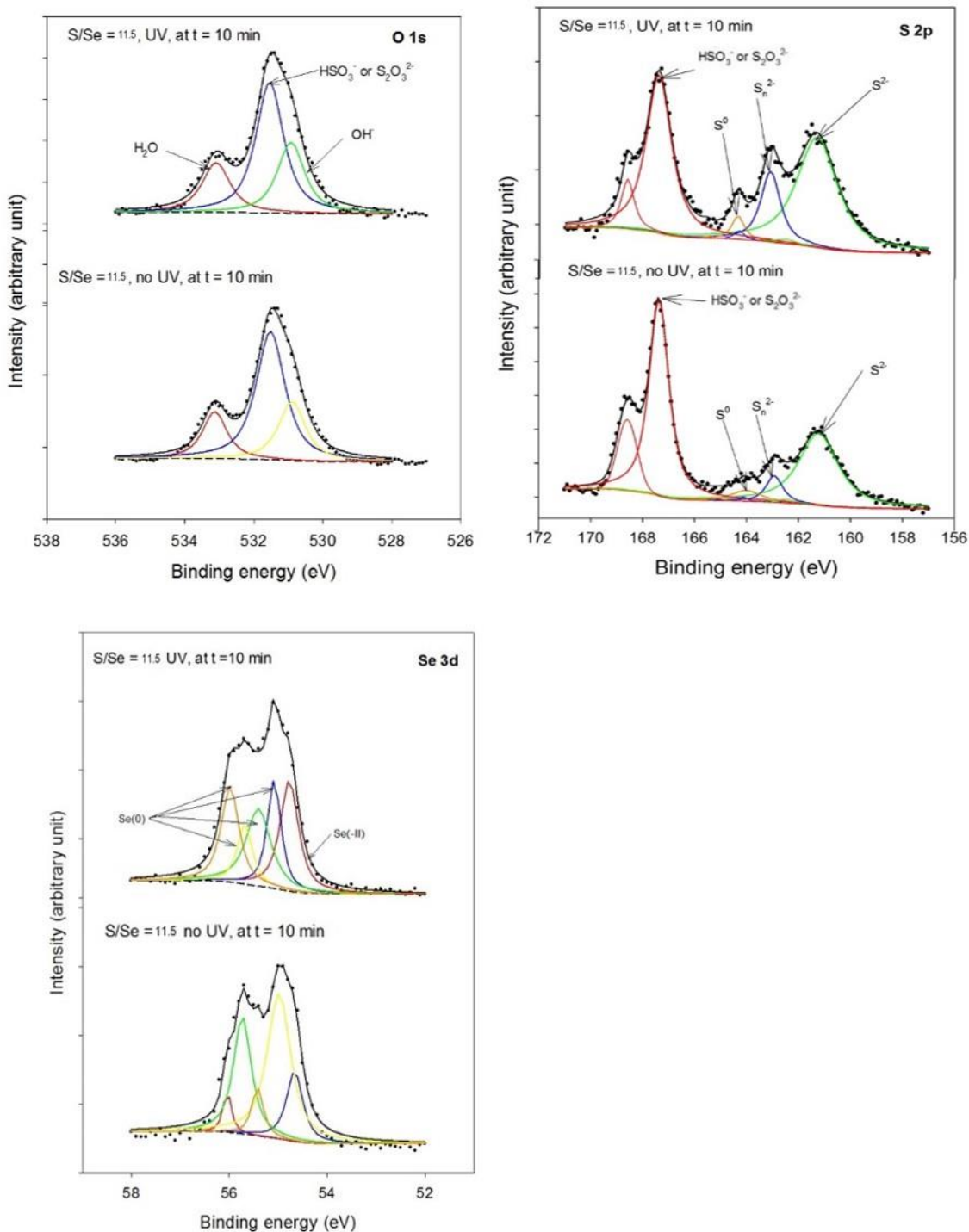


Figure 32. High-resolution O 1s, S 2p, and Se 3d XPS de-convolution spectra of the solid formed in Se(IV)-S(-II) solution in the presence of UV-L and the absence of UV-L light. Experiment conditions: [Se(IV)]₀ = 0.11 mM, [S²⁻]₀ = 1.27 mM, pH 7, t = 10 min.

5.3.5 Effect of Humic Acids

HA is a major compound of humic substrates, with a molecular structure presented in Figure 33,⁸³ However, it can have different molecular structure depending on the molecular weight.⁸⁴ It is soluble in alkaline to weak acidic solutions.⁸⁵ It was reported that HA can act as free radicals scavenger in AOPs.^{83,85} In previous studies on iron reduction, Li et al.⁸⁶ reported that HA aided in the electron transfer process due to the presence of functional groups (e.g., quinone, phenolic and carboxylate moieties). Hence, it is considered as a redox-active organic compound that can affect oxidation-reduction reactions if it present in contaminated waters.⁸⁶ Nevertheless, the dependency on HA in the reduction of contaminants is not clear. HA can either aid the reduction/ removal of selenite or enhance it, depending on the nature of the interaction between the species in the solution. The binding mechanism of HA is highly depended on several factors including cation bridging, water bridging, anion exchange, ligand exchange, hydrogen binding and van der Waals forces, and the pH of the surrounding environment.⁸⁷

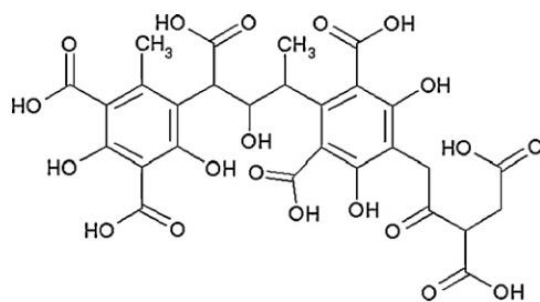


Figure 33. Humic acid molecular structure.

Batch kinetic experiments were conducted to investigate the effect of the presence of humic acids (HA) on selenite removal with sulfide. The experiments were conducted using quartz cell of 17 mL capacity (1 cm thickness) as the reactor. The molar ratio of reducing reagent dose to initial selenite concentration was 46. The reaction time was 60 minutes. Table 8 shows the initial conditions and Se(IV) removal efficiency as affected by the concentration of HA. Figure 34 shows the effect of HA on the kinetics of Se(IV) removal. As the concentration of HA increases, the removal of selenite is hindered and the reduction rate decreased with no change in pH regardless of the presence of UV light. De Carvalho et al.⁸⁸ reported that selenium forms complexes with HA. Kamei-Ishikawa et al.⁸⁹ reported that selenium is sorbed on HA surfaces.

Nevertheless, the presence of UV light enhanced the removal of selenite as the reaction time proceeds in the presence of high concentrations of HA. De Carvalho et al.⁸⁸ reported that HA effect is eliminated upon UV irradiation. Wang et al.⁹⁰ reported that the molecular charge variation upon UV irradiation of HA enhanced HA removal at pH above 7. This could support the decrease in selenite concentration over the irradiation time at high concentrations of HA. Furthermore, Wang et al.⁹⁰ reported that UV light produces small molecular HA, which agglomerates. Therefore, it is proposed that selenite is entrapped or sorbed on these HA agglomerates. The solid formed during the experiments in the presence of HA was not influenced by the presence of UV, rather it was getting darker as HA concentration increases. The greyish-brown color is expected to be due to the presence of HA rather than Se-S precipitates.

Table 8. Experimental conditions for investigating the effect of humic acids.

No.	^a Initial Se(IV) Conc.	HA conc. (mg/L)	UV irradiation		pH		Removal (%)
	(mM)		Type	Light intensity ($\mu\text{W}/\text{cm}^2$)	Initial	Final	
1	0.110	0.00	None	-	7.04	7.24	95.3
2	0.0988	0.00	UV-L	5030	7.04	7.22	99.9
3	0.120	10.0	None	-	7.12	7.32	96.8
4	0.117	10.0	UV-L	4245	7.02	7.08	98.9
5	0.105	50.0	None	-	7.18	7.27	50.3
6	0.103	50.0	UV-L	4158	7.00	7.08	85.1
7	0.110	100.0	None	-	6.97	7.48	41.9
8	0.108	100.0	UV-L	4220	7.03	7.17	86.4

^a Measured concentrations right after mixing Se(IV) and reducing reagent before starting UV irradiation.

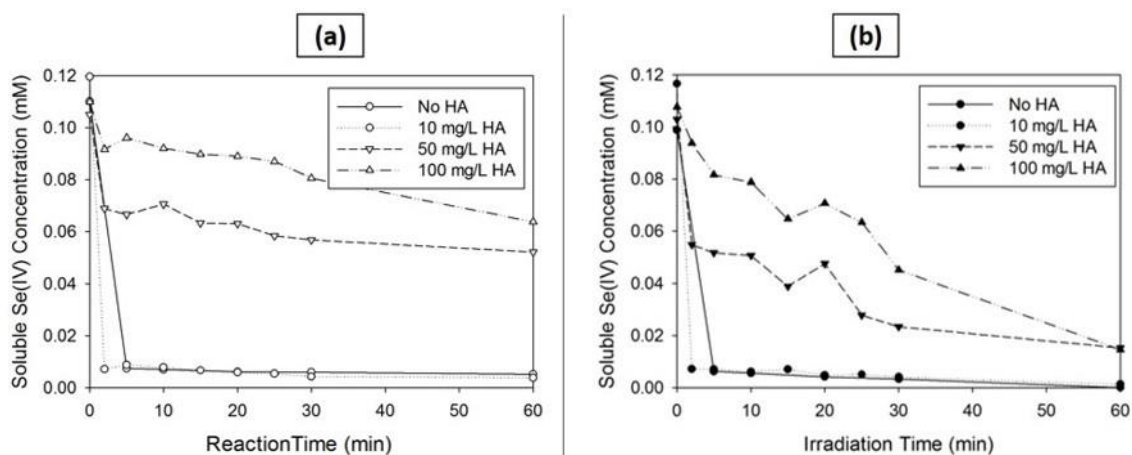


Figure 34. The effect of humic acids concentration on selenite concentrations at different initial HA concentrations in the absence of UV light (a) and in the presence of UV light (b) when the molar ratio of S^{2-}/Se was 46. Experimental conditions: $[\text{Se(IV)}]_0 = 0.11 \text{ mM}$, light intensity = $4207 \mu\text{W}/\text{cm}^2$, and pH 7.0.

5.3.6 Effect of Sulfate and Carbonate on Se(IV) Removal with Sulfide

Batch experiments were conducted to investigate the effect of the presence of sulfate and carbonate inorganic salts on selenite removal in sulfide solution. The molar ratio of reducing reagent concentration to selenite concentration was 46. The reaction time was 120 minutes. Table 9 shows the initial experimental and removal efficiencies of selenite in the presence of sulfate or carbonate. Figure 35 shows the effect of these compounds on the kinetics of Se(IV) removal.

Table 9. Experimental conditions for investigating the effect of inorganics.

No.	^a Initial Se(IV) Conc.	Inorganic		UV irradiation		pH		Removal (%)
	(mM)	Type	conc. (mM)	Type	Light intensity ($\mu\text{W}/\text{cm}^2$)	Initial	Final	
1	0.115	None	0.00	None	-	7.04	7.35	92.5
2	0.104	None	0.00	UV-L	5030	7.04	7.43	100
3	0.108	Sulfate	1.04	None	-	6.95	7.59	97.4
4	0.108	Sulfate	1.04	UV-L	3505	6.95	7.52	100
5	0.108	Carbonate	1.67	None	-	7.06	8.54	95.6
6	0.108	Carbonate	1.67	UV-L	3250	7.06	7.75	98.8

^a Measured concentrations right after mixing Se(IV) and reducing reagent before starting UV irradiation.

Figure 35 shows that these inorganic salts did not have significant effects on the kinetics or the removal efficiency of selenite. However, the presence of anions under UV irradiation resulted in slightly higher Se(IV) concentration during the first 30 minutes of

reaction. The change of solution pH was around 0.5 units for experiments that were conducted under UV irradiation regardless of the presence of anions. However, in the case of carbonate and in the absence of UV, the pH increased by 1.48 units. The solid formed were orange, and the color became lighter with time in the absence of UV, while in the presence of UV, the solid formed was pale yellow to light green. It is worth noting that total carbonate concentration at pH 7 is 83.99 % carbonic acid (H_2CO_3) and 15.96 % bicarbonate (HCO_3^-).⁷⁰ Fujikawa and Fukui⁹¹ reported that selenite sorption on magnetite and hematite was reduced in the presence of sulfate. Goh and Lim⁹² reported the inconsequential influence of sulfate on selenium sorption on iron.

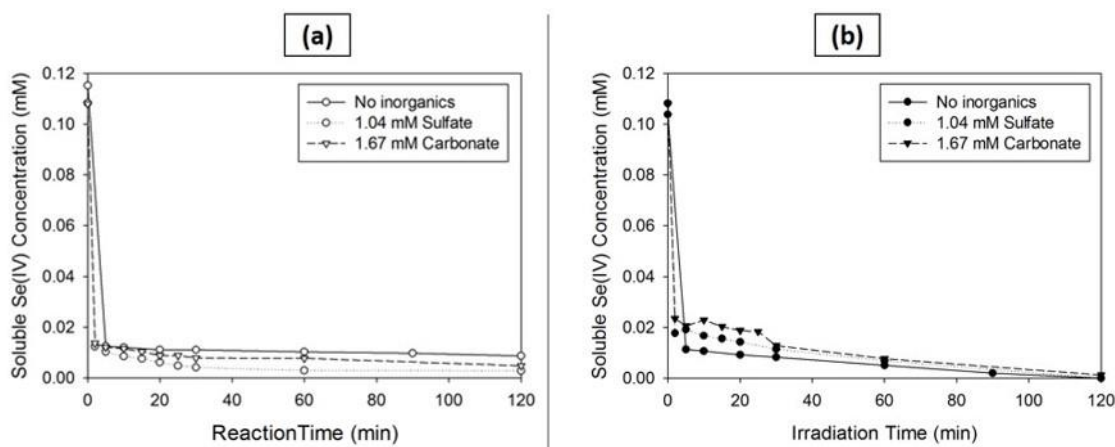


Figure 35. Selenite concentrations and pH changes with 100 mg/L inorganic salts in the absence of UV light (a) and in the presence of UV light (b). Experimental conditions: $[\text{Se(IV)}]_0 = 0.11 \text{ mM}$, $[\text{S}^{2-}] = 5.0 \text{ mM}$, light intensity = $3378 \mu\text{W}/\text{cm}^2$, and pH 7.0.

5.4 Solid Surface Analysis: XRD Results

Solid precipitates were produced at a high initial concentration of selenite (2.54 mM) with S^{2-}/Se molar ratio of 3 to precipitate enough solid for XRD analysis. The solution color turned immediately milky orange. Black (dark gray), fine precipitates were formed in the absence of UV, and in the presence of UV, large agglomerated orange precipitates were formed (Figure 36), and the filtrate in both cases was clear. Figure 37 shows XRD patterns of the solid forms in the absence of UV light and its presence. In the absence of UV light, XRD scan showed major peaks of high-intensity corresponding to the spectra of elemental Se (00-042-1425), with minor peaks corresponds to the spectra of $Se_{3.3}S_{4.7}$ (01-071-0247). In the presence of UV light, XRD scan showed major peaks similar to that of cyclic selenium sulfides ($Se_{3.02}S_{4.98}$) (01-070-9556), in addition to minor peaks of elemental selenium and elemental sulfur. The assignment of peaks of XRD patterns are shown in Figure 38 and Figure 39. Geoffroy and Demopoulos²¹ reported that the precipitates formed in selenium and sulfide solution consisted of sulfur-selenium ring molecules with the formula of Se_nS_{8-n} , with n ranging between 2.5 - 3, in the region of $1.7 < S/Se < 11$ and $1.7 < pH < 7$. Additionally, Šedo et al.⁹³ Also, they reported the formation of heterocyclic compounds having the formula Se_mS_n ($m+n = 8$ or 9) when laser pulses were applied onto a selenium-sulfur mixture.

The XRD analysis confirmed the observation from SEM images and XPS analysis. The observation of irregular particles aggregates that were formed in the presence of UV light, indicating the presence of selenium as Se-S precipitates. Also, aggregates with

layered plate shape were formed in the absence of UV light, indicating the formation of elemental selenium.

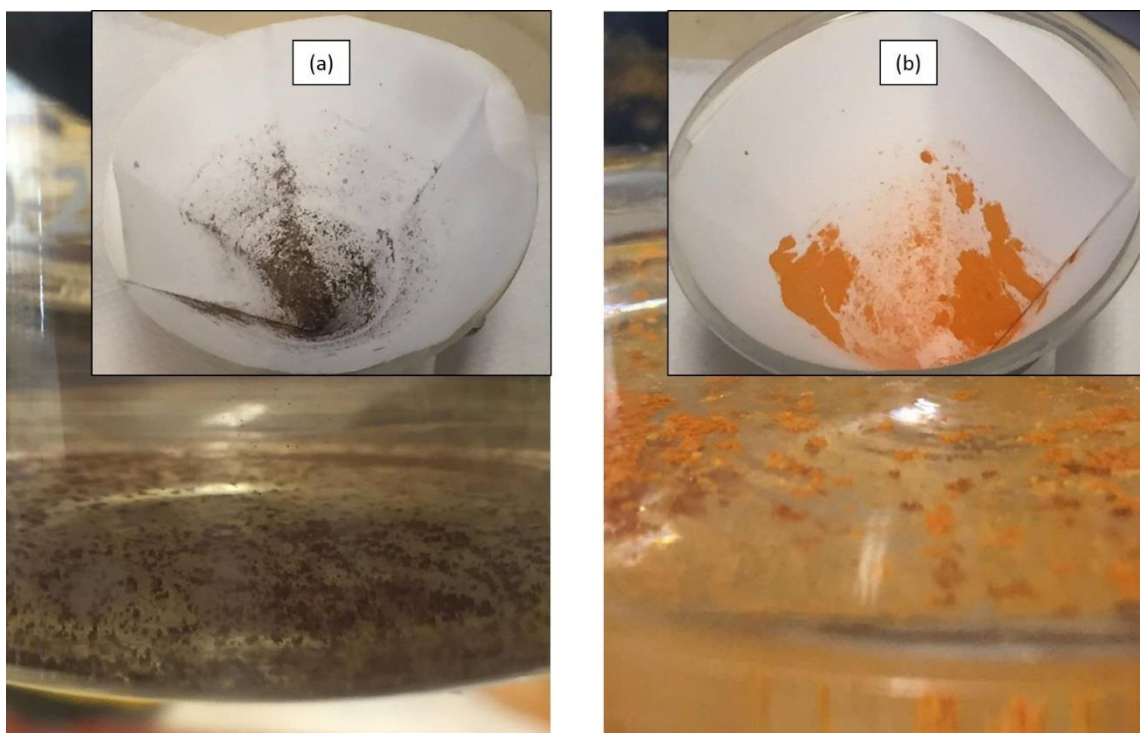


Figure 36. Solids formed in Se-S^{2-} solutions in the absence of UV light (a) and in the presence of UV light (b). Experimental conditions: $[\text{Se(IV)}]_0 = 2.54 \text{ mM}$, $[\text{S}^{2-}]_0 = 7.66 \text{ mM}$ light intensity = $6977 \mu\text{W}/\text{cm}^2$, and pH 7.

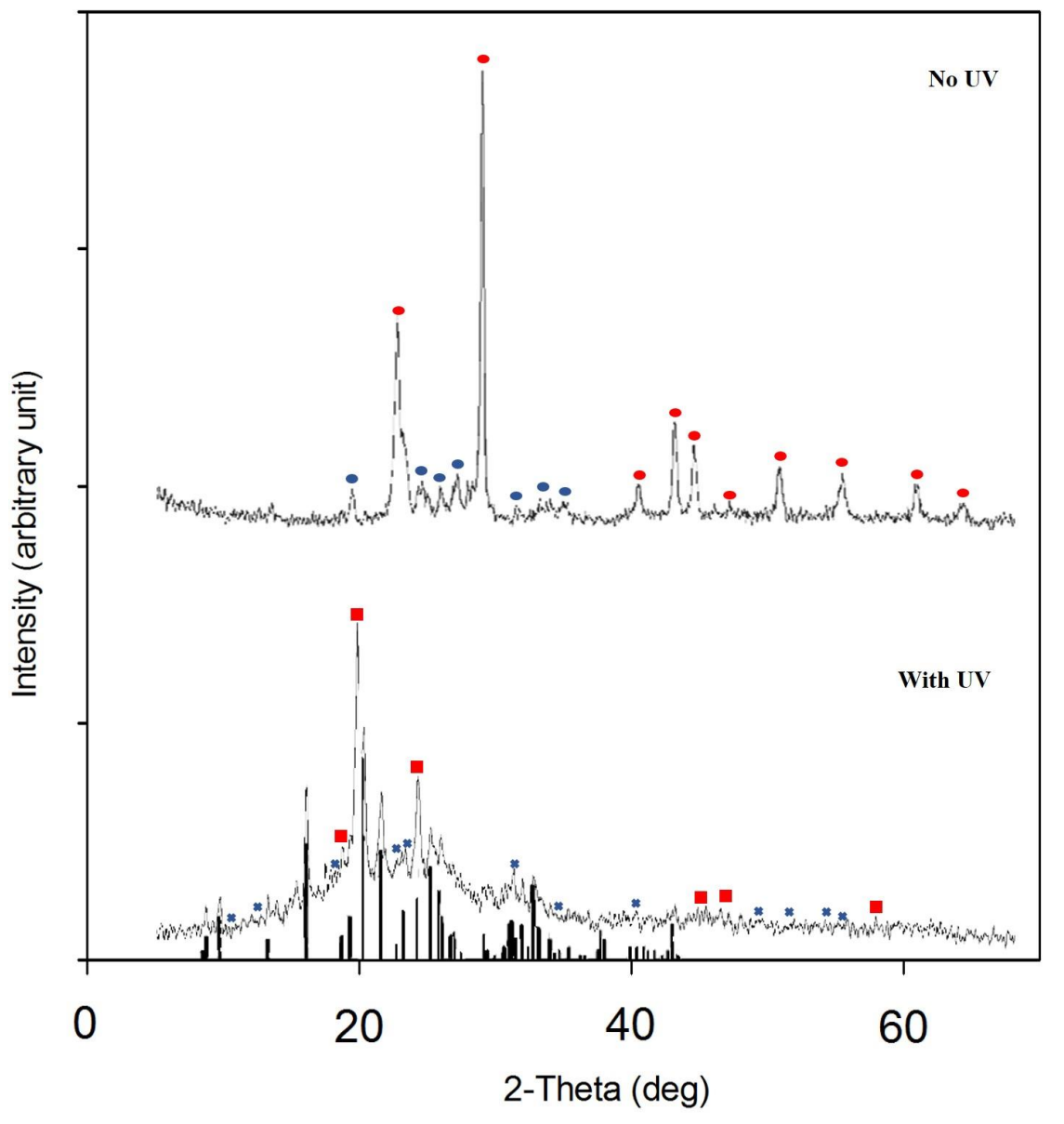


Figure 37. XRD pattern of the precipitates formed from selenium-sulfide solution in the absence and in the presence of UV, elemental selenium (03-065-1876) (red dots) and (01-070-9556) (red squares), sulfur (00-042-1278) (blue crosses), $\text{Se}_{3.3}\text{S}_{4.7}$ (1-071-0247) (blue circles) and $\text{Se}_{3.02}\text{S}_{4.98}$ (00-031-122) (black peaks). Experimental conditions: $[\text{Se(IV)}]_0 = 2.54 \text{ mM}$, $[\text{S}^{2-}]_0 = 7.66 \text{ mM}$, light intensity = $6977 \mu\text{W}/\text{cm}^2$, and pH 7.

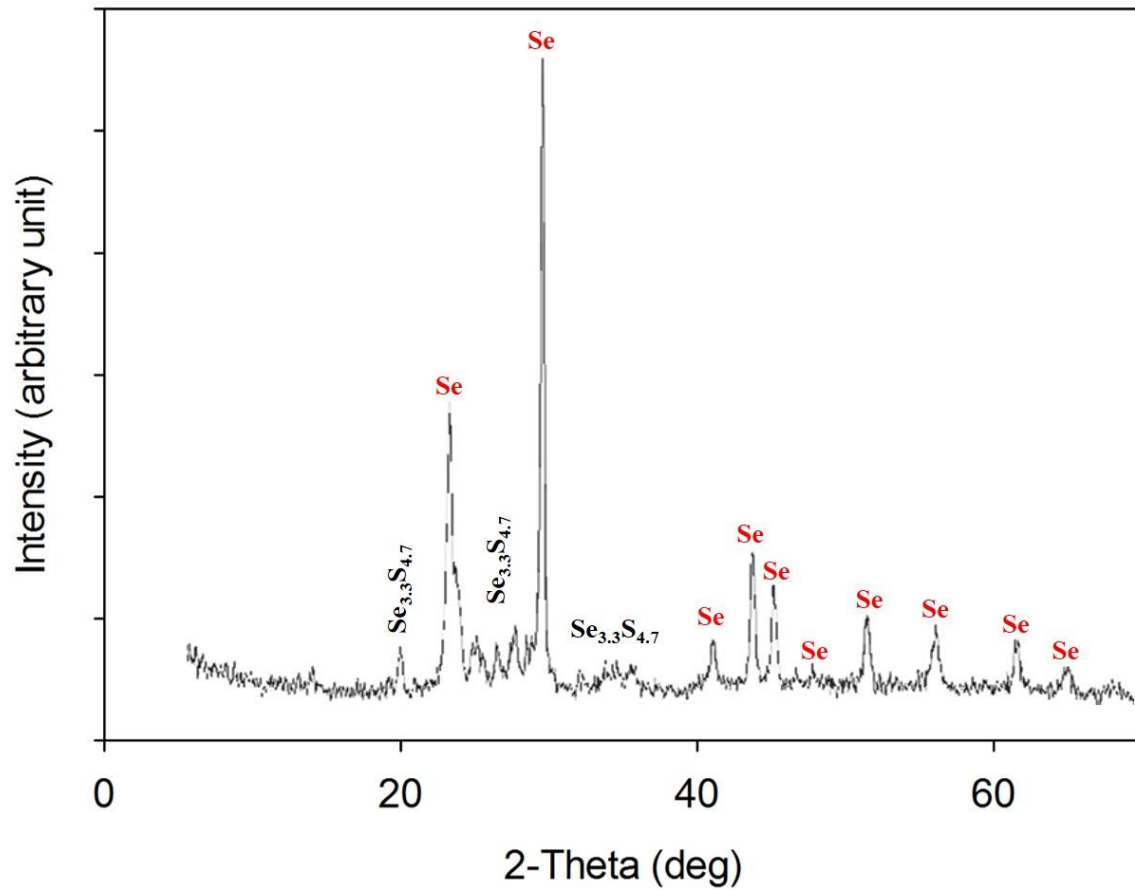


Figure 38. Peak assignments of XRD pattern of the precipitates formed from selenium-sulfide solution in the absence of UV. Experimental conditions: $[\text{Se(IV)}]_0 = 2.54 \text{ mM}$, $[\text{S}^{2-}]_0 = 7.66 \text{ mM}$, and pH 7.

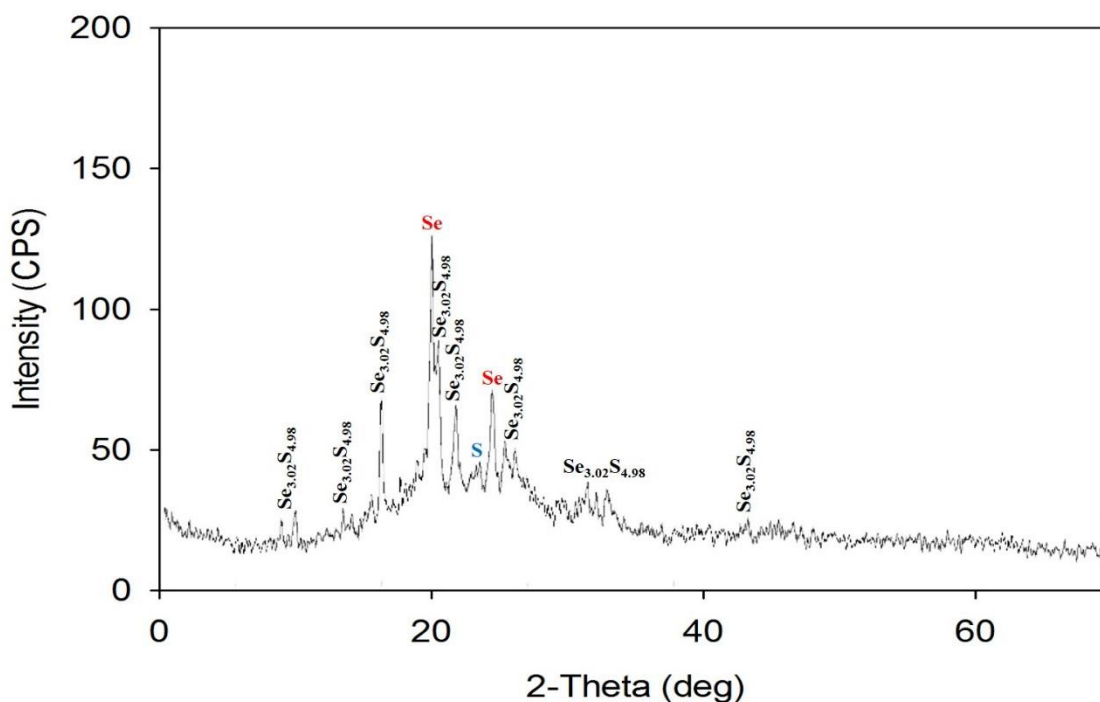


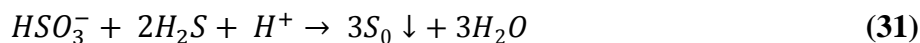
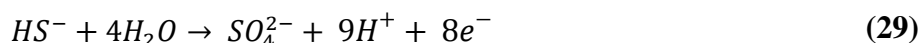
Figure 39. Peak assignments of XRD pattern of the precipitates formed from selenium-sulfide solution in the presence of UV. Experimental conditions: $[\text{Se(IV)}]_0 = 2.54 \text{ mM}$, $[\text{S}^{2-}]_0 = 7.66 \text{ mM}$, light intensity = $6977 \mu\text{W}/\text{cm}^2$, and pH 7.

5.5 Reaction Mechanism of Se(IV) Reduction by Sulfide

A proposed mechanism for the reduction of Se(IV) by sulfide in the absence and presence of UV will be presented in this section based on the UV absorbance measurements, XPS and XRD results. At pH 7, HS^- and H_2S co-exist and HSeO_3^- is the dominant selenium species and SeO_3^{2-} exist as well as a minor species. The presence of Se(-II) from XPS results indicates the reduction of selenite to lower oxidation states than Se(0) in the presence of high sulfide dose. As shown in Figure 23, maximum selenite removal, theoretically, is achieved at S^{2-}/Se molar ratio of 2.6-3, regardless of the presence of UV light.

As shown Eq. (24) – Eq. (27), HS^- is the primary sulfur species involved in the reduction of selenite. According to XPS results at pH 7, with S^{2-}/Se molar ratio of 46 in the absence of UV, the species present are H_2O , HSO_3^- , SO_4^{2-} , S^{2-} , $Se(0)$ and $Se(-II)$. From the equations above (Eq. (32) – Eq. (35)), the formation of H_2O , $Se(0)$ and $Se(-II)$ are proposed.

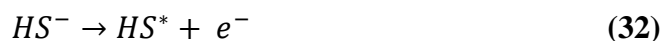
The oxidation of bisulfide ion to sulfate can be represented by the half-reaction shown in Eq. (29), and the oxidation of elemental sulfur to bisulfite takes place as shown in Eq. (31) where the yellow color of the precipitates formed proves the formation of elemental sulfur.⁹⁴ An alternative path for sulfur production in the reaction is reported by De Carvalho²⁰ as shown in Eq. (31).



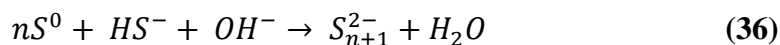
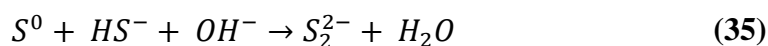
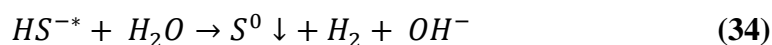
High-resolution S 2p de-convolution spectra show no elemental sulfur peak, only S_n^{2-} that disappeared over reaction time. This proves that the oxidation of elemental sulfur took place. Therefore, in the absence of UV light, selenite will react with H_2S to produce elemental selenium and elemental sulfur.

On the other hand, in the presence of UV light, the photolysis of HS^- occurs but the reaction of HS^- and $Se(IV)$ is rapid enough to be completed before a significant amount of HS^- is photolyzed. The major difference between the presence and absence of UV light is the side reactions of the produced species due to HS^- photolysis.

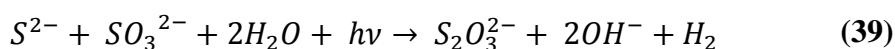
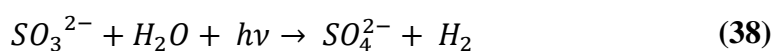
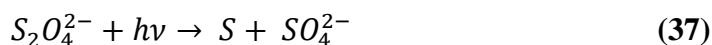
In the presence of UV light, the detection of Se(-II) by XPS results indicates the formation of Se-S precipitates, and the presence of S(-II) indicates the formation of SeS₂ precipitates or due to excess sulfide concentration (Eq. (1)). According to XPS results at pH 7, with S²⁻/Se molar ratio of 46 in the absence of UV, the species present are H₂O, HSO₃⁻, SO₃²⁻, SO₄²⁻, S²⁻, S_n²⁻, S(0), Se(0) and Se(-II). Based on the detected species, the following reactions are proposed to take place in the system when the solution is irradiated with UV light. Steudel⁹⁵ reported that at pH 7, S* is more reactive radical compared to HS*, where HS* is produced when HS⁻ is exposed to free electrons; refer to Eq. (32) and Eq. (33).⁹⁵



The produced sulfur radical will react spontaneously via dimerization, producing S₂²⁻, which can react with sulfur radical (S^{*-}) to produce disulfide radical (S₂^{*-}).⁹⁵ Steudel⁹⁵ reported that disulfide radical can combine with sulfur radical producing trisulfide (S₃²⁻) or dimerize to produce tetrasulfide (S₄²⁻). Larger polysulfides can be produced by analogous reaction approach, or trisulfide and tetrasulfide can be oxidized by HS* or S*⁻ to form S_n²⁻.⁹⁵ This explains the presence of elemental sulfur and polysulfide ions in precipitated solids identified by XPS results under UV irradiation (Figure 17 and Figure 26); refer to Eq. (34) – Eq. (36).

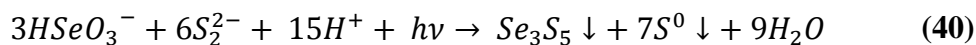


Additionally, the broad peak at high wavelength (Figure 17) was not present when absorbance of Se-S solution was measured (Figure 26), indicating the consumption of these species during the reaction and there was no significant increase in pH at S²⁻/S molar ratio of 46, but there was 0.97 increase in pH (from 7.09 to 8.06) when S²⁻/S molar ratio was 115. This can be described by the following reactions⁷¹,



Furthermore, Eq. (24) – Eq. (27) supports the formation of H₂O, and Se(0) in the presence of UV as well. From the proposed reactions above, H₂S is not directly involved in the reduction of Se(IV); rather it dissociates to maintain the equilibrium in the system. This is supported by the absorbance data (Figure 26). In the presence of UV, the 230 nm peak decreases drastically with time indicating the consumption of HS⁻.

Figure 39 shows the presence of Se-S precipitates having a formula of Se_{3.02}S_{4.98} (Se₃S₅). In the presence of UV light, the reaction between hydrogen sulfide and disulfide produced by sulfide photolysis can be expressed as shown in Eq. (40).



6. CONCLUSION

Reductive precipitation was a major reaction mechanism for selenite removal. Selenite was effectively reduced by sulfide at neutral pH and anoxic conditions. Complete removal of selenite was achieved at molar ratios of sulfide dose to initial Se(IV) concentration above 11.5. The reaction between the two species involves the reduction of selenite and oxidation of sulfide to their elemental states or the formation of Se-S precipitates. These results were confirmed by solids analysis. XPS results obtained for all experimental conditions investigated, high-resolution S 2p and Se 3d narrow scan showed peaks attributed to elemental sulfur and elemental selenium, respectively. UV light irradiation did not affect the removal efficiency or the kinetics of selenite removal. However, UV light affected the morphology and composition of the precipitated solids. SEM/EDS analysis of solids formed showed that particle morphology was affected by sulfide dose and irradiation time, and the presence of UV light. More irregular particles aggregates were formed in the presence of UV light, indicating the formation Se-S precipitates. Aggregates with layered plate shape were formed in the absence of UV light, indicating the formation of elemental selenium.

These results were confirmed by XRD analysis. XRD patterns showed that in the absence of UV light irradiation, elemental selenium was dominant. Whereas, when the solution was irradiated with UV light, Se-S precipitates consisting of 8-member ring molecules (Se_3S_5) were formed beside elemental selenium.

The presence of HA affected the kinetics and removal efficiency. As the concentration of HA increased, the removal efficiency of Se(IV) decreased. For prolonged UV irradiation over time in the presence of HA, Se(IV) removal was enhanced at long reaction times. The presence of sulfate and carbonate, at the tested conditions, did not have significant effects on the kinetics of Se(IV) removal.

REFERENCES

1. Lemly AD. Aquatic selenium pollution is a global environmental safety issue. *Ecotoxicol. Environ. Saf.* 2004;59(1):44-56. doi:10.1016/S0147-6513(03)00095-2.
2. Environmental Protection Agency. Consumer factsheet on: Selenium. *National Primary Drinking Water Regulations*. 1974. Available at: <http://www.epa.gov/ogwdw/pdfs/factsheets/ioc/selenium.pdf>.
3. Janz DM. Selenium. Fish physiology: Homeostasis and toxicology of essential metals. *Elsevier Inc.* 2011;31(11):327-374. doi:10.1016/S1546-5098(11)31007-2.
4. Walker HH, Runnels JH, Merryfield R. Determination of trace quantities of selenium in petroleum and petroleum products by atomic absorption spectrometry. *Anal. Chem.* 1976;48(14):2056-2060. doi:10.1021/ac50008a005.
5. Zhang N, Lin LS, Gang D. Adsorptive selenite removal from water using iron-coated GAC adsorbents. *Water Res.* 2008;42(14):3809-3816. doi:10.1016/j.watres.2008.07.025.
6. Peak D, Saha U, Huang P. Selenite adsorption mechanisms on pure and coated montmorillonite: An EXAFS and XANES spectroscopic study. *Soil Sci. Soc. Am. J.* 2006;70:192. doi:10.2136/sssaj2005.0054.
7. Han DS, Batchelor B, Abdel-Wahab A. Sorption of selenium(IV) and selenium(VI) onto synthetic pyrite (FeS₂): spectroscopic and microscopic analyses. *J. Colloid Interface Sci.* 2012;368(1):496-504. doi:10.1016/j.jcis.2011.10.065.
8. Cassella RJ, Sant Ana OD De, Rangel AT, Fatima M De, Santelli RE. Selenium determination by electrothermal atomic absorption spectrometry in petroleum refinery aqueous streams containing volatile organic compounds. *Microchem. J.* 2002;71(1):21-28.

9. Wasewar KL, Prasad B, Gulipalli S. Removal of selenium by adsorption onto granular activated carbon (GAC) and powdered activated carbon (PAC). *CLEAN - Soil, Air, Water* 2009;37:872-883.
10. Smith K, Lau AO, Vance FW. Evaluation of treatment techniques for selenium removal. In: *70th Annual International Water Conference*. Orlando, Florida, USA: Engineerings Society of Western Pennsylvania (ESWP); 2009:35-52.
11. EPA. Basic information about selenium in drinking water. 2014. Available at: <http://water.epa.gov/drink/contaminants/basicinformation/selenium.cfm>. Accessed June 1, 2015.
12. EPA. Effluent limitation guidelines and standards for the steam electric power point source category: Final Rule. 2015;80.
13. Han DS, Batchelor B, Abdel-Wahab A. Sorption of selenium(IV) and selenium(VI) to mackinawite (FeS): effect of contact time, extent of removal, sorption envelopes. *J. Hazard. Mater.* 2011;186(1):451-7. doi:10.1016/j.jhazmat.2010.11.017.
14. Lemly AD. Ecological basis for regulating aquatic emissions from the power industry: the case with selenium. *Regul. Toxicol. Pharmacol.* 1985;5(4):465-486. doi:10.1016/0273-2300(85)90010-8.
15. Mayland BHF, Gough LP, Stewart KC. Selenium mobility in soils and its absorption, translocation, and metabolism in plants. In: *Symposium on Selenium*. Western U.S.; 2010:57-64.
16. Yang Z. Removal of selenium from wastewater using ZVI and hybrid ZVI/iron oxide process. [Master's thesis]. Texas A&M University. 2012.
17. CDC. Public health statement: Selenium. *Agency Toxic Subst. Dis. Regist.* 2003;(September):1-10. Available at: <http://www.atsdr.cdc.gov/ToxProfiles/tp201-c1.pdf>.

18. Twidwell LG, McCloskey J, Miranda P, Gale M. Technologies and potential technologies for removing selenium from process and mine wastewater. In: *REWAS'99 Global Symposium on Recycling, Waste Treatment and Clean Technology*. San Sabastian, Spain; 1999:1645-1656.
19. Kauffman JW, Laughlin WC, Baldwin RA. Microbiological treatment of uranium mine waters. *Environ. Sci. Technol.* 1986;20(3):243–248. doi:10.1021/es00145a003.
20. Geoffroy N, Demopoulos GP. Reductive precipitation of elemental selenium from selenious acidic solutions using sodium dithionite. *Ind. Eng. Chem. Res.* 2009;48(23):10240-10246. doi:10.1021/ie9008502.
21. Geoffroy N, Demopoulos GP. The elimination of selenium(IV) from aqueous solution by precipitation with sodium sulfide. *J. Hazard. Mater.* 2011;185(1):148-54. doi:10.1016/j.jhazmat.2010.09.009.
22. Golder Associates Inc. Literature review of treatment technologies to remove selenium from mining influenced water. Technical Bulletin No. 08-1421-0034 Rev. 2, *Tech Coal Limited*, Office: Lakewood, Co. 2009.
23. Sandy T, DiSante C. NAMC Final report: Review of available technologies for the removal of selenium from water. *North American Metals Council: CH2M Hill.* 2010.
24. WHO. Selenium in drinking-water: background document for development of WHO guidelines for drinking-water quality. *World Heal. Organ. Geneva* 2011. doi:WHO/HSE/WSH/10.01/14.
25. LaDrega M, Buckingham PL, Evans JC. *Hazardous Waste Management*. 2nd Edition. Long Grove, Ill. : Waveland Press, Inc; 2010.
26. Frankenberger WT, Engberg RA. *Environmental Chemistry of Selenium.*; CRC Press. Marcel Dekker, Inc: New York. 1998.

27. Bouroushian M. *Electrochemistry of Metals Chalcogenides*. 1st Edition. Springer-Verlag Berlin Heidelberg; 2010. doi: 10.1007/978-3-642-03967-6.
28. Ralston N, Unrine J, Wallschläger D. Biogeochemistry and analysis of selenium and its species. *North American Metals Council*. Washington, D.C., 2010;1:1-58.
29. Abdel-Wahab A. Advanced reduction processes for destroying persistent oxidized contaminants. In: *Annual TAMUQ-QAFCO Conference*. Doha, Qatar; 2013.
30. Dabkowski B. Applying oxidation reduction potential sensors in biological nutrient removal systems. *Proc. Water Environ. Fed.* 2008;2008(13):3033-3042. doi:10.2175/193864708788733341.
31. Bye R. Critical examination of some common reagents for reducing selenium species in chemical analysis. *Pergamon Press Ltd* 1983;30(12):993-996. doi:10.1016/0039-9140(83)80232-X
32. Murty ASR. Thiourea in analysis: Part I - Estimation of selenium and tellurium. Karnatak University, Dharwar. *Indian J. Chem* 1965;3:298-299.
33. Schoeller WR. Stannous chloride as a quantitative reagent for selenium and tellurium. *Royal Society Chemistry*. 1939;64:318-323. doi: 10.1039/AN9396400318.
34. Tomicek O. Determination of selenium and of tellurium by means of titanium trichloride. *Bull. Soc. Chim* 1972;41:1389-1399.
35. Marchant WN, Dannenberg RO, Brooks PT. *Selenium Removal from Acidic Waste Water Using Zinc Reduction and Lime Neutralization: Report of Investigation 8312*. Salt Lake City, UT; 1978.
36. Ling L, Pan B, Zhang W. Removal of selenium from water with nanoscale zero-valent iron: Mechanisms of intraparticle reduction of Se(IV). *Water Res.* 2015;71(34):274-281. doi:10.1016/j.watres.2015.01.002.

37. Schalk S, Adam V, Arnold E, Brieden K, Voronov A, Witzke H. UV-Lamps for disinfection and advanced oxidation - Lamp types, technologies and applications. *IUVA News* 2005;8(1):32-37.
38. Bensalah N, Nicola R, Abdel-Wahab a. Nitrate removal from water using UV-M/S₂O₄²⁻ advanced reduction process. *Int. J. Environ. Sci. Technol.* 2013;11(6):1733-1742. doi:10.1007/s13762-013-0375-0.
39. Liu X, Zhang T, Shao Y. Aqueous bromate reduction by UV activation of sulfite. *CLEAN - Soil, Air, Water* 2014;42(10):1370-1375. doi:10.1002/clen.201300646.
40. Yoon S, Han DS, Liu X, Batchelor B, Abdel-Wahab A. Degradation of 1,2-dichloroethane using advanced reduction processes. *J. Environ. Chem. Eng.* 2014;2(1):731-737. doi:10.1016/j.jece.2013.11.013.
41. Vellanki BP, Batchelor B, Abdel-Wahab A. Advanced Reduction Processes: A New Class of Treatment Processes. *Environ. Eng. Sci.* 2013;30(5):264-271. doi:10.1089/ees.2012.0273.
42. Liu X, Yoon S, Batchelor B, Abdel-Wahab A. Photochemical degradation of vinyl chloride with an Advanced reduction process (ARP) - effects of reagents and pH. *Chem. Eng. J.* 2013;215-216:868-875. doi:10.1016/j.cej.2012.11.086.
43. Vellanki BP, Batchelor B. Perchlorate reduction by the sulfite/ultraviolet light advanced reduction process. *J. Hazard. Mater.* 2013;262:348-56. doi:10.1016/j.jhazmat.2013.08.061.
44. Liu X, Yoon S, Batchelor B, Abdel-Wahab A. Photochemical degradation of vinyl chloride with an advanced reduction process (ARP) – effects of reagents and pH. *Chem. Eng. J.* 2013;215-216:868-875. doi:10.1016/j.cej.2012.11.086.
45. Liu X, Yoon S, Batchelor B, Abdel-Wahab A. Degradation of vinyl chloride (VC) by the sulfite/UV advanced reduction process (ARP): effects of process variables and a kinetic model. *Sci. Total Environ.* 2013;454-455:578-83. doi:10.1016/j.scitotenv.2013.03.060.

46. Bensalah N, Liu X, Abdel-Wahab A. Bromate reduction by ultraviolet light irradiation using medium pressure lamp. *Int. J. Environ. Stud.* 2013;70(4):566-582. doi:10.1080/00207233.2013.813755.
47. Weiner ER. *Applications of Environmental Aquatic Chemistry - A Practical Guide*. 2nd Edition. CRC Press. Taylor and Francis Group, New York; 2008. doi:10.1201/9781420008371.
48. Linkous C, Huang C, Fowler JR. UV photochemical oxidation of aqueous sodium sulfide to produce hydrogen and sulfur. *J. Photochem. Photobiol. A Chem.* 2004;168(3):153-160. doi:10.1016/j.jphotochem.2004.03.028.
49. Dzhabiev TS, Tarasov BB. Photochemical decomposition of an aqueous solution of sodium sulphide. *J. Photochem. Photobiol. A Chem.* 1993;72:23-27. doi:10.1016/1010-6030(93)85080-R.
50. Dogliotti L, Hayon E. Flash photolysis study of sulfite, thioeyanate, and thiosulfate ions in solution. *J. Phys. Chem.* 1968;72.
51. Fennema OR. *Food Chemistry*. 3rd Edition. Marcel Dekker, Inc. New York; 1996. ISBN 10: 0824793463.
52. Hemat RAS. *Principles of Orthomolecularism*. Urotext, London; 2004. ISBN: 1-903737-05-2 (e).
53. Yu C, Luo M, Zeng F, Wu S. A fast-responding fluorescent turn-on sensor for sensitive and selective detection of sulfite anions. *Anal. Methods* 2012;4(9):2638. doi:10.1039/c2ay25496d.
54. Horvath AK, Nagypal I. Kinetics and mechanism of the oxidation of sulfite by chlorine dioxide in a slightly acidic medium. *J. Phys. Chem. A* 2006;110(14):4753-8. doi:10.1021/jp060246b.
55. Hayon E, Treinin a., Wilf J. Electronic spectra, photochemistry, and autoxidation mechanism of the sulfite-bisulfite-pyrosulfite systems. SO₂⁻, SO₃⁻, SO₄⁻, and

- SO5-radicals. *J. Am. Chem. Soc.* 1972;94(1):47–57. doi:10.1021/ja00756a009.
56. Getman FH. The ultraviolet absorption spectra of aqueous solutions of sulphur dioxide and some of its derivatives. *J. Phys. Chem.* 1925;30(2):266-276. doi:10.1021/j150260a008.
57. Holman DA, Bennett DW. A multicomponent kinetics study of the anaerobic decomposition of aqueous sodium dithionite. *J. Phys. Chem.* 1994;98:13300-13307.
58. Cermak V, Smutek M. Mechanism of decomposition of dithionite in aqueous solutions. *Collect. Czechoslov. Chem. Commun.* 1975;40(11):3241-3264. doi:10.1135/cccc19753241.
59. Burlamacchi L, Guarini G, Tiezzi E. Mechanism of decomposition of sodium dithionite in aqueous solution. *Trans. Faraday Soc.* 1969;65:496. doi:10.1039/tf9696500496.
60. Youssif S. Recent trends in the chemistry of pyridine N-oxide. *Russ. Acad. Sci. Turpion Ltd* 2001;2001(1):242-268. doi:10.3998/ark.5550190.0002.116.
61. Ellis ME. The technology of mechanical pulp bleaching: Hydrosulfite (dithionite) bleaching. In: *Pulp Bleaching; Principles and Practice.*; 1996:491-512.
62. Spencer MS. Chemistry of sodium dithionite. Part 1 - Kinetics of decomposition in aqueous bisulphite solution. *R. Soc. Chem.* 1967;63:2510-2515. doi: 10.1039/TF9676302510.
63. Lindholm CA. Handbook for pulp & paper technologies, *Papermaking Science and Technology: Mechanical Pulping*, Chapter 11: Bleaching. TAPPI Press, Helsinki, Finland. 1999: 311-343.
64. Amonetter JE., Szecsody JE., Schaef HT., Templeton JC., Gorby YA., Fruchter JS. Abiotic reduction of aquifer materials by dithionite: A promising in-situ remediation technology. *J. Chem. Inf. Model.* 1994;53:160.

doi:10.1017/CBO9781107415324.004.

65. Lambeth DO., Palmer G. Kinetics and mechanism of reduction of electron transfer proteins and other compounds of biological interest by dithionite. *J. Biol. Chemisry* 1973;248(17):6095-6103.
66. ThermoScientific. *Cimarec Stirring Hot Plates: Operation manual and parts list.*; 2009.
67. CasaXPS. Basic quantification of XPS spectra. *Casa Software. Ltd.* 2008:1-7. Available at:
http://www.casaxps.com/help_manual/manual_updates/Basics_Quantification_of_XPS_Spectra.pdf.
68. Sasaki K, Blowes DW., Ptacek CJ. Spectroscopic study of precipitates formed during removal of selenium from mine drainage spiked with selenate using permeable reactive materials. *Geochem. J.* 2008;42(1999):283-294.
69. Guenther EA., Johnson KS., Coale KH, Landing M, Laboratories M, Landing M. Direct ultraviolet spectrophotometric determination of total sulfide and iodide in natural waters. *Am. Chem. Soc.* 2001;73(14):3481-3487.
70. Gustafsson JP. Visual MINTEQ 3.1, beta. 2013.
71. Hara K, Sayama K, Arakawa H. UV photoinduced reduction of water to hydrogen in Na₂S , Na₂SO₃ , and Na₂S₂O₄ aqueous solutions. *J. Photochem. Photobiol. A Chem.* 1999;128:27-31.
72. Naumkin AV., Kraut-Vass A, Gaarenstroom SW, Powell CJ. NIST X-ray photoelectron spectroscopy database. *Natl. Inst. Stand. Technol.* 2012.
73. Naveau F, Monteil-rivera F, Guillon E. Interactions of aqueous selenium(-II) and (IV) with metallic sulfide surfaces. *Environ. Sci. Technol.* 2007;41(15):5376-5382.

74. Smart RSC, Skinner WM, Gerson AR. XPS of sulphide mineral surfaces: Metal-deficient, polysulphides, defects and elemental sulphur. *John Wiley Sons, Ltd* 1999;105(November 1998):101-105.
75. Rickett BI, Payer JH. Composition of copper tarnish products formed in moist air with trace levels of pollutant Gas: sulfur dioxide and sulfur dioxide/nitrogen dioxide. *J. Electroanal Chem.* 1995;142(11).
76. Lindberg J, Hamrin K, Johansson G, et al. Molecular spectroscopy by means of ESCA. II. Sulfur compounds. Correlation of electron binding energy with structure. *Phys. Scr.* 1970;1:286-298.
77. Kretzschmar J, Jordan N, Brendler E, et al. Spectroscopic evidence for selenium(IV) dimerization in aqueous solution. *R. Soc. Chem.* 2015:10508-10515. doi:10.1039/c5dt00730e.
78. Hockin SL, Gadd GM. Linked redox precipitation of sulfur and selenium under anaerobic conditions by sulfate-reducing bacterial biofilms. *Am. Soc. Microbiol.* 2003;69(12):7063-7072. doi:10.1128/AEM.69.12.7063.
79. Scheinost AC, Kirsch R, Banerjee D, et al. X-ray absorption and photoelectron spectroscopy investigation of selenite reduction by FeII -bearing minerals. *J. Contam. Hydrol.* 2008;102(3-4):228-245. doi:10.1016/j.jconhyd.2008.09.018.
80. Doyle COSD, Endelewicz TOMK, Ostick BECB, Rown GOEB. Soft X-ray spectroscopic studies of the reaction of fractured pyrite surfaces with Cr(VI)-containing aqueous solutions. *Elsevier* 2004;68(21):4287-4299. doi:10.1016/j.gca.2004.02.015.
81. Li B, Liu N, Li Y, et al. Reduction of selenite to red elemental selenium by rhodospseudomonas palustris strain N. *PLoS One* 2014;9(4):1-10. doi:10.1371/journal.pone.0095955.
82. Laboratory LN. Periodic Table of Elements: Selenium. Available at: <http://periodic.lanl.gov/34.shtml> . Accessed February 9, 2015.
83. Wei M, Wang K, Hsiao T, et al. Effects of UV irradiation on humic acid removal

- by ozonation, Fenton and Fe0 air treatment: THMFP and biotoxicity evaluation. *J. Hazard. Mater.* 2011;195:324-331. doi:10.1016/j.jhazmat.2011.08.044.
84. Kamei-ishikawa N, Nakamaru Y, Tagami K, Uchida S. Sorption behavior of selenium on humic acid under increasing selenium concentration or increasing solid/liquid ratio. *J. Environmental Radioact.* 2008;99:993-1002. doi:10.1016/j.jenvrad.2007.11.005.
85. Imai D, Dabwan AHA, Kaneco S, et al. Degradation of marine humic acids by ozone-initiated radical reactions. *Chem. Eng. J.* 2009;148:336-341. doi:10.1016/j.cej.2008.09.013.
86. Li X, Chii S, Qi Z. Effect of Fe(III) on the bromate reduction by humic substances in aqueous solution. *J. Environmental Sci.* 2008;20:257-261.
87. Abate G, Masini JC. Influence of pH and ionic strength on removal processes of a sedimentary humic acid in a suspension of vermiculite. *Colloids Surfaces A Physicochem. Eng. Asp.* 2003;226:25-34. doi:10.1016/S0927-7757(03)00418-7.
88. Carvalho LM De, Schwedt G, Henze G, Sander S. Redoxspeciation of selenium in water samples by cathodic stripping voltammetry using an automated flow system. *ARoyal Soc. Chem.* 1999:1803-1809.
89. Kamei-Ishikawa N, Tagami K, Uchida S. Sorption kinetics of selenium on humic acid. *J. Radioanal. Nucl. Chem.* 2007;274(3):555-561. doi:10.1007/s10967-006-6951-8.
90. Wang W, Wang W, Fan Q, Wang Y, Qiao Z, Wang X. Effects of UV radiation on humic acid coagulation characteristics in drinking water treatment processes. *Chem. Eng. J.* 2014;256:137-143. doi:10.1016/j.cej.2014.06.113.
91. Fujikawa Y, Fukui M. Radionuclide sorption to rocks and minerals: Effects of pH and inorganic Anions. Part 2. Sorption and speciation of selenium. *Radiochim. Acta* 1997;76(3):163-172.

92. Goh K, Lim T. Geochemistry of inorganic arsenic and selenium in a tropical soil: effect of reaction time , pH , and competitive anions on arsenic and selenium adsorption. *Chemosphere* 2004;55:849-859. doi:10.1016/j.chemosphere.2003.11.041.
93. Šedo O, Alberti M, Havel J. Laser ablation synthesis of new binary chalcogen molecules from the selenium – sulfur system. *Polyhedron* 2005;24:639-644. doi:10.1016/j.poly.2005.01.012.
94. Geoffroy N. Selenium removal from aqueous solutions. [Doctoral dissertation]. McGill University. Montréal, Canada. 2011;(March).
95. Steudel R. Mechanism for the formation of elemental sulfur from aqueous sulfide in chemical and microbiological desulfurization processes. *Ind. Eng. Chem. Res.* 1996:1417-1423. doi:10.1021/ie950558t.
96. Robinson JW, Frame EMS, Frame II GM. *Undergraduate Instrumental Analysis*. 7th Edition. CRC Press; 2014.
97. Mycroft JR, Bancroft GM, McIntyre NS, Lorimer JW, Hill IR. Detection of sulphur and polysulphides on electrochemically oxidized pyrite surfaces by X-ray photoelectron spectroscopy and Raman spectroscopy. *J. Electroanal Chem.* 1990;292:139-152.
98. Sekiyama H, Kosugi N, Kuroda H, Ohta T. Sulfur K-edge absorption spectra of Na₂SO₄, Na₂SO₃, Na₂S₂O₃, and Na₂S₂O_x (x=5-8). *Bull. Chem. Soc. Jpn.* 1986;(59):575-579.
99. Liang X, Hart C, Pang Q, Garsuch A, Weiss T, Nazar LF. A highly efficient polysulfide mediator for lithium – sulfur batteries. *Nat. Commun.* 2015;6:1-8. doi:10.1038/ncomms6682.
100. Strandberg H, Johansson L. The formation of black patina on copper in humid air containing traces of SO₂. *Electrochem. Soc. Inc* 1997;144(1):81-89.

101. Peterson PJ. *Corrosion of Electronic and Magnetic Materials*. Philadelphia: ASTM; 1992.
102. Watanabe M, Ando H, Handa T. Comparative XPS study of silver and copper surfaces exposed to flowing air containing low concentration of sulfur dioxide exposed to flowing air containing low concentration. *Zairyo-to-Kankyo* 2007;(56):10-15.
103. Briggs D, Seah MP. *Practical Surface Analysis, Auger and X-Ray Photoelectron Spectroscopy*. 2nd Edition. New York: John Wiley & Sons Inc; 1993.
104. Shenasa M, Sainkar S, Lichtman D. XPS study of some selected selenium compounds. *J. Electron Spectros. Relat. Phenomena* 1986;40:329-337.
105. Wagner CD, Riggs WM, Davis LE, Moulder JF. *Handbook of X-Ray Photoelectrons Spectroscopy*. Eden Prarie: Perkin-Elmer Corporation; 1979.
106. Hamdadou N, Bernede JC, Khelil A. Preparation of iron selenide films by selenization technique. *J. Cryst. Growth* 2002;241:313-319.

APPENDIX A

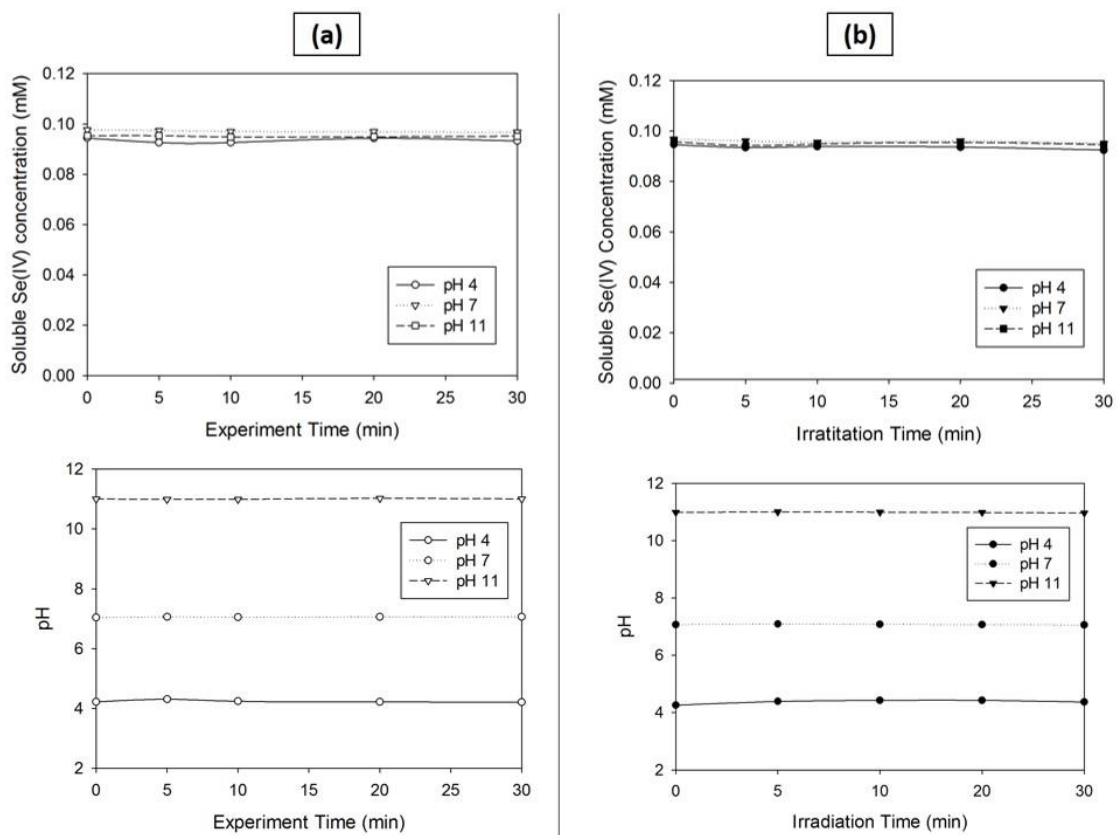


Figure A1. Selenite concentrations and pH changes in blank control (no reagent, no UV) (a) and light control (no sulfide, UV-L) (b). Experimental conditions: $[\text{Se(IV)}]_0 = 0.11 \text{ mM}$, light intensity = $6298 \mu\text{W}/\text{cm}^2$.

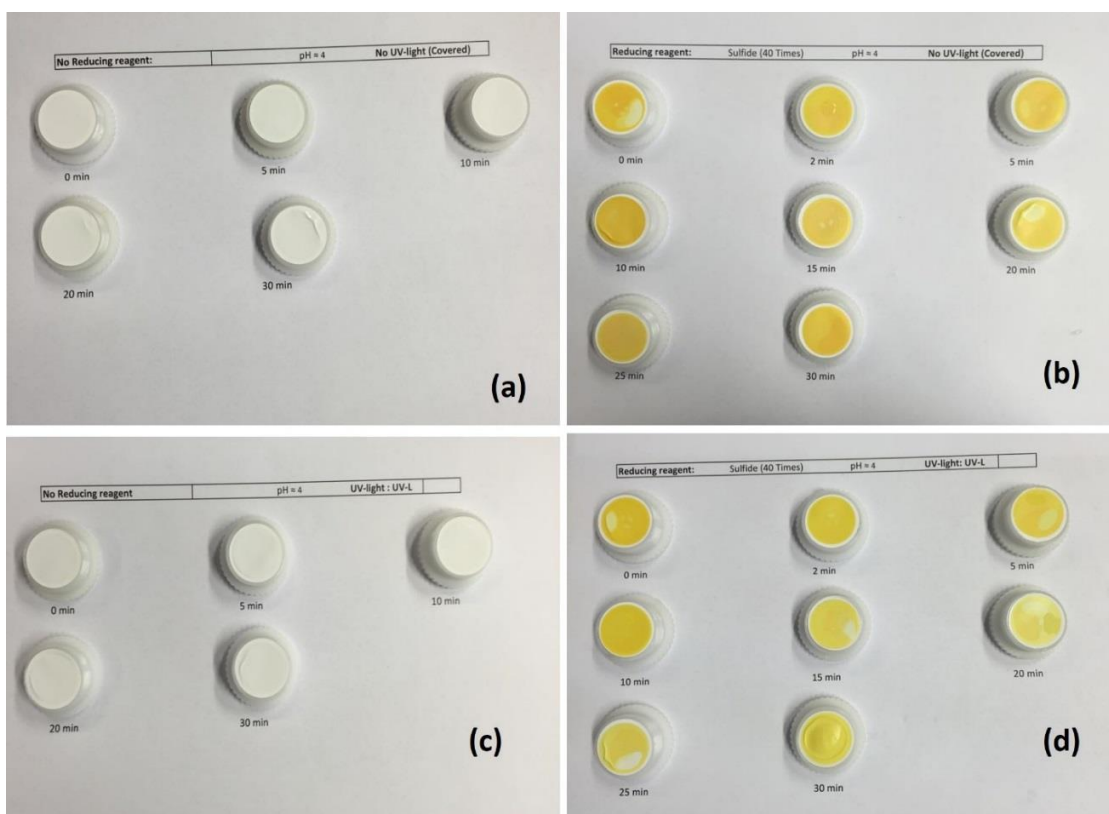


Figure A2. Solids produced in Se^{4+} - S^{2-} solution at pH 4 in a blank (a), light control (b), reagent control (c), and reactor (d). Experimental conditions: the initial Se concentration was 0.11 mM and UV light intensity = $6442 \mu\text{W}/\text{cm}^2$.

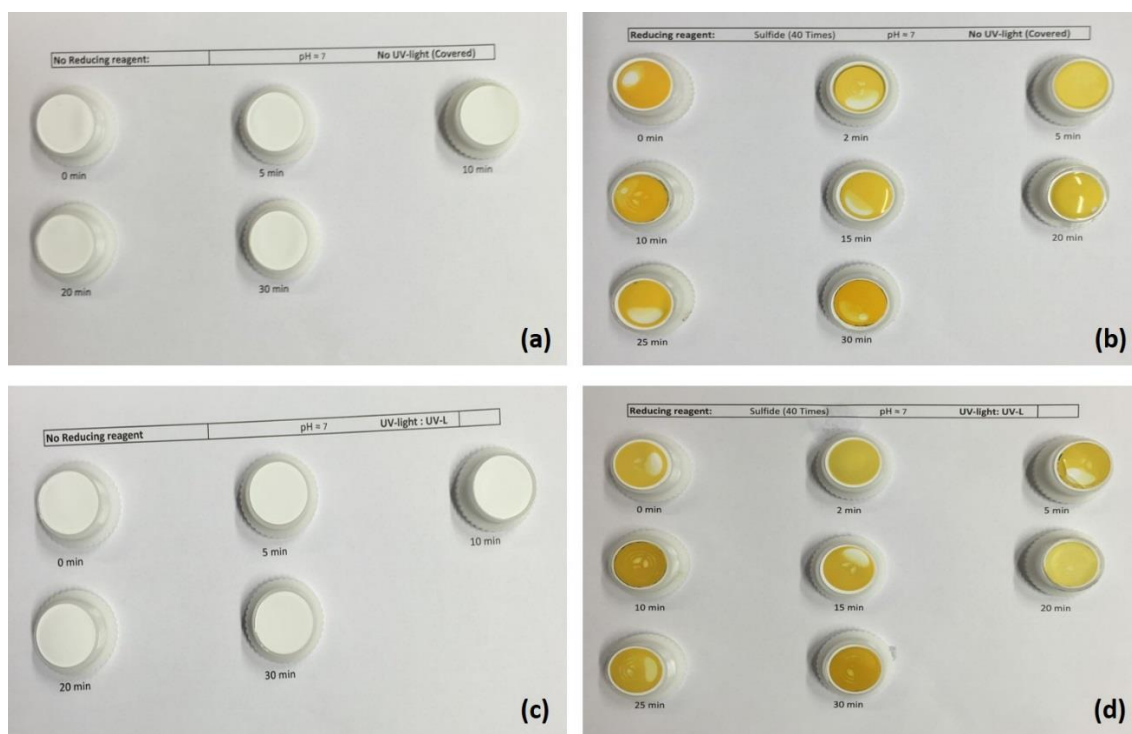


Figure A3. Solids produced in $\text{Se}^{4+}\text{-S}^{2-}$ solution at pH 7 in a blank (a), light control (b), reagent control (c), and reactor (d). Experimental conditions: the initial Se concentration was 0.11 mM and UV light intensity = $6520 \mu\text{W}/\text{cm}^2$.

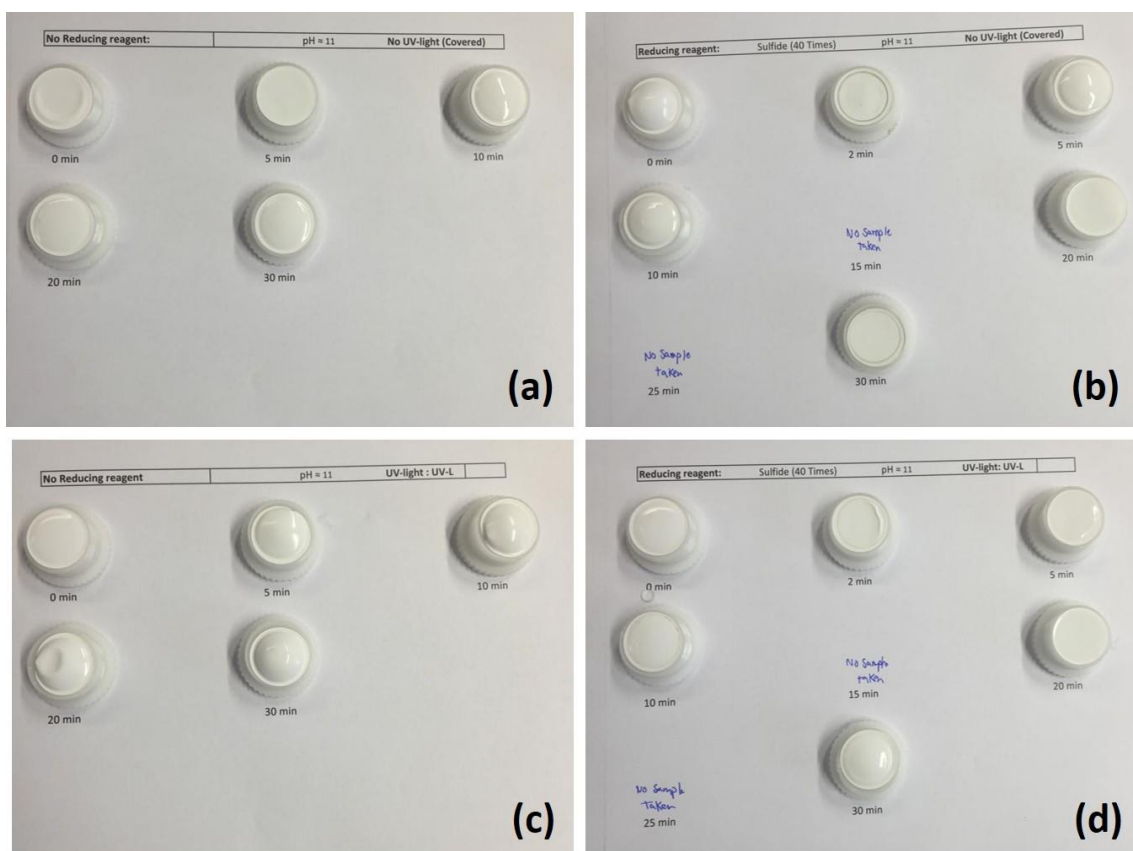


Figure A4. Solid formation throughout the experiment at pH 11. (a) Se and no UV-L. (b) Se and Sulfide and no UV-L. (c) Se and UV-L. (d) Se and Sulfide and UV-L. Experimental conditions: $[\text{Se(IV)}]_0 = 0.11 \text{ mM}$, light intensity = $6298 \mu\text{W}/\text{cm}^2$.

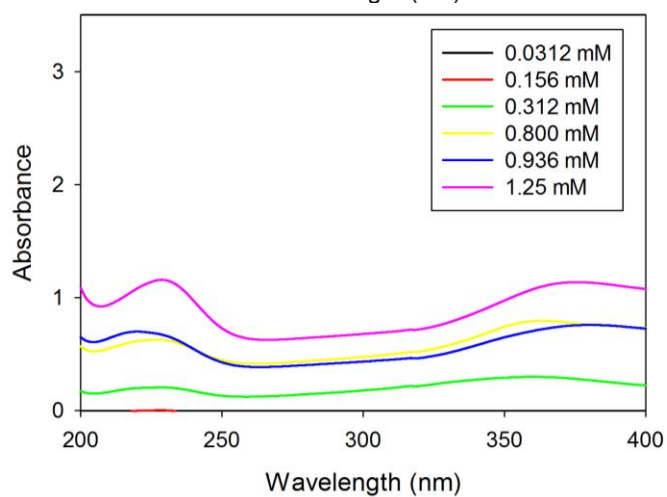
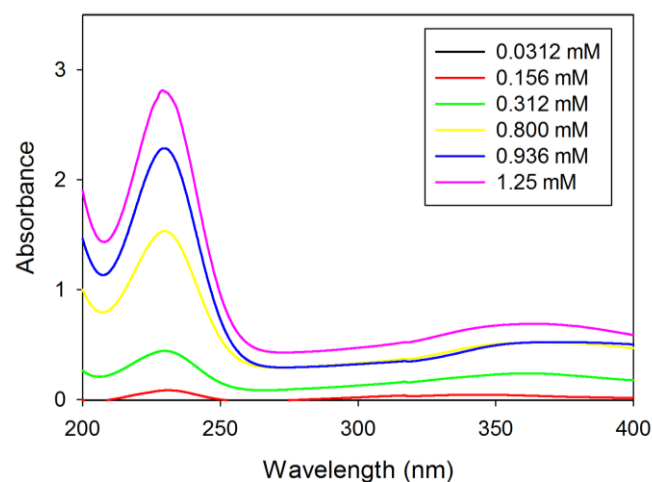
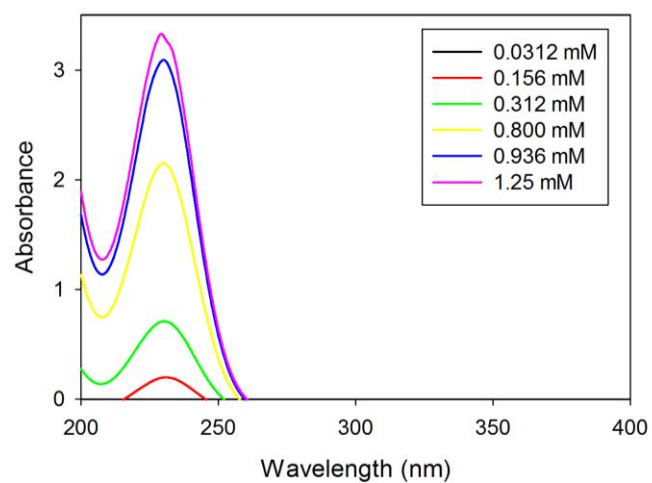


Figure A5. Absorbance spectra of Se-sulfide solution for different concentration in the absence of UV light (a), in the presence of UV-L light for 10 min (b) and the presence of UV-L light for 30 min. Experimental conditions: light intensity = $4041 \mu\text{W}/\text{cm}^2$, and pH 7.

Table A1. Binding energies of O 1s XPS spectra from the literature.

Species	BE (eV)	Formula	Reference
O 1s	532.8, 533.1, 533.3, 534.8, 535.1, 538	H ₂ O	⁷²
O 1s	532.2, 534.2	H ₂ O	⁷⁹
O 1s	531.1, 531.3, 532.1	Na ₂ SO ₄	⁷²
O 1s	532.3	Na ₂ SO ₄	⁷⁶
O 1s	532.5	H ₂ SO ₄	⁷²
O 1s	531.9	CuSO ₄	⁷⁵
O 1s	530.7, 531.2, 531.7	Na ₂ SO ₃	⁷²
O 1s	531.9	Na ₂ SO ₃	⁷⁶
O 1s	531.4	NaHSO ₃	⁷⁵
O 1s	531.6, 531.8	Na ₂ S ₂ O ₃	⁷²
O 1s	531.4	Na ₂ S ₂ O ₃	⁷⁵
O 1s	531.8	Na ₂ S ₂ O ₃	⁷⁶
O 1s	531.3	Na ₂ S ₂ O ₄	⁷⁵
O 1s	531.8	Na ₂ S ₂ O ₅	⁷⁶
O 1s	531.6	Na ₂ S ₂ O ₆	⁷²
O 1s	529.4, 529.9, 530.1	Se ₂ O ₃	⁷²
O 1s	531.0, 531.1	OH ⁻	⁷⁹
O 1s	531.2	Cu(OH) ₂	⁷⁵

Table A2. Assignment of S 2p_{3/2} from elemental sulfur collected from the literature.

Spectral line	BE (eV)	Formula	Chemical state	reference
S 2p	163.6, 164	S	S(0)	⁷²
S 2p _{3/2}	162.9-164.8	S	S(0)	⁷²
S 2p _{3/2}	162.9-164.8	S ₈	S(0)	⁷²
S 2p	163.6, 164	S ₈	S(0)	⁷²
S 2p	164	S ₈	S(0)	⁷²
S 2p _{3/2}	164.5	S	S(0)	⁷⁹
S 2p _{3/2}	164.0	S	S(0)	⁹⁶
S 2p _{3/2}	163.6-164.2	Sulfur bulk (S ₈ ⁰)	S(0)	⁹⁷
S 2p _{3/2}	163.2-163.6		S(0)	⁷⁴

Table A3. Assignment of S 2p_{3/2}: sulfides (S²⁻, S₂²⁻) and polysulfides (S_n²⁻) from the published data.

Spectral line	BE (eV)	Formula	Chemical State	Reference
S 2p _{3/2}	160.6	Na ₂ S	S ²⁻	72
S 2p _{3/2}	161.8	Na ₂ S	S ²⁻	72
S 2p _{3/2}	161.2-162.8		S ²⁻	7
S 2p _{3/2}	162.3		S ²⁻	79
S 2p _{3/2}	162.3	Bulk	S ²⁻	79
S 2p _{3/2}	161.5	Surface	S ²⁻	79
S 2p _{3/2}	160.1-161.2		S ²⁻	74
S 2p _{3/2}	162.7-164.1		S ₂ ²⁻	7
S 2p _{3/2}	162.1-162.6	Pyrite FeS ₂	S ₂ ²⁻	74
S 2p _{3/2}	162.5	Pyrite S ₂ ²⁻	S ₂ ²⁻	97
S 2p _{3/2}	161.9-163.2		S _n ²⁻	74
S 2p _{3/2}	163.5		S _n ²⁻	79
S 2p _{3/2}	163.1-163.5		S _n ²⁻	7

Table A4. Binding energies of S 2p components HSO_3^- , SO_3^- , SO_4^{2-} , $\text{S}_2\text{O}_3^{2-}$, $\text{S}_2\text{O}_4^{2-}$, $\text{S}_2\text{O}_5^{2-}$, $\text{S}_2\text{O}_6^{2-}$, $\text{S}_2\text{O}_8^{2-}$, and $\text{S}_4\text{O}_6^{2-}$ from the published data.

Spectral line	BE (eV)	Formula	Reference
S 2p	169	Na_2SO_4	98
S 2p	168.4, 168.6, 169.2	Na_2SO_4	72
S 2p _{3/2}	170.2	SO_4^{2-}	99
S 2p _{3/2}	168.5	SO_4^{2-}	100
S 2p _{3/2}	167.5, 168.6, 168.7, 168.8	Na_2SO_4	72
S 2p	166.7	Na_2SO_3	98
S 2p	166.6, 166.9, 167, 167.4	Na_2SO_3	72
S 2p _{3/2}	165.6, 166.4, 166.6, 167, 167.2	Na_2SO_3	72
S 2p _{3/2}	166.5	Na_2SO_3	100
S 2p _{3/2}	167	SO_3^{2-}	100
S 2p	166.4, 166.7	NaHSO_3	101
S 2p	166.7, 167.4	NaHSO_3	75
S 2p	167.6	NaHSO_3	72
S 2p _{3/2}	166.9	NaHSO_3	72
S 2p	162.5, 162.9, 168.4	$\text{Na}_2\text{S}_2\text{O}_3$	72
S 2p	161.8, 167.9	$\text{Na}_2\text{S}_2\text{O}_3$	101
S 2p	161.8, 167.9	$\text{Na}_2\text{S}_2\text{O}_3$	75
S 2p	167.2, 161.3	$\text{Na}_2\text{S}_2\text{O}_3$	98
S 2p _{3/2}	161.7, 162.4, 162.5, 162.9, 167.7, 162.9, 168.5, 168.6	$\text{Na}_2\text{S}_2\text{O}_3$	72
S 2p _{3/2}	161.7, 167.7	$\text{Na}_2\text{S}_2\text{O}_3$	100
S 2p _{3/2}	167.2	$\text{S}_2\text{O}_3^{2-}$	99
S 2p	166.1, 168.2	$\text{Na}_2\text{S}_2\text{O}_4$	101
S 2p	166.1 168.2	$\text{Na}_2\text{S}_2\text{O}_4$	75
S 2p _{3/2}	166.6	$\text{Na}_2\text{S}_2\text{O}_4$	100
S 2p _{3/2}	165.9, 167.5	$\text{S}_2\text{O}_5^{2-}$	102
S 2p	168.8	$\text{Na}_2\text{S}_2\text{O}_6$	72
S 2p	168.4	$\text{Na}_2\text{S}_2\text{O}_6$	98
S 2p	168.7	$\text{Na}_2\text{S}_2\text{O}_8$	98
S 2p _{3/2}	163.8, 167, 168.8, 169	$\text{Na}_2\text{S}_4\text{O}_6$	72
S 2p _{3/2}	167.2-167.6	$\text{S}_4\text{O}_6^{2-}$	7

Table A5. Se 3d_{5/2} binding energies of selenium compounds from the literatures.

Compound	Oxidation state	Binding energy	References
Se	Se(0)	54.9 eV	103
Se	Se(0)	55.5 eV	104
Se	Se(0)	56.3 eV	105
Se	Se(0)	54.64-57.5	72
Na ₂ SeO ₃	Se(+4)	59.1	72
Na ₂ SeO ₄	Se(+6)	61.6	72
Na ₂ SeO ₃	Se(+4)	58.2 eV	105
Na ₂ SeO ₃	Se(+4)	58.2 eV	73
Na ₂ Se(S ₂ O ₃) ₂	Se(+2)	56.9	72
SeO ₂	Se(+4)	58.5 eV	106
SeO ₂	Se(+4)	58.8, 59.8, and 59.9 eV	72
H ₂ SeO ₃	Se(+4)	59.1 eV	105
H ₂ SeO ₃	Se(+4)	59, and 59.9 eV	72
Pyrite +Se(-II)	Se(-2) or Se(-1)	54.8 eV	73
Pyrite + Se(IV)	Se(-2) or Se(-1)	54.8 eV	73

Table A6. Experimental conditions of samples for XPS analysis.

No.	Molar ratio of [S ²⁻] ₀ /[Se(IV)] ₀	pH ^a	UV ^b	Time ^c (min)
1	11.5	7	Yes	10
2	11.5	7	No	10
3	115	7	No	10
4	46	4	Yes	10
5	46	4	No	10
6	46	7	No	10

^aThe solution pH was buffered to pH 7 using 10 mM phosphate solution, ^bApplied UV light is UV-L lamp (Philips TUV PL-L lamp at 254 nm), and ^cTime is UV irradiation time or reaction time.

Table A7. Binding energies, full width at half maximum (FWHM), and area for peaks in the Se 3d, S 2p, and O 1s XPS spectra of samples 1-9 in this study.

Sample no.	Species	BE (eV)	FWHM	Area	Chemical State
1	Se 3d	54.77	0.453	215.17	Se(-II) or Se(-I)
		55.08	0.335	155.90	Se(0)
		55.4	0.6	198.88	Se(0)
		55.68	0.5	94.34	Se(0)
		55.98	0.430	176.38	Se(0)
	S 2p	161.30	1118.05	1.874	S ²⁻
		162.50	22	0.937	* Doublet
		163.10	342.713	0.897	S _n ²⁻
		164.30	21.414	0.448	* Doublet
		164.35	73.369	0.586	S(0)
		165.55	4.0	0.293	* Doublet
		167.4	1005.909	1.173	HSO ₃ ⁻ or S ₂ O ₃ ²⁻
	168.6	158.919	0.587	* Doublet	
	O 1s	530.92	0.94	1187.08	OH ⁻
		531.54	0.96	2224.26	HSO ₃ ⁻ or S ₂ O ₃ ²⁻
533.09		0.97	856.50	H ₂ O	
2	Se 3d	54.66	0.4	120.567	Se(-II) or Se(-I)
		54.98	0.58	360	Se(0)
		55.42	0.5	58.608	Se(0)
		55.73	0.434	218.474	Se(0)
		56.04	0.197	34.3523	Se(0)
	S 2p	161.22	1138.07	1.823	S ²⁻
		162.42	27	0.912	* Doublet
		162.92	177.213	0.76	S _n ²⁻
		164	130	1.38	* Doublet
		164.12	14	0.38	S(0)
		165.2	13	0.69	* Doublet
		167.37	1535	0.9	HSO ₃ ⁻ or S ₂ O ₃ ²⁻
	168.59	400	0.89	* Doublet	
	O 1s	530.89	0.93	2236.28	OH ⁻
		531.51	1	5218	HSO ₃ ⁻ or S ₂ O ₃ ²⁻
533.12		0.84	1599.22	H ₂ O	

Table A7. Continued

Sample no.	Species	BE (eV)	FHWM	Area	Chemical State
3	Se 3d	54.6	0.5	195.911	Se(-II) or Se(-I)
		54.83	0.5	20.877	Se(0)
		55.21	0.4786	131.702	Se(0)
		55.63	0.51	331.679	Se(0)
		56.1	0.56	55.5013	Se(0)
	S 2p	161.15	1328.396	1.797	S ²⁻
		162.35	45	0.899	* Doublet
		162.93	201.324	1.1	S _n ²⁻
		164.13	12	0.55	* Doublet
		164.2	33	0.5	S(0)
		165.4	11	0.25	* Doublet
		167.37	1945.782	1.041	HSO ₃ ⁻ or S ₂ O ₃ ²⁻
	168.57	444	0.52	* Doublet	
	O 1s	530.87	0.98	3567.94	HSO ₃ ⁻ or S ₂ O ₃ ²⁻
531.53		1.04	6898.19	H ₂ O	
533.05		0.87	1814.16	H ₂ O	
4	Se 3d	55.17	0.5	1532.86	Se(-II) or Se(-I)
		55.43	0.41	1779.89	Se(0)
		55.65	0.21	272.445	Se(0)
		55.9	0.5	1220.35	Se(0)
		56.26	0.5	2215.69	Se(0)
	S 2p	161.55	8777	1.73	S ²⁻
		162.75	133	0.865	* Doublet
		163.23	1710	0.89	S _n ²⁻
		164.43	100	0.445	* Doublet
		164.5	255	0.506	S(0)
		165.7	22	0.253	* Doublet
		167.51	4600	1.25	HSO ₃ ⁻ or S ₂ O ₃ ²⁻
	168.71	444	0.625	* Doublet	
	O 1s	531.56	1.41	14701.2	HSO ₃ ⁻ or S ₂ O ₃ ²⁻
533.30		0.86	2111.67	H ₂ O	

* The doublet is associated with the previous peak

Table A7. Continued.

Sample no.	Species	BE (eV)	FHWM	Area	Chemical State
5	Se 3d	54.83	0.6	2600	Se(-II) or Se(-I)
		55.06	0.19	200	Se(0)
		55.68	0.72	2270	Se(0)
		55.9	0.5	150	Se(0)
		55.98	0.5	94	Se(0)
	S 2p	161.5	902.085	2.04	S ²⁻
		162.7	140.756	1.02	* Doublet
		164	45	0.8	S _n ²⁻
		165.2	8	0.4	* Doublet
		167.4	1579.545	0.79	HSO ₃ ⁻ or S ₂ O ₃ ²⁻
		168.6	50.015	0.395	* Doublet
		168.5	1017.857	1.14	SO ₄ ²⁻
	169.7	8	0.57	* Doublet	
	O 1s	531.28	1.45	8110	HSO ₃ ⁻ or S ₂ O ₃ ²⁻
		532.26	0.89	535.0007	SO ₄ ²⁻
533		0.9	1000	H ₂ O	
6	Se 3d	54.67	0.5	22.99	Se(-II) or Se(-I)
		54.95	0.438234	133.7898	Se(0)
		55.25	0.315907	61.7494	Se(0)
		55.56	0.419969	147.703	Se(0)
		56.15	0.98	385.2236	Se(0)
	S 2p	161.26	1201.212	1.928	S ²⁻
		162.46	44	0.964	* Doublet
		163.23	133	0.964	S _n ²⁻
		164.43	16	0.48	* Doublet
		167.53	1820.135	0.969	HSO ₃ ⁻ or S ₂ O ₃ ²⁻
		168.4	92.723	0.721	* Doublet
		168.73	312	0.485	SO ₄ ²⁻
	169.6	6	0.36	* Doublet	
	O 1s	531.34	1.26	9383.62	HSO ₃ ⁻ or S ₂ O ₃ ²⁻
		532.99	0.72	1200	SO ₄ ²⁻
533.44		0.51	390.0313	H ₂ O	

* The doublet is associated with the previous peak